

Topical Review

Mechanical metamaterial sensors: from design to applications

Hugo de Souza Oliveira^{1,2,3,*} , Niloofar Saeedzadeh Khaanghah¹ , Giulia Elli¹ ,
Luisa Petti¹ , Giuseppe Cantarella⁴ , Edoardo Milana^{2,3}  and Niko Münzenrieder^{1,5,*} 

¹ Faculty of Engineering, Free University of Bozen-Bolzano, 39100 Bozen-Bolzano, Italy

² Department of Microsystems Engineering—IMTEK, University of Freiburg, Freiburg 79110, Germany

³ Cluster of Excellence livMatS @ FIT-Freiburg Center for Interactive Materials and Bioinspired Technologies, University of Freiburg, 79110 Freiburg, Germany

⁴ Department of Physics, Informatics, Mathematics, University of Modena and Reggio Emilia, 41125 Modena, Italy

⁵ Sensor Technology Research Centre, University of Sussex, Brighton BN1 9QT, United Kingdom

E-mail: hugo.oliveira@livmats.uni-freiburg.de and niko.muenzenrieder@unibz.it

Received 25 May 2024, revised 26 July 2024

Accepted for publication 23 January 2025

Published 5 February 2025



Abstract

The integration of mechanical metamaterials with sensor technology has opened new frontiers in the design and application of advanced sensing systems due to their ability to impart unique mechanical properties that enhance sensor functionality. Mechanical metamaterials, with properties derived from their engineered structures rather than their material composition, offer unique advantages such as negative Poisson's ratio, high strength-to-weight ratios, and programmable behaviors. This review explores the dual approaches of incorporating sensors with mechanical metamaterials: metamaterial-supported sensors, where metamaterials provide structural support and enhanced durability to traditional sensors, and metamaterial-integrated sensors, where the metamaterial itself serves as the sensing element. Incorporating metamaterials in sensor design can offer increased sensitivity and precision, enhanced structural integrity and durability, programmability and reconfigurability, as well as lightweight and compact design solutions. Key advancements in the field are presented, highlighting how metamaterials properties can enhance sensor performance in terms of sensitivity, precision, and operational versatility. The review covers the primary materials and fabrication techniques used, including additive manufacturing, molding, and physical vapor deposition, and discusses the challenges associated with the mechanical integration of metamaterials and sensors. Practical applications in pressure, strain, temperature, and biomedical sensing are examined, demonstrating the transformative potential of mechanical metamaterials in creating

* Authors to whom any correspondence should be addressed.



Original Content from this work may be used under the terms of the [Creative Commons Attribution 4.0 licence](https://creativecommons.org/licenses/by/4.0/). Any further distribution of this work must maintain attribution to the author(s) and the title of the work, journal citation and DOI.

high-performance, multifunctional sensor systems. The discussion concludes with an outlook on future research directions and potential advancements in the field.

Keywords: sensors, metamaterials, flexible electronics, 3D printing, microfabrication, soft robots

1. Introduction

Metamaterials, also known as artificial materials [1], are a class of materials designed to present unique properties and behaviors that are hardly found in natural materials [2, 3]. These materials derive their special characteristics from their complex designed structure, rather than their chemical composition alone [4]. The main types include electromagnetic metamaterials [5, 6], designed to control electromagnetic waves for applications like cloaking and superlenses; acoustic metamaterials [7, 8], which manipulate sound waves for advanced soundproofing and acoustic imaging; mechanical metamaterials [9, 10], engineered to exhibit unique mechanical properties such as negative Poisson's ratio and programmable deformation (section 2).

The first attempts to develop metamaterials can be traced to experiments with microwaves, attributed to Jagadis Chunder Bose, who explored architected twisted structures to manipulate waves at the end of the 19th century [24, 25]. Subsequently, in 1914, efforts were made to develop artificial twisted media using randomly oriented small wire helices in a host medium [25, 26]. Thirty-five years later, lightweight microwave lenses were designed by periodically positioning spheres, strips, and disks, making it possible to tune the effective refractive index of artificial media [25, 27].

In parallel to the advancements of this new class of materials, mechanical metamaterials began attracting attention [28]. Similarly to the metamaterials designed to manipulate electromagnetic waves, they are engineered to exhibit properties that are not found in naturally occurring materials [29, 30], often through their unique geometric or microstructural design. These properties can include unusual mechanical behavior such as negative Poisson's ratio [19], negative thermal expansion (NTE) [31], and high strength-to-weight ratio (see section 2). In 1987, Lakes first described a foam-based mechanical metamaterial [28]. In the past decade, the advent of advanced fabrication methods, such as additive manufacturing has boosted interest in mechanical metamaterials, because of its ability to fabricate complex geometries and features that are challenging or even impossible to achieve with traditional manufacturing methods [32–34].

Mechanical metamaterials have been explored in various structures to realize devices, such as metamaterial mechanisms [35], metamaterial foams [36–39], resonators for reducing vibrations [40–43], stents for biomedical applications [44–47], structures for energy impact absorption [48–52], and sports equipment [53]. Nonetheless, a very promising application for metamaterials lies in incorporating them in sensor design, as they can offer unique advantages, including increased sensitivity [11, 17] and precision [13], enhanced structural integrity and durability [15, 18, 19, 54], programmability and

reconfigurability [55], and lightweight and compact design solutions [56].

The exploration of metamaterials in sensing applications typically follows two distinct approaches. In the first approach, sensors are embedded or housed within a metamaterial structure; however, these sensors can operate independently of the metamaterials [15, 18, 19, 57]. The primary role of the metamaterial in such systems is to provide mechanical support, enhance durability, or enable the adaptation of sensors to complex surface geometries that would otherwise be challenging to manage [19, 58]. This arrangement preserves the sensor's original functionality while leveraging the unique properties of metamaterials—such as their engineered structural features—to enhance the overall performance of the device. In the second approach, the sensing elements themselves are designed using the principles of metamaterial structures. Here, metamaterials are not just supportive frameworks but integral components that interact directly with the target stimuli [11, 12, 14, 16, 17, 21, 23, 54, 55, 59, 60]. The design often exploits the mechanical properties of metamaterials to enhance the sensitivity, the specificity, or the operational bandwidth of the sensors. For the purposes of this work, the first approach is referred to as metamaterial-supported sensors, and the second as metamaterial-integrated sensors. Figure 1 shows a brief overview of the of mechanical metamaterials relying on many established technologies to realize diverse types of sensors.

Most reviews on mechanical metamaterials typically focus on briefly describing their potential applications and advantages over conventional materials [61], conducting broad analyses covering various aspects [10, 34], or examining their use in sensing applications without discussing the nuances of the design principles, material choices, optimization techniques, integration with electronics, fabrication technologies and limitations [62]. Herein, however, we present a review of the recent advancements and applications of mechanical metamaterials in sensor technology from the perspective of metamaterial-supported and metamaterial-integrated sensor design. This review outlines the fundamental principles of each approach, discusses their technological implementation, and examines the impact of the mechanical metamaterial properties on the performance enhancements of sensor systems. The discussion covers the main properties of metamaterials that are explored in the design of the sensors, such as negative Poisson's ratio, NTE, and high strength-to-weight ratios, which can be harnessed to enhance sensor performance in various fields. By critically analyzing the structural and functional interaction between metamaterials and sensors, we provide an overview of how these materials can enhance the sensor's capabilities. Through advances in fabrication techniques and careful material selection, we demonstrate how the incorporation

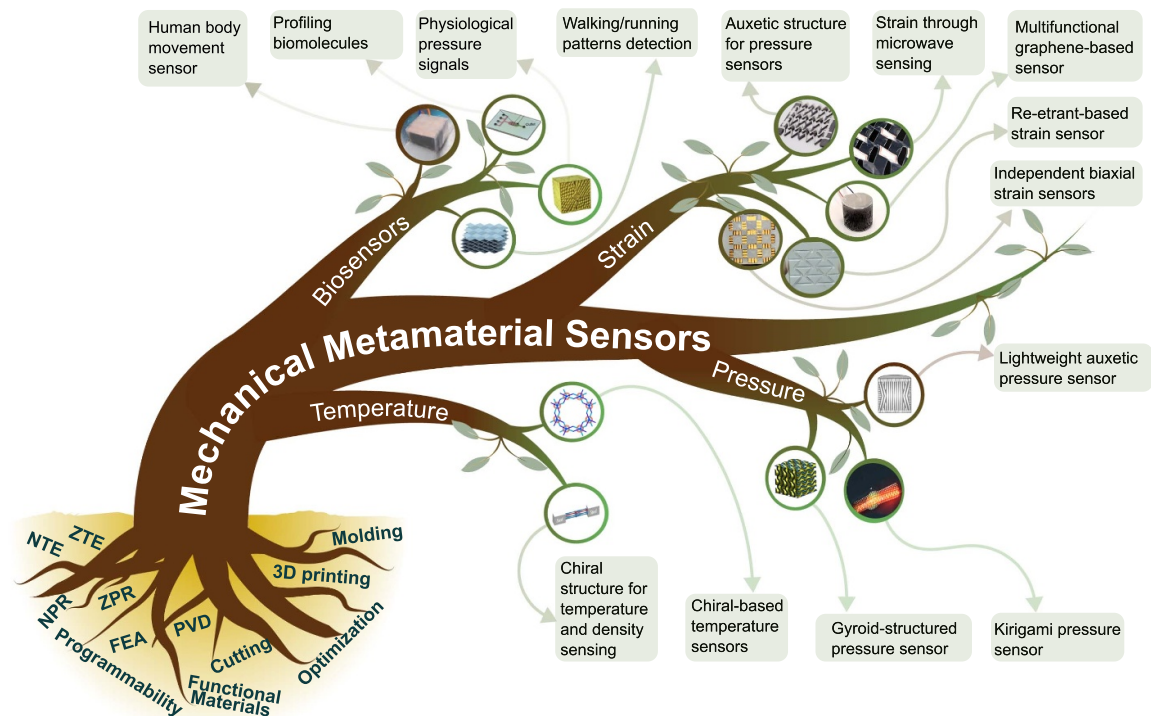


Figure 1. Overview of mechanical metamaterial sensors categorized into: biosensors [11–14], strain [15–19], temperature [20, 21], and pressure sensors [16, 22, 23]. The tree diagram highlights key and foundational technologies and material properties that support metamaterial-based sensor development. Reprinted from [11], Copyright (2022), with permission from Elsevier. © [2023] IEEE. Reprinted, with permission, from [12]. Reproduced from [13], with permission from Springer Nature. Reprinted from [14], Copyright (2023), with permission from Elsevier. Reproduced from [15]. CC BY 4.0. Reprinted from [16], Copyright (2023), with permission from Elsevier. [17] John Wiley & Sons. [© 2018 WILEY-VCH Verlag GmbH & Co. KGaA, Weinheim]. Reprinted with permission from [18]. Copyright (2020) American Chemical Society. © [2022] IEEE. Reprinted, with permission, from [19]. Reproduced from [20]. CC BY 4.0. Reprinted from [21], Copyright (2024), with permission from Elsevier. [22] John Wiley & Sons. [© 2022 Wiley-VCH GmbH]. [23] John Wiley & Sons. [© 2023 Wiley-VCH GmbH].

of metamaterials can lead to sensors with increased sensitivity, precision, and durability.

In section 2, we present the unique and most explored properties of mechanical metamaterials that make them attractive for sensor design. In section 3, we discuss the methodologies for designing them, focusing on forward and inverse design approaches. Section 4 exhibits the main fabrication technologies along with the materials utilized to fabricate the metamaterial-based sensors. In section 5 we present the practical aspects of incorporating metamaterials in sensor design. Section 6 shows applications of metamaterial-based sensors for pressure, biomedical, strain, and temperature sensing. In section 7, we summarize the important points, highlight the main contributions of this work, and present an outlook of potential further exploration of metamaterial-supported and metamaterial-integrated sensor design.

2. Exploring the unique properties of mechanical metamaterials for designing sensors

Mechanical metamaterials can be designed to exhibit various unique properties, such as negative Poisson's ratio,

NTE, negative compressibility, high energy absorption, attributes like programmability/reprogrammability, and extreme anisotropy [15]. However, the most explored properties for developing sensors are negative Poisson's ratio, negative expansion, high strength-to-weight ratio, and attributes like programmability and re-programmability, which offer significant opportunities for innovation in the development of metamaterial-supported and metamaterial-integrated sensors. The other properties can also be promising for sensor development, but have not been extensively explored, as this field is still immature and many aspects remain unexplored (section 7).

These properties can benefit sensor applications by redistributing stresses and strains [15, 19], thus protecting sensitive functional materials from damage or the influence of deformation in their behavior. They allow for minimal or zero strain in specific regions through careful metamaterial design, creating optimal locations for placing delicate sensing elements [15, 19]. Additionally, the metamaterial properties can enhance sensitivity [16, 60] or facilitate the development of novel [20], lightweight [56], and highly sensitive sensors [12, 17]. This section will discuss the main characteristics of the negative Poisson's ratio, negative/zero thermal expansion, high strength-to-weight ratio, and programmable/reprogrammable

Table 1. Effect of Poisson's ratio on mechanical properties for isotropic materials.

Poisson's ratio (ν)	Physical significance
1	Preservation of area in 2D material
0.5	Preservation of volume (incompressibility)
0	Preservation of cross section
-0.5	Preservation of moduli $E = G$
-1	Preservation of materials' shape

behavior demonstrating their potential for sensor development and integration.

2.1. Negative Poisson's ratio

The Poisson's ratio ν is a mechanical property of materials that describes the ratio of transverse strain to axial strain when the material is uni-axially stressed. It indicates how much a material will contract or expand in the perpendicular direction to an applied force. Poisson's ratio offers valuable insights into the mechanical behavior of a material. Most conventional materials exhibit characteristic positive Poisson's ratios (PPR). For instance, rubber-like materials typically present a Poisson's ratio of approximately $\nu = 0.5$, while for steel-like materials it is around $\nu = 0.3$ [63]. For isotropic materials, the Poisson's ratio can be described by the relation $E/G = 2(1 + \nu)$ [64, 65]. Table 1 summarizes the effect of the Poisson's ratio values on the mechanical properties and characteristics of an isotropic material [64, 65].

Negative Poisson's ratio (NPR) and zero Poisson's ratio (ZPR) are properties of certain materials that exhibit the counter-intuitive mechanical behavior of expanding laterally when stretched and contracting laterally when compressed, which is the opposite of what is observed in PPR materials [66–68]. While the theoretical possibility of NPR has been in discussion for some time in elastic theory [69], practical demonstrations are relatively recent, as the first documented material exhibiting a negative Poisson's ratio was reported by Lakes [28] in 1987. Since then, NPR materials have gained significant attention due to their potential in diverse application areas, ranging from aerospace [70, 71] to medical applications [72]. This is driven by unique abilities, such as enhanced energy dissipation [73], and achieve lightweight and high-strength structures [16].

NPR materials, also known as auxetic materials [74], are a subclass of mechanical metamaterials [51, 66, 68]. Auxetic behavior can be found in nature [75], such as in cubic crystal lattices [76, 77] and some forms of snakeskin [3, 51]. Figure 2 illustrates the main difference between PPR and NPR materials both with an initial length L_1 and height L_2 . Upon stretching, the PPR material shrinks laterally, while the NPR material expands. The difference is quantified by the Poisson's ratio $\nu = (L_4 - L_2)/(L_3 - L_1)$, which is universally applied for any material, regardless of whether it exhibits PPR or NPR behavior. The counter-intuitive behavior of the NPR material is a result of the inner arrangements in the material's structure and the way it deforms when a load is applied [15]. These

inner arrangements can be designed by exploring various unit-cell configurations, such as re-entrant, semi-reentrant, rotation polygonal units, kirigami and origami, or missing rib approaches (section 3). Additionally, the deformation mechanism in auxetic materials can occur at any scale, as Poisson's ratio is scale-independent [78, 79], which means their deformation mechanism is effective from the nano-level to the macro-scale [80, 81].

NPR-based designs have been explored in metamaterials-integrated sensors, providing enhanced sensitivity and detection range [11–14, 16, 17, 21, 23, 54–56, 60]. It can also be used in metamaterial-supported sensors, offering resilience against stretching, impact, and other potential damage [18, 19, 22, 59]. This embedding approach allows sensors to maintain their core functionality while benefiting from the unique advantages of NPR materials.

To exemplify metamaterial-supported sensors exploring NPR, a PPR and NPR designs were combined to create a hybrid material leveraging the superposition of the two Poisson's ratio [15], as verified in figure 3(a). The structure achieved an overall Poisson's ratio of 0.07 for a uniaxial tensile strain of 10%. Figure 3(b) shows a ZPR structure used as a substrate for pressure sensors showing a Poisson's ratio of 0.061 at a stretching of 15% [19].

Figures 3(c)–(f) show examples of metamaterial-integrated sensors. Figure 3(c) refers to a re-entrant structure (section 3.1.1) that exhibits an overall Poisson's ratio of 0.41 to 0.19. The main function of the frame was to enhance the deformation of the sensing material [17]. Similarly, figure 3(d) shows a sensor that leverages an NPR structure integrated into the sensing material. The NPR structure facilitated the formation of electrical pathways, reducing the electrical resistance of the whole sensitive material. The Poisson's ratio of the sensitive structure reached 0.18 [12]. Figure 3(e) shows a NPR material used to enhance the sensitivity of a self-powered strain sensor. The Poisson's ratio of the structure was -1 at a deformation of 30% [60]. Figure 3(f) shows the NPR as the sensing element of the pressure sensor. Here, the NPR material shows an unconventional oblique transversal expansion improving the sensitivity of the sensor. The configuration resulted in a Poisson's ratio of -4.2% at a longitudinal strain of 25% [16]. Additionally, a conductive porous material based on re-entrant structures was explored in designing biomedical sensors [11]. In this case, a symmetric hyperbolic re-entrant pattern combined with a rhombus structure was developed to show NPR and high contraction in the transverse and longitudinal directions under compression. The NPR varied with the compression experiments in the range of -0.48 to 0.175 with a maximum compressive strain of -80%.

2.2. Negative and zero thermal expansion

Most common materials exhibit positive thermal expansion coefficients (PTE) $\beta > 0$, which means they expand and contract upon heating and cooling, respectively [82]. This behavior is attributed to the increased vibrational energy of the atoms, as they vibrate more intensely and occupy more space with the temperature increases, consequently causing the

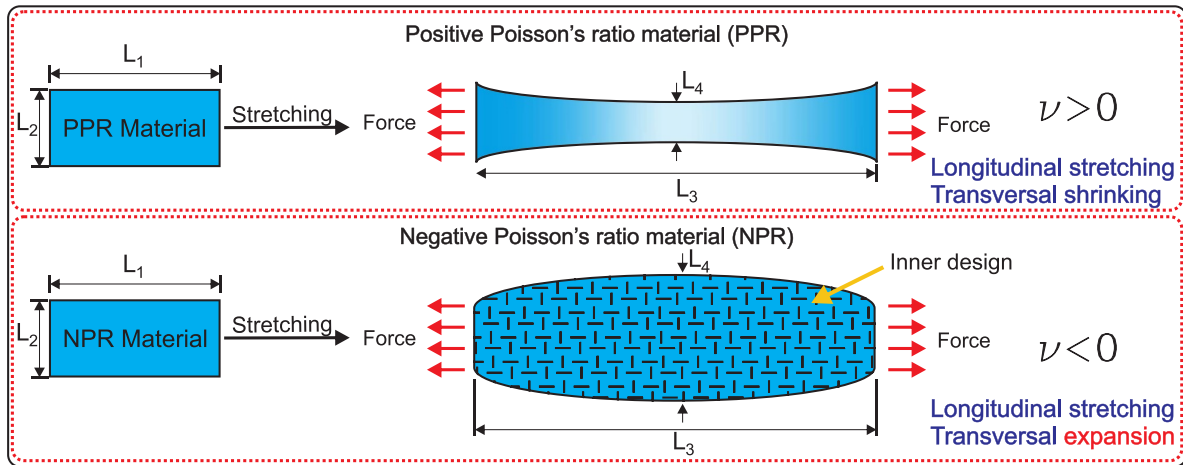


Figure 2. Description of PPR and NPR materials behavior.

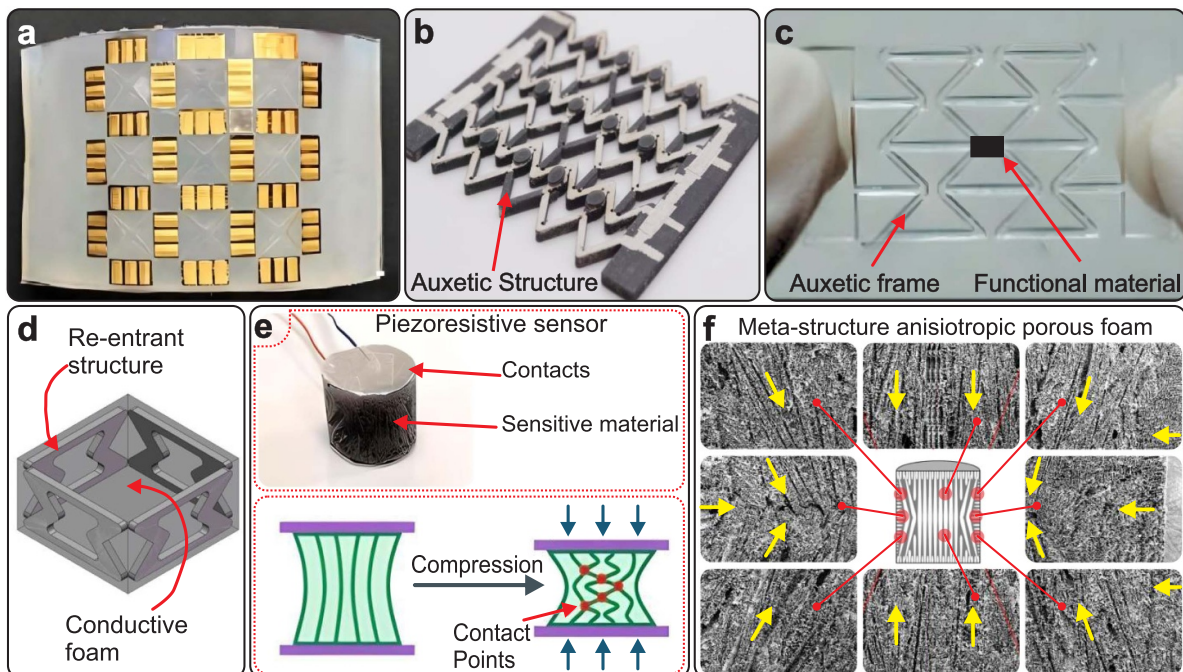


Figure 3. NPR structures to realize metamaterial-based-sensors (a) Combination of PPR and NPR [15]. Reproduced from [15]. CC BY 4.0.; (b) Semi re-entrant auxetic ZPR material [19]. © [2022] IEEE. Reprinted, with permission, from [19].; (c) Strain sensor based on a re-entrant frame [17]. [17] John Wiley & Sons. [© 2018 WILEY-VCH Verlag GmbH & Co. KGaA, Weinheim].; (d) Combination of conductive foam and a re-entrant structure [12]. © [2023] IEEE. Reprinted, with permission, from [12].; (e) Lightweight auxetic foam-based pressure sensor [16]. Reprinted from [16], Copyright (2023), with permission from Elsevier.; (f) Detailing of the inner structure of the conductive foam [16]. Reprinted from [16], Copyright (2023), with permission from Elsevier.

material to expand, as shown in figure 4(a). Nevertheless, this expansion can be reduced or even eliminated in materials that exhibit NTE behavior, $\beta < 0$; or zero thermal expansion (ZTE) coefficients, $\beta = 0$. Figure 4(b) demonstrates the behavior of a NTE material contracting with increasing in temperature and expanding with decreasing the temperature, while figure 4(c) shows a ZTE material insensitive to temperature variations.

NTE-based materials exhibit the unique property of contracting upon heating, contrasting with the expansion observed

in conventional materials [31, 32]. This counter-intuitive behavior is observed in some bulk synthesized materials, like Zirconium Tungstate ZrW_2O_8 [83], and natural materials, such as ice. It occurs because the apparent distance between the unit cells decreases during positive temperature increments, although the actual distance between these cells may increase or remain constant [31]. The NTE effect is the fundamental principle that allows metamaterials to contract upon heating, in contrast to the conventional expansion seen in most materials [31]. Metamaterials engineered to exhibit NTE can

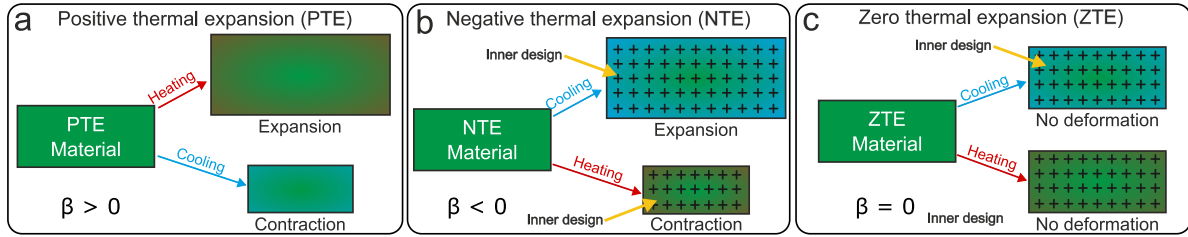


Figure 4. Expansion and contraction of materials upon heating and cooling: (a) Ordinary PPE material; (b) NTE materials; (c) ZTE materials.

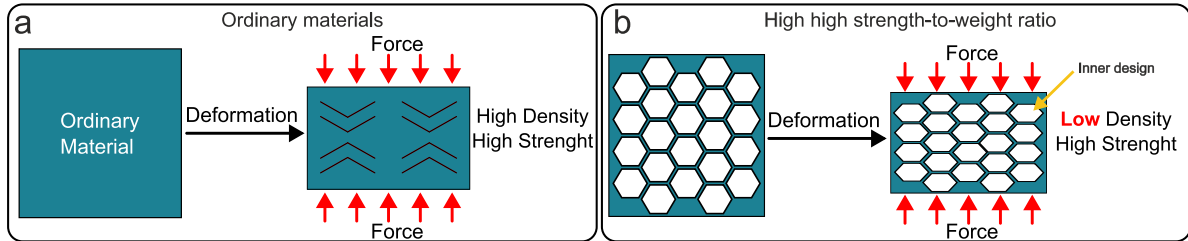


Figure 5. Description of high strength-to-weight ratio materials: Normal material with high density exhibiting high strength; (b) Metamaterial exhibiting low density and high strength.

significantly reduce internal stress levels, especially in scenarios involving mechanical deformation-induced stress [82, 84]. By effectively countering the expansion typically induced by temperature increases, they offer a novel solution for enhancing the structural integrity and the durability of materials under varying thermal and mechanical conditions [82]. The NTE effect is achieved by manipulating the geometry and material composition of the unit cells in response to temperature changes [31]. The fundamental mechanisms that enable this response involve the unique inner design of metamaterials, which explores the thermo-stretching-dominated or the thermo-bending-dominated designing aspects [31, 84]. Thermo-stretching-dominated NTE metamaterials typically exhibit high stiffness due to the axial thermal expansion of struts leading to a reduction in transverse distance [31]. In contrast, thermo-bending-dominated NTE metamaterials show pronounced NTE behavior due to the increased curvature of bi-material curved beams under temperature changes, effectively reducing the longitudinal distance between the ends of the beams [31].

Similarly to NTE, zero thermal expansion (ZTE) is a property of some materials in which there is no change in volume or dimensions under temperature variations [32]. This phenomenon occurs despite the typical behavior of materials to expand upon heating due to increased atomic or molecular vibrations. ZTE is also realized through the design of a material’s structure and the strategic selection and arrangement of its components, allowing for dimensional stability across a range of temperatures [84]. By adjusting these factors, the overall thermal expansion properties of the composite can be manipulated to achieve ZTE, which is particularly valuable in applications requiring high precision and stability under thermal stress [32].

The NTE effect can be explored in metamaterial-integrated and metamaterial-supported sensors. For the integrated type,

the geometrical changes in the internal structure in response to temperature variations can be merged with functional materials to monitor environmental parameters such as temperature or moisture [20]. On the other hand, for the supported type, the NTE effect may be employed to mitigate internal stresses and strains, thereby reducing the risk of sensor breakage within the metamaterial framework.

2.3. High strength-to-weight ratio

The property of high strength-to-weight ratio in mechanical metamaterials is related to their ability to exhibit substantial mechanical strength with minimal mass [85]. Figures 5(a) and (b) illustrate the contrast between ordinary materials, which exhibit high density and strength, and high strength-to-weight ratio materials, which achieve comparable strength with much lower density, primarily due to their internal design.

This characteristic is directly associated with the relative density of the metamaterial’s unit cell, which is defined as the ratio of the solid material’s volume to the total volume of the unit cell, including empty spaces and voids [86–88]. The relative density property is important for influencing the mechanical properties of metamaterials [86–89].

As the size of the unit cell increases or decreases, the volume of material within the cell changes accordingly, which in turn alters the relative density [87]. If the amount of material within the unit cell remains constant while the overall dimensions of the cell increase, the relative density will decrease because there is a larger volume of space relative to the amount of material [88]. Conversely, if the unit cell size is reduced while maintaining the same amount of material, the relative density will increase [86, 89]. For stretching-dominated structures [87], both the elastic modulus and strength exhibit a linear relationship with the relative density, in contrast

to bending-dominated structures, in which these properties demonstrate an exponential dependence [87].

The high strength-to-weight ratios characteristic of mechanical metamaterials offer significant advantages in sensor design. These properties enable the creation of lightweight yet robust sensor components capable of withstanding high stresses and strains without compromising performance [90]. This is particularly beneficial for sensors deployed in harsh environments, such as those subject to vibration or impact. Here, the metamaterials' increased resilience and durability, coupled with their reduced weight, ensure they will not significantly influence the modal parameters of the object being observed [91]. Furthermore, their lightweight and unobtrusive nature makes mechanical metamaterial-based sensors ideal for wearable applications where comfort and seamless integration are important aspects [92, 93].

The high strength-to-weight property is especially interesting for metamaterial-supported sensors. With a reduced mass, they can offer enough stability and protection to the sensors embedded in the metamaterial structure, reducing the likelihood of breakage or excessive stress and strain [15, 19, 22]. In metamaterial-integrated sensors, the high strength-to-weight ratio allows for creating lightweight but mechanically resistant materials that can be used as pressure sensors [16, 56].

For example, the high strength-to-weight ratio property was explored in the design of a multifunctional ceramic/graphene metamaterial [56]. The designed structure resulted in a flyweight density of 1.8 mg cm^{-3} . The relative density was also explored as a central parameter in the design of a metamaterial-based pressure sensor so that by altering the relative density of the structure from 30% to 80% the young modulus increased from 0.32 mPa to 3.61 mPa, influencing the sensitivity and the sensing range [23].

2.4. Programmable and reprogrammable metamaterials

While mechanical metamaterials offer a range of innovative properties, their practical applications are often hindered by limitations such as insufficient tunability and a tendency towards single functionality. However, endowing metamaterials with programmable and reprogrammable functionalities could potentially reduce or eliminate these limitations [94, 95]. This adaptability is critical in developing more efficient, responsive, and intelligent sensor systems that can operate in complex, and changing environments [96].

Programmable metamaterials are designed with the ability to change their physical properties, geometry, or functionality in a predetermined manner. The term 'programmable' implies that these changes are not spontaneous but initiated or controlled by a programmed mechanism [95]. The programming can be performed by introducing contact and non-contact methods [95], enabling the adjustment of certain characteristics, and introducing programmability into these materials. Contact tuning employs external force stimuli [97, 98] and relies on deformable materials to achieve desired changes. Non-contact tuning, on the other hand, utilizes magnetic [99–102], electric [103, 104], and temperature [105–108] fields to manipulate the metamaterials' properties, requiring the

materials to be responsive to these external fields. The key aspect of programmable metamaterials is the ability to precisely control the change in properties or shape according to a pre-defined sequence [95].

To exemplify the programmability of mechanical metamaterials integrated with sensors, a multifunctional composite was developed [109]. The SCMM system features programmable self-sensing and self-powering functionalities via tailored triboelectric microstructures. This design enables precise control of electrical output, generating voltages up to 0.85 V under cyclic loading. The system's programmability is further demonstrated by its snapping behavior, which modulates electrical signals. For instance, the generated current increases from $0.1 \mu\text{A}$ to $0.5 \mu\text{A}$ as the loading amplitude varies from 5 mm to 10 mm, showcasing its potential for active sensing and energy harvesting applications. In another example, conductive mechanical metamaterials with programmable elastic instabilities that work as electronic logic gates on mechanical stress input combinations, were developed exploring rotating rigid units (section 3.1.2) [55], as shown in figure 6(a). The structure responds to mechanical stress in discrete modes leading to changes in the compliant conductor network to realize all digital logic functions and logic assemblies. Although no sensor was specifically integrated into the structure, Ag microflakes-based conductive lines were deposited on the TPU structure to serve as an electrical contact under mechanical stress, indicating the deformation state of the structure. Six logic gates were realized (AND, NAND, OR, XOR, and XNOR) by combining the deformation modes of the metamaterial units, as verified in figure 6(b).

Reprogrammable or reconfigurable metamaterials can undergo reconfiguration after initial fabrication [110], distinguishing them from systems that exhibit fixed behaviors or configurations following their initial programming [111–113]. They can adjust to new requirements or functionalities as needed, without being permanently locked into their original programming, state, or function [113]. For example, a structure that leverages origami elements with heterogeneous mechanical properties, exhibiting a variety of mechanical behavior patterns was developed [114], as shown in figure 7(a). By employing functional group transformations, the metamaterial structure demonstrates the ability to switch mechanical behavior between positive and negative stiffness. This switching is achieved through the anisotropic assembly of two different elements into a functional group, leading to the metamaterial's zero Poisson's ratio $\nu = 0$ in stretching/compression, and negative Poisson's close to $\nu = -2$ ratio auxetic deformation, as verified in figure 7(b). This structure can be integrated with electrical networks to achieve mechanical computing, representing a sensor that indicate the deformation state of each functional group.

Recently, efforts have been devoted to developing metamaterials that are self-programmable [112, 115] and self-reprogrammable [113]. The former can reconfigure itself using external mechanisms, actuators, and reference frames, while the latter uses autonomous mechanisms intrinsic to the system [113]. As an example of self-programmable materials, self-folding origami structures were developed by integrating

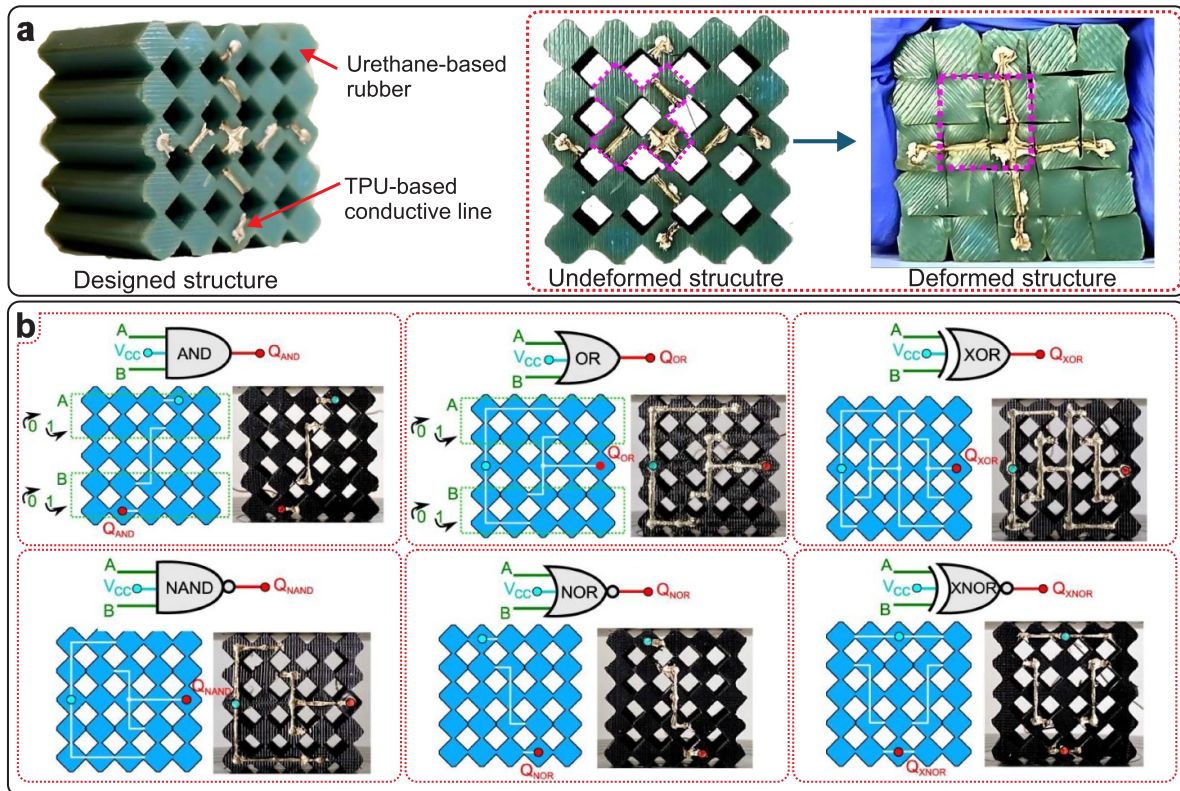


Figure 6. Programmable metamaterial: (a) Polymeric structure developed [55]. Reproduced from [55]. CC BY 4.0.; (b) Possible combinations achieved through mechanical stress [55]. Reproduced from [55]. CC BY 4.0.

wood elements with shape memory polymer [115]. At a certain temperature the structure starts self-folding, adapting to the increase in the temperature, as illustrated in figures 7(c) and (d). The folding dependence on the temperature increase can be explored as a temperature sensor, although the structure was not intentionally designed to be used in this manner. Similarly, a programmed self-folding structure at the millimeter scale was developed [112]. Here, a $50\mu\text{m}$ -thick aluminum substrate was combined with $18\mu\text{m}$ -thick shape memory polyolefin, as the active material; and a $2.5\mu\text{m}$ -thick polyester, as the flexural layer; was employed to devise a composite material. The external temperature around 130° triggers the polyolefin material, causing the structure to adapt to the high temperature by folding the composite and changing its geometry (figures 7(e) and (f)).

3. Designing mechanical metamaterials

The unique properties of mechanical metamaterials are realized through well-defined lattices and unit cells [17, 65, 78, 116], which manifest in various unique shapes and designs, such as re-entrant [11, 17, 19, 117, 118], semi re-entrant [19], chiral [13, 21], origami and kirigami-based [14, 18, 22, 54], and missing rib approaches [59], providing the materials with their unique properties. Each design approach brings unique strengths and tradeoffs [17], enabling fine-tuning of a metamaterial's behavior to match specific application requirements.

The design of metamaterials-supported or metamaterial-integrated sensors is typically carried out following the forward and inverse design methodologies, as demonstrated in figure 8. They enable the precise engineering of structures allowing for the manipulation of properties such as stiffness, energy absorption, and even counterintuitive behaviors like negative Poisson's ratios or NTE (section 2). This precise control creates opportunities for signal amplification [12, 16, 17] and innovative sensing modalities [16, 21, 60], leading to attractive applications in sensor systems [11–19, 21–23, 59, 60]. This section presents how these design methodologies facilitate the creation of unique material properties, enhancing the functionality and sensitivity of sensors.

3.1. Forward design methodology

The most common method for designing metamaterials, either metamaterial-integrated or metamaterial-supported, is the forward design methodology [66]. In this approach, designers leverage their knowledge and creativity to conceptualize structures that can achieve specific properties, such as NPR and NTE (section 2). Biomimetic approaches [119], mathematical control [120, 121], and even basic geometric manipulations [122, 123] are all tools employed at this stage, although the role of design experience is often more pronounced [66, 68]. The designer's familiarity with successful metamaterial architectures and their properties significantly guides the

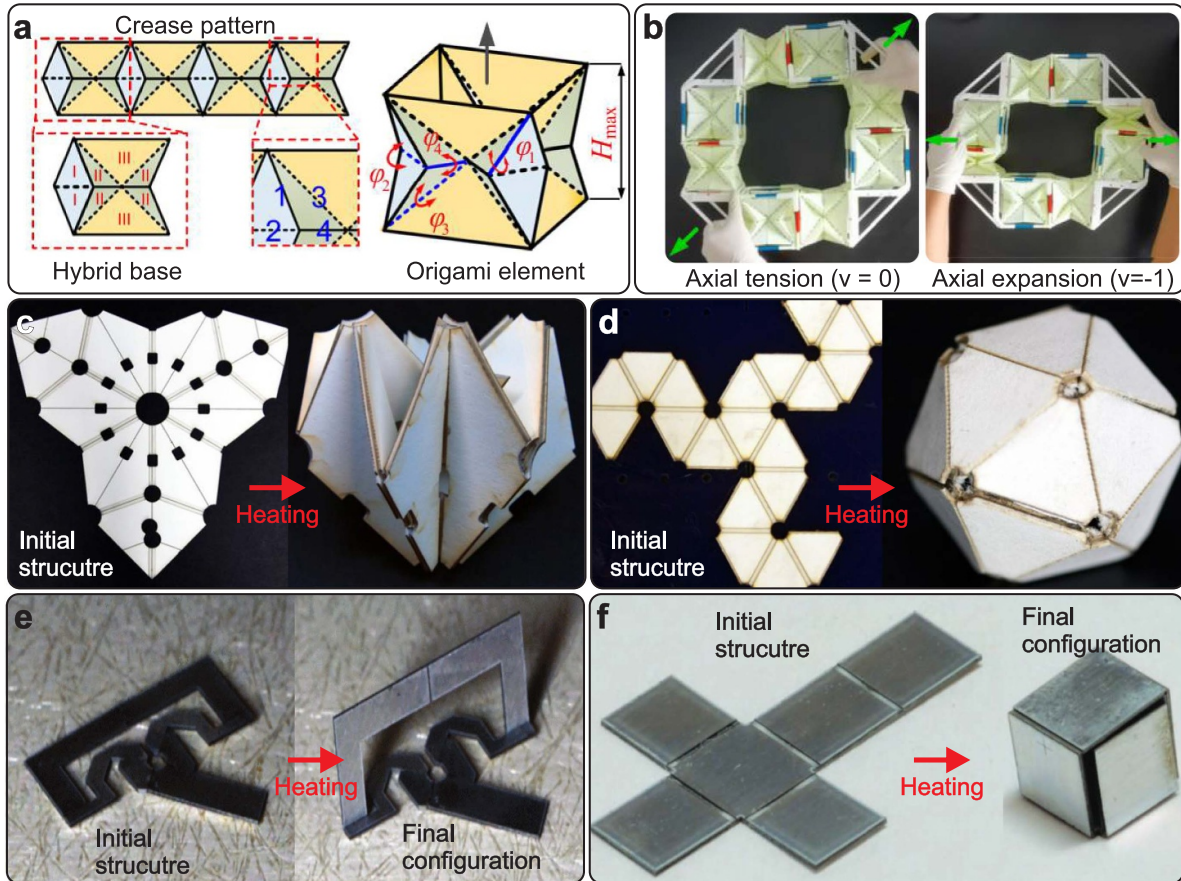


Figure 7. Reprogrammable metamaterials and self-programmable materials: (a) Origami reprogrammable design [114]. Reproduced from [114]. CC BY 4.0.; (b) Origami reprogrammable structure [114]. Reproduced from [114]. CC BY 4.0.; (c) Self-folding flower [115]. Reproduced from [115]. © IOP Publishing Ltd All rights reserved.; (d) Self-folding icosahedron [115]. Reproduced from [115]. © IOP Publishing Ltd All rights reserved.; (e) Self-folding five-bar linkage [112]. © [2014] IEEE. Reprinted, with permission, from [112].; (f) Self-folding cube [112]. © [2014] IEEE. Reprinted, with permission, from [112].

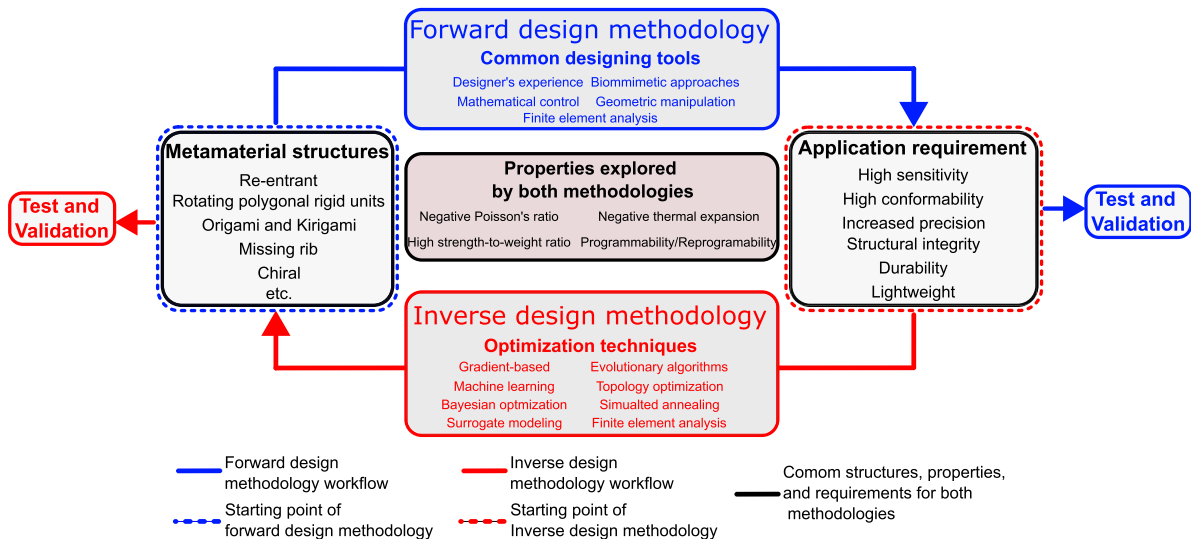


Figure 8. Forward and inverse design methodologies for designing metamaterials.

initial conceptualization and tool selection. After a structure is developed, techniques such as finite element analysis simulations (FEA) or mechanical testing are employed

to assess its performance. Designers often rely on well-established structural patterns and internal arrangements to achieve desirable properties (section 2), which are important

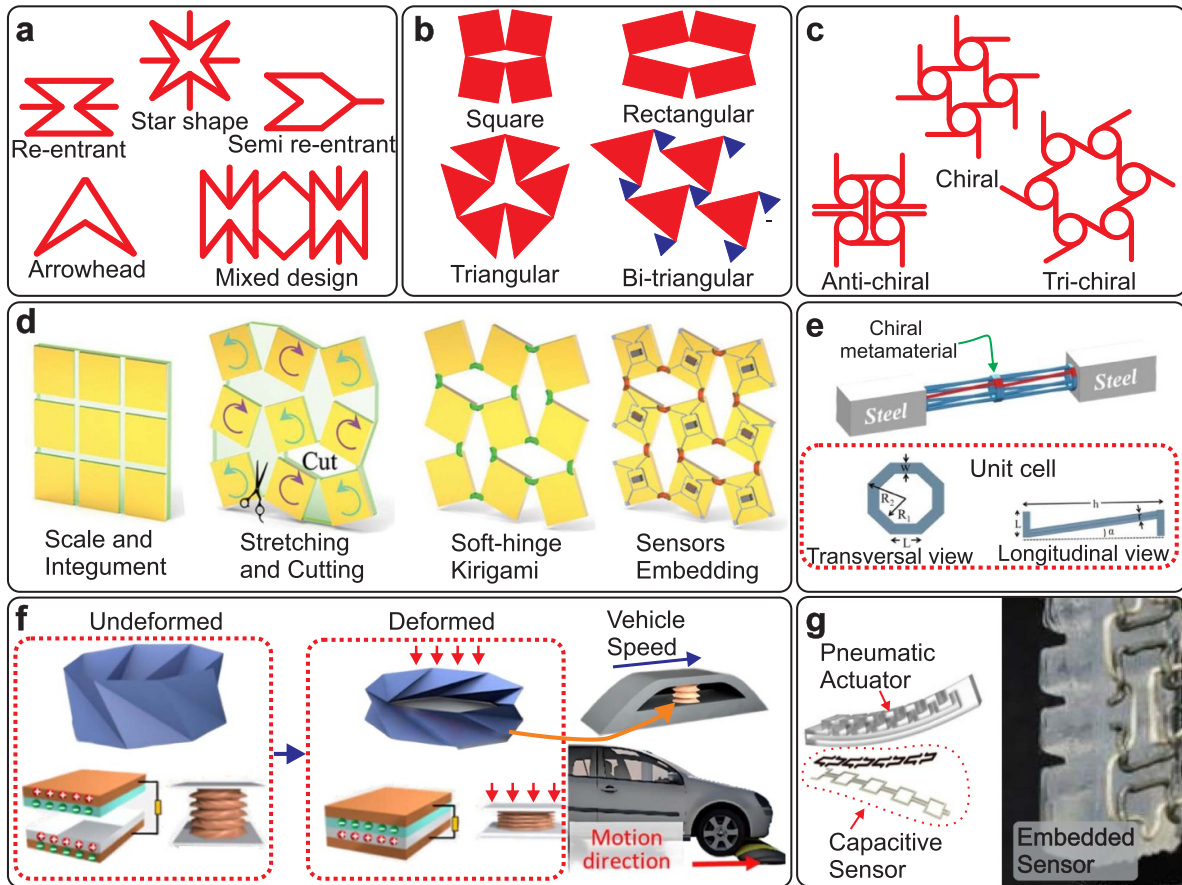


Figure 9. Negative Poisson's ratio structures: (a) Re-entrant unit-cells ; (b) Rotating polygonal units; (c) Chiral structures; (d) Rotating square units embedded with sensors [22] John Wiley & Sons. [© 2022 Wiley-VCH GmbH].; (e) Chiral structure for temperature and density measurement [21]. Reprinted from [21], Copyright (2024), with permission from Elsevier.; (f) Origami structure for mechanoelectrical multistability applications [54]. Reprinted with permission from [54]. Copyright (2023) American Chemical Society.; (g) Missing-rib structure for soft actuator adaptability [59]. Reproduced from [59]. CC BY 4.0.

in the design of sensor-based metamaterials. Figure 8 summarizes the design process of the forward design methodology. This section will showcase and discuss some of the main explored unit cells and structures to realize metamaterial-integrated and supported sensor design in the forward design methodology.

3.1.1. Re-entrant structures. Re-entrant structures are the most basic configuration for unit cells to present NPR or ZPR behavior (section 2.1). The unit cell geometry contains nodes and connecting ribs oriented inwardly [51]. Figure 9(a) shows some of the most explored designs. This structure encompasses various unit cell topologies, such as re-entrant [17, 60, 124–126] and semi-re-entrant [19] honeycombs, mixed honeycombs [19, 80, 127–130], struts [116], arrowhead [131], peanut [132], sinusoidal [46], and star shaped designs [133]. These configurations are highly anisotropic, offering increased transverse Young's and shear moduli [78]. When the structure is deformed, the auxetic behavior of re-entrant structures takes place due to the reconfiguration of nodes and ribs [65].

The integration of re-entrant structures in the design of deformable sensors is essential for enhancing their performance by leveraging the unique properties of NPR or ZPR materials (section 2.1). When these materials are deformed, the inward orientation of the nodes and connecting ribs in re-entrant configurations allows the structure to expand laterally when stretched or to shrink when compressed [11, 17], contrary to the behavior of conventional materials. This characteristic expansion or shrinking can be utilized to increase the number of electrical contact points within the sensor material, significantly enhancing its ability to detect changes in pressure or strain [11, 12, 17, 56]. Increasing contact points is important for maintaining the sensor's sensitivity and accuracy under deformation. Consequently, re-entrant structured materials are particularly effective for applications that require high sensitivity and can endure large deformations [11, 17, 19]. Additionally, re-entrant structures can also be utilized to protect and support the sensing materials, not necessarily being part of them, thus providing structural stability and extending the functional lifespan of the sensors [15, 19, 118]. Such design flexibility not only supports a wide range of mechanical properties but also enables the creation of sensors that

can reliably operate under various operational conditions [15, 17, 19, 22, 118].

3.1.2. Rotating polygonal rigid units. Rotating polygonal rigid unit cells refer to polygonal components within the metamaterial that can rotate relative to each other without deforming [134]. This structure was one of the earliest designs to show the NPR mechanical property [135, 136] and was first proposed by Grima *et al* [137]. A variety of configurations have been explored, such as rotating squares, rectangles [138], rhombi, triangles [139], parallelograms, and combined geometries [136, 140]. Figure 9(b) shows the examples of unit cells normally employed in the design of rotation polygonal rigid units.

As an example of a rotating rigid with sensing capabilities, a kirigami structure was developed following the design concept of rotation polygonal units [22]. Here, the flexibility and bendability of the polymeric substrate were enhanced by the cutting patterns, allowing to deform significantly, as shown in figure 9(d).

3.1.3. Chiral configuration. The concept of chirality was introduced by Lord Kelvin in 1904 [68] and describes a geometric property in which an object cannot be superimposed onto its mirror image through simple rotations and translations [141, 142]. The design of metamaterials often leverages this concept to create structures with unusual properties, such as NPR and NTE. Chiral-based metamaterials are characterized by their unique mechanical properties, such as the compression-twisting effect, where compression induces shearing and a twisting behavior [142]. The design and application of chiral mechanical metamaterials take advantage of the unique deformation features of node rotation and ligament bending in the unit cells [141]. The structure can transform linear deformation into rotation at the unit cell scale [143]. Moreover, chiral geometry exhibits a deterministic handedness, which results in a very stable Poisson's ratio, making them less susceptible to manufacturing errors across small and large deformations [17]. While asymmetric lattices in metamaterials typically lead to anisotropic behavior, chiral lattice patterns can result in isotropic properties. Despite their inherent asymmetry, these chiral patterns can distribute properties uniformly in all directions [144]. Chiral-based metamaterials can be classified into chiral [143], anti-chiral [31], and meta-chiral categories [141]. They are noteworthy for their multi-functional properties, including vibration attenuation and bandgap features [145], impact energy absorption [68], and a negative coefficient of thermal expansion [141, 146, 147]. These properties make chiral-based unit cells attractive for applications where control over mechanical and thermal responses is critical. Figure 9(c) shows some designs for chiral unit cells explored in the design of mechanical metamaterials.

To illustrate the use of chiral design in the development of sensors, a chiral syndiotactic unit cell—which was composed of two chiral sub-cells and with inclined rods attached to

octagonal plates—was employed as a temperature sensor for water, exploring the Fano resonance [21], as shown in figure 9(e).

3.1.4. Origami and Kirigami structures. The exploration of origami and kirigami in the development of auxetic metamaterials has emerged as a significant approach in the fabrication of mechanical metamaterials [4, 14, 18, 22, 114, 148–155]. They are particularly effective in realizing NPR structures due to their efficient design, fabrication, and reconfigurability of mechanical properties [48], which is particularly valuable in applications requiring materials that exhibit large deformations without failure.

The origami-inspired metamaterials are primarily constructed by folding thin sheets along carefully predefined creases [85], resulting in intricate structures that can be used in diverse applications, ranging from mechanical vibration attenuation [114, 156–158] to stents for biomedical applications [159]. Meanwhile, the kirigami technique involves cutting and folding thin and sheet-like materials to create structures [160]. This technique allows for the manufacturing of metamaterials with unique mechanical properties, such as a high strength-to-weight ratio, and has been applied in applications ranging from energy harvesting [161–163] to healthcare [164–166]. For instance, the origami structure was used to create a mechanically responsive substrate that could undergo controlled deformations and maintain multistable mechanical states [54]. These structures, consisting of octagonal, hexagonal, and conical origami units, were important in enabling the effectively trigger triboelectric pairs integrated into their design (figure 9(f)). It was integrated into a self-detectable speed bump designed to monitor vehicle speeds, showcasing their application in a practical, real-world setting.

3.1.5. Missing rib structures. The missing rib design is a specific pattern explored to induce or enhance the negative Poisson's ratio of mechanical metamaterials [167]. This design approach involves creating patterns or structures within the material that unfold or expand in unconventional ways. It consists of removing selected ribs from the designed structure [168] and is particularly relevant in the development of expandable [59], flexible [78], or adaptable structures [169], often verified in metamaterials.

As an example, the missing rib structure was explored in a soft actuator to create a deformable system that can maintain its functionality under expansion and contraction [59]. This structure enabled the actuator to exhibit enhanced mechanical properties, such as increased stretchability and resilience, necessary for soft robotics applications that require robust performance in varying physical conditions figure 9(g). The integration of this auxetic pattern within the actuator allowed for the seamless embedding of sensors that could continuously monitor deformation, thereby providing real-time feedback crucial for adaptive control systems in robotics.

3.2. Inverse design methodology

Inverse design offers a contrasting approach to the traditional forward design methodology [170]. Unlike forward design's focus on the initial fabrication of a structure, inverse design prioritizes specific properties of the structure [171–174]. This method begins by defining the target properties, such as high strength or specific Poisson's ratio [175, 176]. Subsequently, optimization algorithms are used to search a vast design space and identify structures that achieve predefined goals. The main optimization techniques in the design of mechanical metamaterials are gradient-based optimization [177], evolutionary algorithms [178, 179], topology optimization [180, 181], machine learning-based optimization [66, 170, 178, 179, 182–185], bayesian optimization [184], simulated annealing [186], and surrogate modeling [170, 171, 187]. A significant challenge in inverse design is balancing the optimal structure with the feasibility of manufacturing it [32, 79, 188]. The naturally inspired forms that emerge from this process are frequently complex and challenging to fabricate (section 4), limiting their application primarily to conceptual levels [86, 189]. Figure 8 summarizes the design process of the inverse design methodology.

To illustrate the adoption of inverse design, topology optimization was employed in the design of a chiral-based metamaterial to increase the mechanical energy absorption [68]. A generic chiral structure was used as a starting point for the optimization. The main goal was to maximize the elements D_{ijkl} of the matrix \mathbf{D} , which is related to the material stress and the chirality of the structure. The structure was tested by having Fiber Bragg Grating pressure sensor that was attached to the structure to monitor the change in the output pressure during the impact on the metamaterial. The topology and parametric optimization resulted in a structure that could absorb 63% more impact energy than the initial generic structure. Figure 10(a) depicts the designed structure.

As an example of machine learning and bayesian optimization, a non-invasive continuous blood pressure meter consisting of a piezoelectric metamaterial-based structure was enhanced using machine learning and Bayesian optimization techniques [184]. Initially, different unit-cell-based metamaterials were compared to a normal square-shaped piezoelectric element in terms of generating electric potential. Afterward, a Bayesian optimization was used to achieve the optimal design of the proposed piezoelectric metamaterial blood pressure sensor. Then, machine learning algorithms were employed to reveal the effect of design parameters on the output voltage through regression models to simulate and visualize relevant parameters. The structure suggested by the Bayesian optimization could produce an electric potential more than two times greater than that of a conventional square-shaped piezoelectric element achieving 936 mV when subjected to a blood pressure of 100 mmHg. Figure 10(b) shows the obtained structure after the optimization process.

Inspired by human skin, neural networks—core building blocks in machine learning—were implemented to develop a heterogeneous multi-layered structure for soft tactile sensors for multiple sensitivities across force sensing ranges [185].

The structure was composed of an array of blocks, where each block consists of stacked unit cells forming layers, as verified in figure 10(c). Here, each unit cell has a design space \mathbf{t} , θ , and \mathbf{h} , for each set of depth \mathbf{D} , height \mathbf{H} , and width \mathbf{W} . Magnetic transduction method was chosen to translate the displacement of the metamaterial into an electrical signal. Due to the multiple design parameters that influence the sensitivity and the force sensing range, the minimization of a cost function resulted in the desired stiffness values of each layer and sensitivity. The parameters obtained in the optimization process resulted in a sensitivity of 0.26 N^{-1} , 0.08 N^{-1} , and 0.03 N^{-1} for each unit cell of the stacked structure.

3.3. Finite element analysis

Finite element analysis (FEA) is one of the most explored tools that facilitates the design of metamaterials through both forward and inverse design methodologies [15, 17–19, 190–193]. Its importance lies in bridging the gap between conceptualizing these structures and realizing their desired properties. While FEA can be used to analyze some traditional materials, it becomes essential for predicting the behavior of mechanical metamaterials [144, 191], especially because of the complex geometries and inner arrangements [194]. FEA allows for testing under various loading conditions, analyzing factors such as stress distribution, deformation, and potential failure points, which is invaluable for optimizing the design of metamaterials [15, 17–19, 144, 190–192, 194]. By iteratively refining the structure based on the FEA results, the desired mechanical properties can be realized, such as negative Poisson's ratio, high strength-to-weight ratios, or tailored stiffness profiles (section 2), without the need for extensive and time-consuming physical prototyping.

To illustrate the use of FEA in the design of metamaterials, finite element simulations were conducted in a kirigami-based strain sensor embedded with an array of wireless microwave resonators to identify the rotation angle of the structure's hinges under axial tension [18], as demonstrated in figure 11(a). The base material used to fabricate the structure was cellulose acetate with a density of 1300 kg m^{-3} , modulus of elasticity 2.4 GPa, and Poisson's ratio of 0.38. The simulations revealed a dominant out-of-plane rotation of the kirigami structure occurring at the hinges, although the metamaterial also experienced in-plane and plastic deformation. Three patterns were simulated (figure AA), showing an out of plane rotation varying from $[\theta \Delta L/L]^{-1} = 3.2\%$ to 3.9% for a deformation of $\Delta L/L < 8\%$.

FEA is also attractive in the process of estimating the mechanical properties of metamaterials. As an example, FEA was utilized to estimate the Poisson's ratio of a hybrid ZPR metamaterial consisting of the superposition of PPR and NPR structures [15]. Figure 11(b) shows the longitudinal deformation contour under 20% transverse tensile strain. The simulations showed some discrepancy in the Poisson's ratio when compared to the experiments, which was attributed to difficulties in accurately controlling the dimensions during fabrication processes and the different material properties.

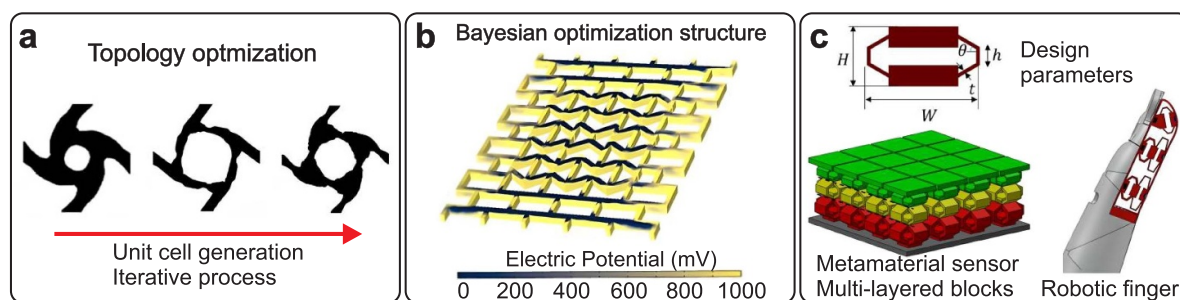


Figure 10. Optimization processes in inverse design methodology: (a) Unit cell generation process through topology optimization [68]. Reproduced from [68]. CC BY 4.0.; (b) Structure obtained through Bayesian optimization [184]. Reprinted with permission from [184]. Copyright (2023) American Chemical Society.; (c) Heterogeneous multi-layered structure for soft tactile sensors developed through FEA. [185]. Reproduced from [185]. CC BY 4.0.

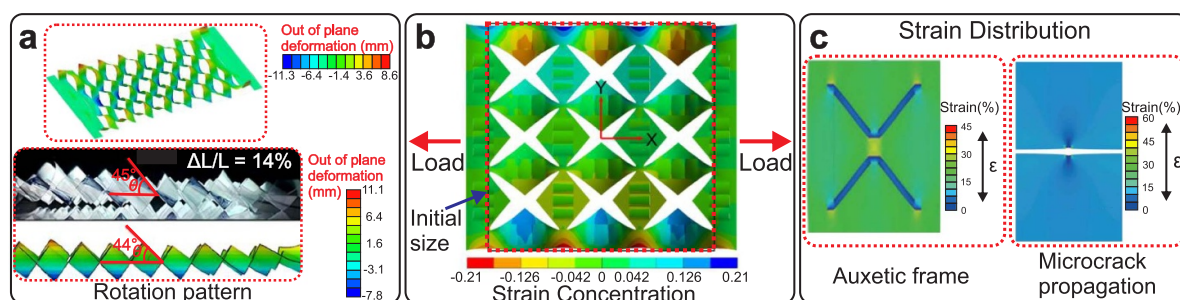


Figure 11. Finite element analysis in the development of metamaterial-based sensors: (a) Simulation of kirigami hinges in a strain sensor [18]. Reprinted with permission from [18]. Copyright (2020) American Chemical Society.; (b) Finite element analysis of a hybrid ZPR metamaterial [15]. Reproduced from [15]. CC BY 4.0.; (c) Simulation of a stretchable strain sensor with a re-entrant structure [17]. [17] John Wiley & Sons. [© 2018 WILEY-VCH Verlag GmbH & Co. KGaA, Weinheim].

Similarly, FEA was also employed in the development of a re-entrant structure in a stretchable strain sensor composed of conductive single-wall carbon nanotube (SWCNT) network on polydimethylsiloxane (PDMS) thin film, with a PDMS auxetic frame [17]. Here, the simulations allowed insights into the auxetic/nonauxetic frames, revealing the regulatory effects of strain redistribution and concentration at a 15% nominal strain and a gauge factor (GF) of ≈ 835 , as verified in figure 11(c).

4. Fabrication technologies and materials

The incorporation of mechanical metamaterials with sensors involves many fabrication technologies. The metamaterials are normally fabricated using additive manufacturing [17, 19, 23, 195–198], traditional molding methods [12, 16, 17, 22], or patterned cutting [15, 18, 60, 115] either for metamaterial-supported or metamaterial-integrated sensors. Several materials can be explored in the fabrication process of the structures, providing mechanical resistance, adequate electrical pathways, and longevity.

The sensitive and functional materials are normally fabricated through microfabrication technologies, including, evaporation [60], sputtering [15, 199], and pulsed laser deposition (PLD) [200], as they allow the creation of small components and thin-film layers, which are very important to realize unobtrusive and imperceptible electronics and sensors [201,

202]. This section will present the materials commonly used in the fabrication of metamaterial-integrated and metamaterial-supported sensors, along with the main fabrication techniques employed in their fabrication.

4.1. Materials

The materials used in the fabrication of metamaterials for sensor applications constitute a critical component of their design and functional capabilities. These materials are typically chosen to enhance and preserve the sensitivity of the sensors and to withstand mechanical deformations [15, 17, 19, 46, 60]. When combined with metamaterial designs, these materials lead to performances that are unattainable with conventional approaches [11, 12, 17, 19]. Functional materials such as conductive polymers, carbon nanotubes, and metallic nanostructures are frequently employed to harness their superior electrical conductivity and mechanical flexibility. Additionally, the integration of these materials within polymeric matrices allows for the exploitation of both the intrinsic properties of the materials and the geometric innovations provided by metamaterial designs (section 3.1).

4.1.1. Metamaterial-integrated sensors. The materials typically used for fabricating metamaterial-integrated sensors can be categorized as either composites, formed through the combination of structures fabricated separately and subsequently

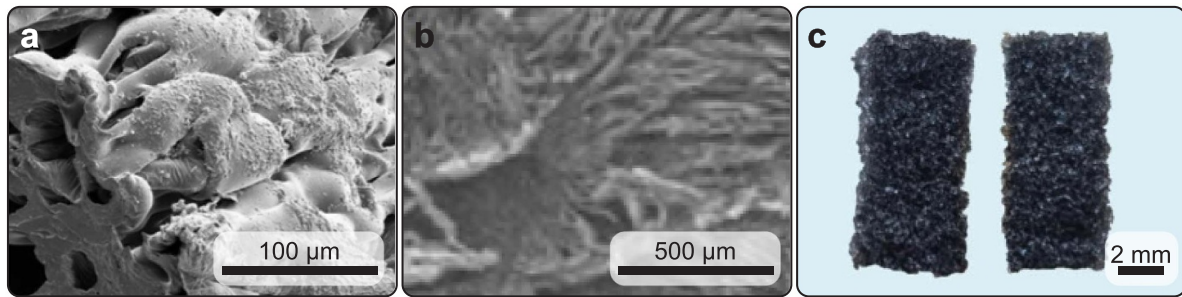


Figure 12. Examples of functional materials integrated in the metamaterial structures. (a) MWCNT integrated in a gyroid-based structure [23]. [23] John Wiley & Sons. [© 2023 Wiley-VCH GmbH].; (b) Mxene mixed in a porous material to make it conductive [11]. Reprinted from [11], Copyright (2022), with permission from Elsevier.; (c) Graphene oxide uniformly absorbed by the structure of the sensor [12]. © [2023] IEEE. Reprinted, with permission, from [12].

joined [17], or as mixtures of different materials aimed at realizing the metamaterial, which constitutes the sensitive part of the sensor. Several conductive materials have been mixed with polymeric materials to realize metamaterial-integrated sensors. These conductive materials include single-walled carbon nanotubes (SWCNT) [11, 17, 23], multi-walled carbon nanotube (MWCNT) [16], titanium carbide (MXene) [11], silver nanowire (SNW) [11, 17, 59], poly(3,4-ethylenedioxythiophene) polystyrene sulfonate (PEDOT:PSS) [11], aluminum (Al) [14], copper *Cu* [54], gold *Au* [13, 60], chromium *Cr* [60], titanium *Ti* [13], graphene oxide [12], and silver microflakes [55].

Carbon nanotubes are mostly employed to facilitate conductive pathways, enhancing the sensitivity and mechanical stability of the sensors [11, 17, 23]. Titanium carbide (MXene) provides high electrical conductivity, enabling the sensors to endure deformations without losing functionality, which is attractive for the detection of physiological signals [11]. Silver nanowires (SNW) can enhance electrical conductivity due to their ability to maintain high electrical conductivity even under repetitive stretch or compression without losing functionality [11]. Unlike SNW, silver microflakes typically exhibit a flat and planar structure that can create a dense, overlapping network when dispersed in a polymeric matrix. This planar orientation tends to form conductive paths more easily across two dimensions [55]. Conductive polymers have also been explored to realize metamaterial-integrated sensors. For example, poly(3,4-ethylenedioxythiophene) polystyrene sulfonate (PEDOT:PSS) offers high electrical conductivity combined with good flexibility and stretchability [11]. Figure 12 show examples of functional materials on parts of the sensors. Figure 12(a) show the deposition of MWCNT on a 3D printed gyroid-based structure. Figure 12(b) shows a Mxene material mixed with the structure of a auxetic-based pressure sensor. Figure 12(c) shows graphene oxide completely absorbed by a foam material that is integrated with an auxetic structure.

These conductive materials are combined with polymeric materials that are shaped to explore mechanical metamaterial properties (section 2) through specific designs (section 3.1). Several polymeric materials are employed, including Polyvinylidene fluoride or polyvinylidene difluoride

(PVDF) [14], Fluorinated Ethylene Propylene [54], vulcanized silicone [59], TPUs [16, 23, 55], PDMS [12], silicone rubber [12], urethane-based rubber [55], shape memory polymers [14], polyvinylpyrrolidone (PVP) [16].

4.1.2. Metamaterial-supported sensors. In the development of metamaterials to support sensors, polymeric materials are often explored due to their flexibility and increased elongation before breakage, high impact resistance, and electrical insulation [201, 203], as well as high tensile strength and chemical resistance [22]. These materials are utilized in fabrication processes including molding [12, 15, 16] and patterned cutting [18, 60] (sections 4.4 and 4.5).

Commonly employed materials include PDMS [15], photopolymer resins suitable for flexible 3D printing [19], and silicone rubber [22]. In the fabrication of structures utilizing sheet-like materials, techniques such as patterned cutting are applied to materials like rubber sheets [60], polyimide (PI) [22], and transparent cellulose acetate sheets [18]. After the fabrication of the structure, the sensors are either fabricated separately [18, 19, 54] — and later embedded in the metamaterial structure — or are fabricated on top of the metamaterial structure [22, 60] by different fabrications process (sections 4.3 and 4.6).

4.2. Additive manufacturing techniques

Additive manufacturing, also known as 3D printing, has become an important tool in the design and fabrication of mechanical metamaterials. Its ability to produce complex shapes with precision provides extensive flexibility in geometric design. Several 3D printing techniques are commonly used for mechanical metamaterials, including fuse deposition modeling (FDM) [204–209], stereolithography (SLA) [34, 210–214], digital light process (DLP) [215–219], masked stereolithography (MSLA) [220–222], direct inking writing (DIW) [223–226], and polyjet [227–229]. 3D printing offers the advantages of rapid prototyping, enabling the creation of complex geometries that would be challenging or unattainable with traditional manufacturing methods [109, 230].

This flexibility facilitates customization, on-demand production [34, 204, 216, 222], rapid prototyping, and iterative design processes [34, 196, 230–233]. However, 3D printing also present some limitations. Print speed can be slow, particularly for high-resolution parts, and material selection may be limited compared to conventional processes. Additionally, printed objects often display anisotropic properties, meaning their mechanical properties might vary depending on the direction of applied stress, a result of the layer-by-layer printing process.

4.2.1. Fused deposition modeling. The Fused Deposition Modeling (FDM) technique is noted for its ability to print mechanically resistant and precise structures [204–206]. However, FDM-printed mechanical metamaterials often suffer from the stair stepping effect [234–236], often resulting in a rough surface finish. This effect is caused by the layer-by-layer deposition of the filament material, which creates visible tracks on the surface [234]. To overcome this issue, various strategies have been explored to improve the surface quality of FDM printed objects, such as post-processing techniques and optimization of printing parameters [237–242]. It has been used to fabricate structures for a variety applications, including devices for mechanical vibrations mitigation [243–246] and auxetic structures [206, 207, 209, 247, 248]. Overall, the use of FDM for mechanical metamaterials offers unique advantages in terms of design flexibility, customization, and rapid prototyping.

For example, the FDM technique was essential in fabricating a pressure sensor exploring a gyroid-based configuration [23] (figure 13(a)). The printed structure was coated with functional to form the sensitive part of the sensor. The fabricated structure exhibited a Young's modulus ranging from 0.32 mPa at 30% relative density to 3.61 mPa at 80% relative density. Additionally, the sensor achieved a high sensitivity of 2.68 mPa⁻¹ and a wide sensing range up to 1.45 mPa.

4.2.2. Stereolithography. Stereolithography (SLA) stands out for its high-resolution capabilities [34, 204]. This technique uses a liquid resin that is cured layer by layer using ultra-violet (UV) light to create solid objects with good detailing [205, 249, 250]. SLA-printed structures normally exhibits smooth surface finishes and high precision, making them suitable for applications requiring fine details and tight tolerances [29, 249, 250]. However, the disadvantages of SLA technology include average resistance to mechanical loads when compared to other 3D printing process [204–206], reduced durability over time, susceptibility to damage from long exposure to the Sun, and the need for troublesome post-processing operations involving potentially hazardous chemicals, and relatively slow printing processes due to low photopolymerization rates during printing [249, 251].

As an example of the use of SLA in the fabrication of metamaterials, ultrasoft bioinspired metamaterials that combined natural fiber-inspired frameworks with graphene-inspired parent structures was engineered [195], as shown in figure 13(b). Here, SLA enabled the precise creation of a layered design, significantly reducing dynamic compressive

strength by 86% and increased energy absorption for applications requiring high-impact resistance and durability. SLA was also important in fabricating 3D and conformal metamaterial structures [196]. The high precision allowed for the creation of 3D orthogonal split-ring resonator (SRR) metamaterials with unit cell sizes of 1.25 mm, ring radii of 500 μm, and split gaps of 300 μm. Figure 13(c) illustrates one of the fabricated structures.

4.2.3. Digital light processing. The DLP technique is similar to the SLA [222]. However, it relies on a continuous liquid interface production. It means that the object is built layer by layer from a liquid resin that is cured using UV light. This method is especially effective in creating complex microstructures, like pneumatic robots [215]. Its cost-effectiveness and high throughput make DLP an attractive option for large-scale applications [216]. The DLP technique's ability to fabricate structures without supporting materials is also attractive [216], offering the advantage of fabricating complex designs faster. The use of DLP for fabricating mechanical metamaterials offers similar advantages to SLA, such as high-resolution capabilities and the ability to create complex geometries with intricate details [216]. However, this technique has increased costs [252], complexity in fabricating large structures, and limited availability of printing materials.

To exemplify the use of DLP in fabricating complex metamaterials, this technique was used in the fabrication of a piezoelectric microphone (figure 13(d)), as it enabled the exploration of a resin mixed with functional materials to create a structure precision and functional customization [197]. Specifically, the printer achieved layer resolutions of 27 μm to integrate a 35 μm finely-tuned acoustic membranes. Moreover, DLP allowed for the embedding of conductive and piezoelectric layers within a single build, facilitating the creation of a complete electro-mechanical system within the structural polymer matrix.

4.2.4. Masked stereolithography. The MSLA technique represents a significant advancement in 3D printing, offering the ability to create graded structures with tunable mechanical properties [222]. MSLA's use of digital masks allows for controlled curing of photopolymers, enabling the fabrication of materials with varying softness [220, 221]. This capability is essential for producing metamaterials with specific mechanical properties and functional gradients. Differently from the SLA and DLP, MSLA does not require dynamic mirrors or a continuous liquid interface, as it works through a stationary mask pattern that selectively cures the resin. In terms of fabrication of mechanical metamaterials, MSLA offers the advantage of greater control over the mechanical properties of the printed structures while maintaining high resolution and fine details.

The MSLA technique was important in the fabrication of a ZPR auxetic structure to house pressure sensors. The layer thickness of 50 μm [19]. Here, the 3D printing technique allowed for the integration of complex geometrical features such as hinges and encapsulation structures critical for

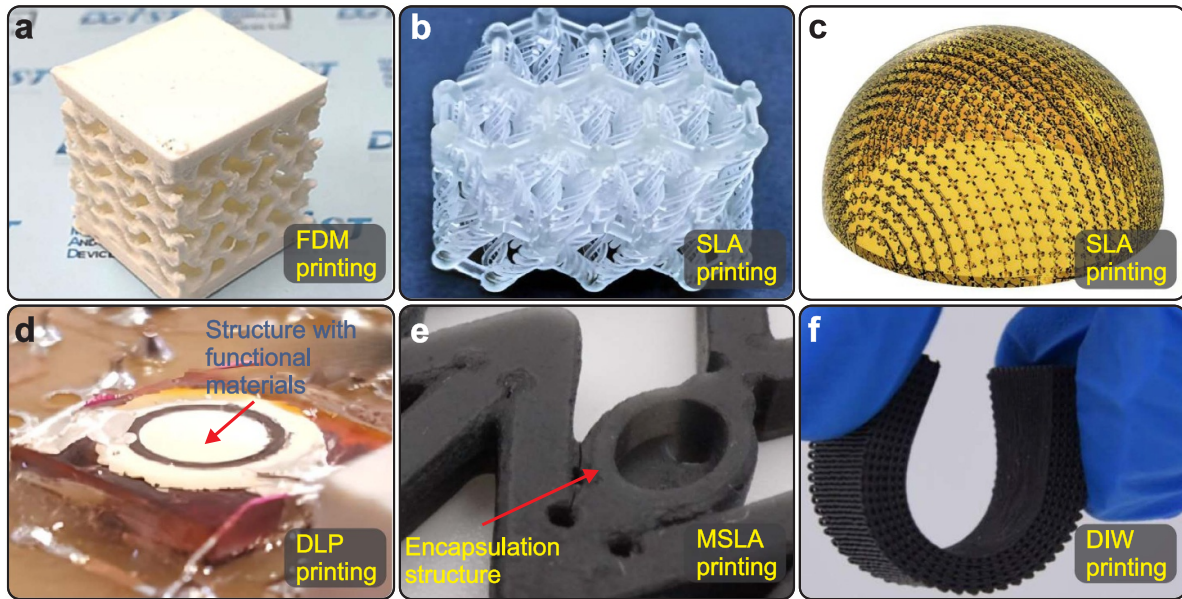


Figure 13. Printing technologies in the development of mechanical metamaterials: (a) A gyroid-based pressure sensor structure showcasing the layering and material functionality typical of FDM processes [23]. [23] John Wiley & Sons. [© 2023 Wiley-VCH GmbH]; (b) Ultrasoft bioinspired metamaterial achieved through SLA [195]. Reprinted from [Gao *et al.*], Copyright (2024), with permission from Elsevier.; (c) Detailed view of 3D orthogonal split-ring resonator metamaterials obtained with SLA [196]. [Zhang *et al.*] John Wiley & Sons. [© 2021 Wiley-VCH GmbH]; (d) DLP printing of a supporting structure of a piezoelectric microphone component [197]. Reproduced from [197]. CC BY 4.0.; (e) Encapsulating part of a ZPR structure printed through MSLA [19]. © [2022] IEEE. Reprinted, with permission, from [19].; (f) DIW printed sample with customized with controlled mechanical properties [198]. Reproduced from [Shi *et al.*]. © IOP Publishing Ltd All rights reserved.

the mechanical flexibility and functionality of the structure, demonstrating the capability of the structure to withstand up to 15% stretch and shear deformations without mechanical failure. This precision and design flexibility were essential for the high performance and durability required in flexible electronics applications. Figure 13(e) shows the encapsulating part that was designed to support and house pressure sensors.

4.2.5. Direct inking writing. DIW is another method for printing multimaterials, particularly metamaterials and soft robots [223]. While DIW has lower resolution when compared to SLA or MSLA, its utility in multimaterial applications is significant, especially in fields requiring a combination of different material properties within a single structure [223]. DIW technique was essential in fabricating the four-layer gradient woodpile metamaterial absorbing structure [198]. The flexibility and conformability of the printed structure were enabled by the printing process. Figure 13(f) shows one of the fabricated samples.

4.2.6. Polyjet printing. Polyjet 3D printing, similar to SLA and DLP, allows for the fabrication of complex geometries with high precision [34, 228, 253, 254]. Its utility in creating customized and unique designs, particularly in the rapid prototyping phase, makes it an important tool in the development of mechanical metamaterials [227–229]. The main advantage of this technique is the ability to print with multiple materials simultaneously, allowing for the creation of mechanically heterogeneous structures with precise control over

material properties [228, 253]. In the fabrication of metamaterials, Polyjet is used to create structures with elaborated internal architectures and variable density, allowing for control over mechanical properties such as stiffness and elasticity [17, 255]. This technique was explored in the fabrication of stretchable strain sensors enhanced by auxetic mechanical metamaterials [17]. This approach utilized a 3D printing-assisted molding method to create molds for PDMS casting, leveraging the fine resolution of PolyJet (16 μm) to precisely control the auxetic structures' fine geometries.

4.3. Transfer techniques

The integration or embedding of sensors on metamaterial structures can be carried out through transfer techniques, in which the electronics and sensors are fabricated in separate steps and then transferred to a final surface. This is important because in some metamaterials, the surface might not be compatible with the fabrication process of the sensors, either because it cannot meet the handling and the fabrication setup requirements, or it is unable to endure the chemical and the temperature conditions during the fabrication of the electronics [256, 257]. As a result, transfer methods have been developed to transfer the electronics from a donor substrate, which can withstand all the fabrication processes to a target substrate.

The transfer methods normally involve bypassing the incompatibilities of the receiver substrate through separated

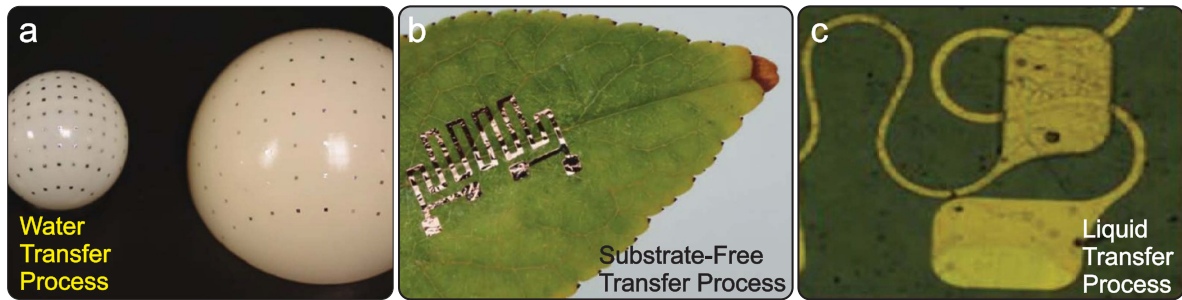


Figure 14. Transfer techniques that can be used to develop metamaterial-based sensors: (a) Water transfer process (WTP) [266]. [266] John Wiley & Sons. [© 2019 WILEY-VCH Verlag GmbH & Co. KGaA, Weinheim].; (b) Substrate-free transfer process (SFT) [257]. Reproduced from [257]. CC BY 4.0.; (c) Liquid transfer process (LTP) [268]. Reproduced from [268]. CC BY 4.0.

fabrication steps using a donor substrate, which is compatible with all the fabrication processes [257]. They enable the exploration of unconventional properties of the target substrates, such as flexibility [258], low cost [259], biocompatibility [260], and biodegradation [261].

Various methods have been developed to transfer the electronics and sensors. For example, the exploration of elastomeric tapes (ET) and stamps have been widely adopted for transferring electronics to planar surfaces [261–265]. For 3D metamaterials with complex large-area surfaces, water transfer printing (WTP) is another technique that has been explored to transfer electronics [266, 267]. Figure 14(a) shows metallic layers transferred to 3D surfaces. When it comes to avoiding damage and deformation in the electronics during the transferring, the liquid transfer printing (LTP) method has shown attractive results with receiver substrates of different materials, patterns, and sizes [268]. Figure 14(b) shows delicate metallic layers transferred to a target substrate. Additionally, a substrate-free technique (SFT) that eliminates intermediate layers between the electronics and the target substrate has also been developed, exhibiting a better conformability of the electronics to uneven receiver substrates, adequate electrical contact, and increased thermal contact conductance between the electronics and the target surface [257]. Figure 14(c) shows the method's versatility with a metallic layer transferred onto a leaf.

4.4. Molding and casting

Molding is a technique typically employed to reproduce complex geometries and structures. It is a simple and common method for preparing mechanical metamaterials [269]. Normally, it involves pouring an uncured material, such as silicone rubber [270], Ecoflex, or PDMS [201, 271] onto a mold, allowing it to cure, and obtaining the desired shape [269]. This technique has been used to fabricate complex structures, such as soft robots [272–274], and mechanical parts, in which elaborated details and surface quality are relevant. Although these characteristics are essential in developing mechanical metamaterials, this technology is not fully explored because of its limitations [275]. For example, it is unsuitable for micro-molding and complex structures with greater levels of customization [275, 276], for which additive

manufacturing technologies can be more suitable (section 4.2). The molding technique can be either used to fabricate the metamaterial-supported [17, 22], or metamaterial-integrated sensors [12, 16, 55].

To illustrate the use of molding in the fabrication of metamaterials-supported sensors, a strain sensor exploring a ZPR structure fabricated with PDMS was designed [15]. Here, the molds were employed to achieve specific geometric patterns that modulated the Poisson's ratio. The fabricated structure had a thickness $200\ \mu\text{m}$, an elastic modulus of $1.62\ \text{mPa}$, and a Poisson's ratio of 0.49 . This approach enabled the fabrication of sensors that could detect independent multiaxial mechanical deformation without interference. Figure 15(a) shows the fabrication process of the structure.

As an example of metamaterials-integrated sensors, an auxetic structure for stretchable strain sensors was developed [17]. The technique facilitated the precise casting of PDMS, shaping auxetic structures with a defined frame thickness of $1\ \text{mm}$ and thin film thickness of $201\ \mu\text{m}$. Figure 15(b) shows the molding process of the auxetic structure. Similarly, the molding technique was employed in the fabrication of an anisotropic cellular foam with a negative Poisson's ratio for high-performance piezoresistive sensors [16]. In this case, through an ambilateral convergent directional freeze casting technique, the process was able to control pore orientation by varying freezing directions and speeds precisely. This method enabled the production of foams with controlled density and porosity levels adjustable by the concentration of the functional material. In another example, the molding technique was important in the fabrication of a flexible pressure sensor utilizing a mixture of elastomeric and functional materials embedded with a NPR structure [12]. By employing a sacrificial sugar template method, sugar cubes embedded with PDMS were molded and subsequently dissolved to create a porous matrix within the silicone rubber, ensuring uniform and controlled porosity.

4.5. Patterned cutting techniques

Cutting techniques are important tools in the fabrication process of metamaterial-based sensors. They allow for the creation of fine details that would be difficult or even impossible to achieve manually. These techniques can rapidly produce

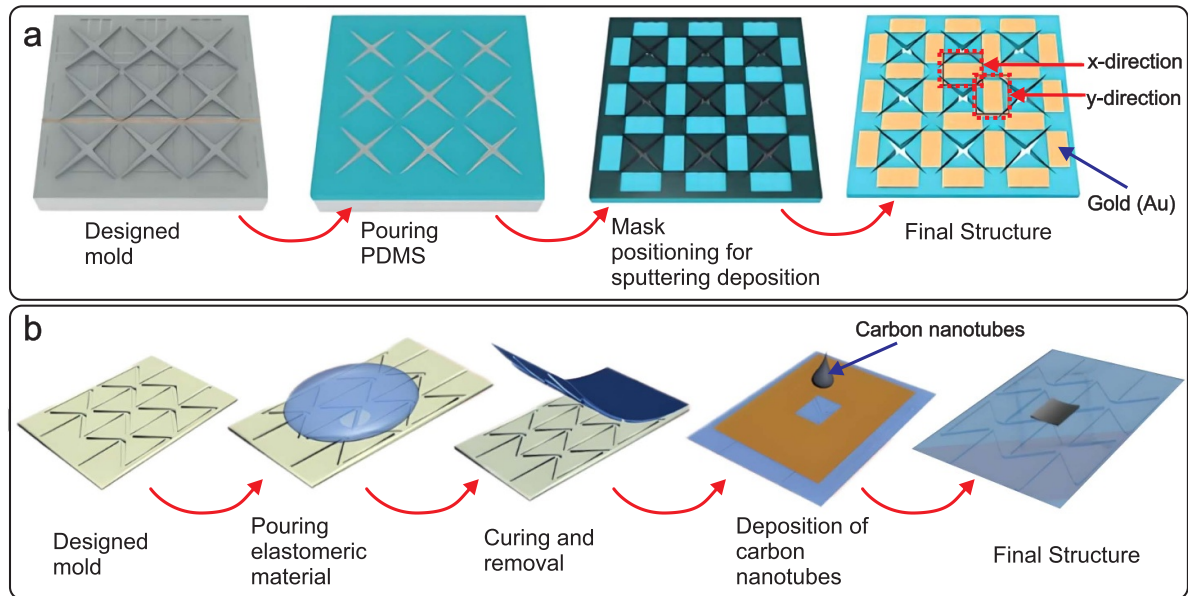


Figure 15. Molding techniques leveraged in the fabrication of metamaterial-based sensors: (a) Fabrication of a metamaterial-supported strain sensor [15]. Reproduced from [15]. CC BY 4.0.; (b) Fabrication of a metamaterial-integrated strain sensor [17]. [17] John Wiley & Sons. [© 2018 WILEY-VCH Verlag GmbH & Co. KGaA, Weinheim].

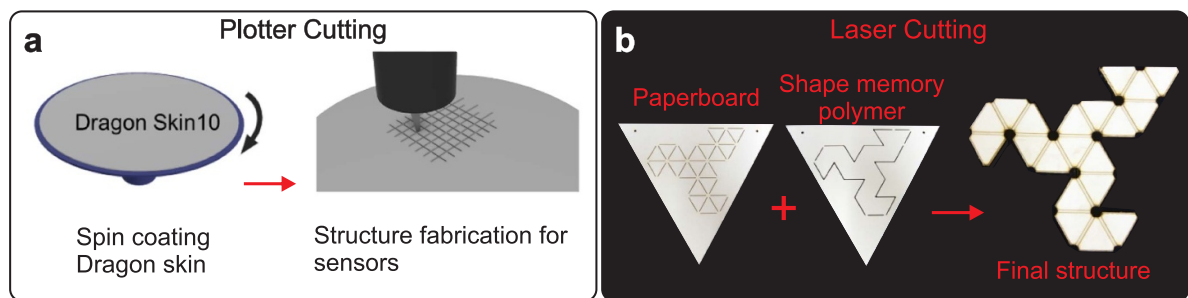


Figure 16. Patterned cutting. (a) Plotter cutting to fabricate an auxetic structure for a stretching sensor [60]. Reprinted from [60], Copyright (2021), with permission from Elsevier. (b) Laser cutting for developing a self-folding structure [115]. Reproduced from [115]. © IOP Publishing Ltd All rights reserved.

multiple identical pieces, which is essential for projects requiring numerous components or consistent reproduction. They enable high customization, as designs can be altered on the fly and quickly tested, which encourages experimentation and iteration during the fabrication process. For flat or sheet-based structures, cutting techniques are often significantly faster than molding or 3D printing, as there's no need for mold creation or layer-by-layer printing. Additionally, cutting techniques can be more cost-effective, especially for smaller batches or when using readily available materials. They also tend to be more accessible and affordable for hobbyists and small-scale makers compared to industrial-grade molding or 3D printing systems. In the fabrication steps of mechanical metamaterials-based sensors, plotter cutting [18, 60] and laser cutting [15, 115] are the most explored tools. Figures 16(a) and (b) show examples of patterned cutting being used to realize sensors.

To exemplify the use of laser cutting tools in the fabrication process of a metamaterial-based sensor, a highly compliant structure inspired by kirigami patterns was developed

[15]. The laser cutting allowed for precise geometric cuts on a 200 μm -thick PDMS substrate, ensuring uniformity and enabling strain concentration in specific parts of the metamaterial structure. Laser cutting was also employed in the fabrication of self-folding structures from shape memory composites [115], as demonstrated in figure 16(b). The precise cut patterns guided the folding behavior by creating predefined gaps ranging from 0.25 mm to 12 mm, directly influencing the fold angles achieved, which were essential for the formation of complex 3D shapes.

The plotter cutting was fundamental in the fabrication of the kirigami-enabled microwave resonator arrays for wireless, flexible, passive strain sensing [18]. The kirigami patterns were fabricated from transparent cellulose acetate sheets with a thickness of 0.127 mm. The cuts enabled the kirigami sheets to undergo large deformations without plastic damage. In another application, this technique was employed to fabricate an auxetic pattern on a Dragon Skin film [60], achieving a unit cell size of 4 mm, resulting in a structure that could

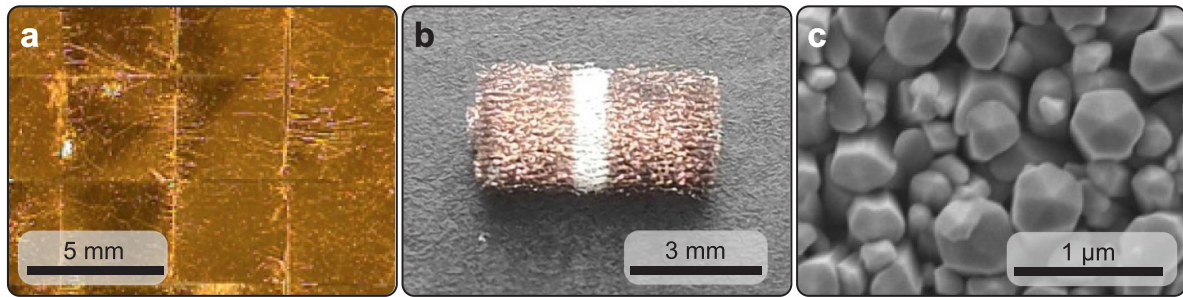


Figure 17. Physical vapor deposition. (a) Evaporation of gold on top of an auxetic structure [60]. Reprinted from [60], Copyright (2021), with permission from Elsevier.; (b) Copper deposited on a porous structure through sputtering [283]. © [2023] IEEE. Reprinted, with permission, from [de Souza Oliveira *et al.*]; (c) ZnO grown by PLD at 600°—100 Pa [200].

undergo bending-dominated deformations with minimal stiffness. Figure 16(a) shows an illustration of the plotter cutting after fabrication of the substrate.

4.6. Physical vapor deposition

Physical vapor deposition (PVD) is a technique that can be used to fabricate thin-films and coatings on different substrates. It allows for the deposition of a variety of materials, including metals, ceramics, glass, and polymers [277–279]. PVD is characterized by a process in which the material transitions from a condensed phase to a vapor phase, by energetic means, with a subsequent deposition of the atoms onto the target substrate, resulting in a physical coating on the substrate [277, 278, 280, 281]. Various deposition methods have been used to develop electronics and sensors, such as thermal evaporation (TE), electron-beam (E-beam) evaporation, physical sputtering, and PLD [277, 279, 282].

4.6.1. Evaporation. In evaporation processes, the material to be deposited, referred to as the source material, is heated beyond its melting point within a vacuum chamber, using a specific heating source. Due to the reduced pressure in the chamber, the evaporated atoms travel in straight lines without collisions and subsequently condense on the substrate [279, 280]. The primary techniques of evaporation include TE and electron beam (E-beam) evaporation.

In TE, the source material is placed in a conductive crucible and melted using either inductive heating or a resistive heater. Within the vacuum chamber, the heated crucible allows the material to evaporate and subsequently deposit onto the substrate [280]. In E-beam evaporation, an electron beam is used to melt the material, facilitating the evaporation of particles. A magnetic field then directs the accelerated electrons onto the source material, causing the released particles to deposit onto the substrate through the plasma present in the chamber [280–282].

Evaporation processes result in highly pure thin films; however, controlling the properties of these films is challenging, and their adhesion is often poor. The primary advantage of TE and E-beam techniques is the ability to achieve high deposition rates [281].

For instance, this technique was used in the fabrication of a strain sensor based on mechanical metamaterials, where Cr and Au films were deposited at thicknesses of 10 and 100 nm, respectively [60]. This method enabled the creation of a light-blocking film that exhibited superior uniformity and high reflectance. Figure 17 shows the deposited layer of gold. In the case of an E-beam evaporator, Ti and Au were deposited with thicknesses of 3 and 10 nm, respectively. These layers played an important role in the functionality of a hydrogel metamaterial within their device [13]. The metamaterial was functionalized with antibodies to detect specific biomarkers present on extracellular vesicles [13].

4.6.2. Sputtering. Sputtering operates through the creation of Argon plasma (Ar) via glow discharge. Ar ions are then accelerated towards the target material. Through momentum transfer, atoms from the target are ejected and transported through the plasma to the substrate. Upon reaching the substrate, these atoms condense to form solid films. The target can be powered either by direct current (DC) or radio frequency, adding flexibility to the process. Notably, sputtering allows for a top-down deposition approach, which is not feasible with TE [284–287].

In microelectronics, sputtering is the predominant PVD technique due to its ability to deposit complex alloy compositions and high-temperature, refractory metals such as Tungsten and Molybdenum [285, 288]. This method achieves well-controlled and uniform depositions, even on large deposition areas. The main advantages include its low-temperature processability (often at room temperature), excellent adhesion, smooth film quality, the ability to tailor the properties of the layers by adjusting the power, and the large availability of sputtering tools [285].

To demonstrate the application of sputtering in sensor technology, gold (Au) was sputtered onto PDMS during the fabrication of ZPR flexible sensors [15]. In another example, sputtering was employed to deposit titanium nitride oxide (TiN_xO_y) and silver (Ag) films onto a BK7 glass substrate for the creation of a surface plasmon resonance (SPR) sensing device. In this case, the DC magnetron sputtering technique was utilized. The final structure of the device featured a multilayer composition of $\text{TiN}_x\text{O}_y/\text{Ag}/\text{TiN}_x\text{O}_y/\text{Ag}$ [199].

Figure 17(b) exemplifies the use of the sputtering technique to develop sensors. Copper and IGZO were sputtered on a porous material, realizing a permeable thermistor that was also sensitive to moisture variations.

4.6.3. Pulsed laser deposition. PLD begins with the ablation of the target material using a high-power laser pulse. This pulse vaporizes the material into a plasma plume which is then deposited onto the substrate. This process can occur either in the presence of a background gas or under ultra-high vacuum conditions, offering flexibility in the deposition environment [289, 290].

The properties of thin films produced by PLD can be optimized by adjusting various parameters, such as laser wavelength, the distance between target and substrate, and the pressure within the deposition environment [289]. A key advantage of this technique is its ability to deposit complex compositions, including multi-elemental materials, with controlled stoichiometry [289]. PLD can be utilized to deposit a diverse range of materials, such as high-temperature superconductors, semiconductors, oxides, nitrides, diamond-like carbons, polymers, and more [291]. However, the technique's main drawback is its difficulty in covering large areas, making it less suitable for producing large-sized samples [291].

PLD was used to deposit ZnO films in the fabrication of optical gas sensing platforms [200]. The films were deposited on Si substrates by either KrF (248 nm) or ArF (193 nm) laser ablation. Smooth and rough films, as well as nanostructures, were obtained, by changing the substrate temperature in the range of 500 °C–700 °C and the oxygen pressure in the range of 1 Pa–100 Pa [200]. Indeed, they studied how the morphology of the thin films (ZnO nanostructures) affected the sensing properties for the detection of NO₂ [200]. Figure 17(c) show one of the morphologies obtained through the technique.

PLD was used to deposit MoO₃ thin-films (0.5 mm) [292]. The deposition was carried out using different parameters, such as temperature ranging from 300° to 400° and substrate to target distance in a range of 3 cm–4 cm. These thin films were then exploited for gas sensing applications, exhibiting good sensitivity towards ammonia [292].

5. Incorporation of metamaterials in the design of sensors

As discussed in previous sections, sensors that incorporate metamaterials can be categorized based on the role of the metamaterial. When metamaterials provide structural benefits, the sensors are termed metamaterial-supported. Alternatively, when metamaterials form the core sensing element, the sensors are described as metamaterial-integrated. This incorporation enables the realization of diverse sensor types, such as temperature [20, 21], strain [15, 17, 18, 59, 60], and pressure [11, 12, 14, 19, 16, 22, 23, 54] exploring common sensing principles, including resistance [11, 17, 19], capacitance [22], and piezoelectricity [14, 54], alongside less common, such as resonant frequency [21] and microwave variation [18]. The realization of these sensors normally involves several steps, utilizing

different fabrication processes (section 4). Table 2 summarizes a selection of sensors developed using various metamaterial characteristics, categorized by their sensing principle, fabrication techniques employed, and their performance. This section will show the development of the main types of sensors found in the literature and discuss some of the main issues related to the integration of metamaterials and sensors.

5.1. Requirements for integration with sensors

Effective integration of mechanical metamaterials with sensors requires careful consideration of several key factors. These aspects include addressing the mismatch of mechanical properties, ensuring fabrication process compatibility, precise sensor positioning, establishing robust electrical connections and wiring, and considering stability and lifetime expectations. Neglecting these factors may result in sensors with unreliable mechanical and electrical behavior and a shortened operational lifespan.

5.1.1. Mismatch of mechanical properties. In the design of metamaterial-supported or metamaterial-integrated sensors, careful attention to material compatibility is necessary [90]. This is important because these sensors are often fabricated by exploring polymeric materials through 3D printing and molding techniques. A significant challenge lies in integrating functional materials with these polymers due to potential adhesion issues arising from mismatched mechanical properties, which can compromise the integrity and functionality of the sensors [19, 293].

Polymeric materials typically exhibit mechanical properties that differ significantly from those of functional materials (section 4.1), such as conductive and semiconductive materials [201]. When functional materials are combined with polymeric substrates using processes such as PVD (section 4.6), there is a considerable potential for a mismatch in mechanical properties. This difference means that under mechanical stress, the metamaterials may undergo deformations exceeding the tolerable limits of the functional materials. Such excessive deformation can lead to cracking and eventual mechanical failure of the functional materials.

The approaches to reducing the mismatch include fabricating functional materials with mechanical properties close to the one exhibited by the polymeric materials [16, 55, 294]; exploring stiff islands designs [58, 295–299], where the functional materials are protected from excessive strain; and designing the metamaterials to keep the tension and strain on the functional materials at levels lower than the mechanical failure levels [297].

To illustrate the fabrication of functional materials whose mechanical properties align closely with those of polymeric metamaterials, a composite ink was developed [55]. It consists of a mixture of 35% silver microflakes and 65% TPU by volume. The resulting mixture forms a flexible conductive material that was deposited into pre-defined channels of a urethane-based rubber metamaterial. This configuration enabled the material to undergo significant

Table 2. Summary of Metamaterial-Based Sensor Applications, Characteristics, and Performance Metrics.

Application	Type of Incorporation	Metamaterial Characteristic	Type of Sensor	Sensing Principle	Main Fabrication Technology	Performance	Reference
Protect pressure sensor	Metamaterial Supported	ZPR, Semi re-entrant structures	Pressure	Piezoresistive	Masked Stereolithography (MSLA)	$\nu = 0.061$, Shear def. of 15%, Strech def. of 15%	[19]
Monitoring deformation	Metamaterial Integrated	Re-entrant unit cells	Strain	Piezoresistive	Molding	$\nu = 0.0061$, gauge factor of $(GF) \approx 835$	[17]
Monitoring health status	Metamaterial Integrated	Re-entrant unit cells	Pressure	Piezoresistive	Molding and directional freeze-drying	Max. com. strain of -80%, Min. $\nu = -0.48$, Sensitivity of 990.4 kPa^{-1}	[11]
Protect flexible electronics	Metamaterial Supported	NPR, Rotating polygonal unit cells, Kirigami	Pressure	Capacitive	Patterned cutting	Out of plane sens. of 4.86 N^{-1} in-plane loading sens. of 0.1 N^{-1}	[22]
Temperature and density Monitoring	Metamaterial Integrated	Chiral unit cells	Temperature	Resonant frequency	Simulations	Sens. of 100 Hz m^{-3}	[21]
Monitoring walking/ running	Metamaterial Integrated	Origami	Pressure	Piezoelectric	Fused Deposition Modeling (FDM)	Sens. of 4.68 V N^{-1} , max. power density of 77 nW cm^{-2}	[14]
Monitoring vehicle speed	Metamaterial Supported	Origami	Pressure	Piezoelectric	3D printing, bonding, folding	Max. power density of $0.96 \mu\text{W cm}^{-2}$	[54]
Tempetature and Moisture monitoring	Metamaterial Integrated	NTE	Temperature	—	Only designed, but not tested	—	[20]
Structural health monitoring	Metamaterial Integrated	Kirigami	Strain	Microwaves	Patterned cutting, assembling	Gauge factor of $GF = 15.51$	[18]
Monitoring soft actuator	Metamaterial Integrated	Missing ribs	Strain	Capacitive	3D printing	Conductivity of 102 S cm^{-1} , capacitance variation of 66%	[59]
Robotic tactile monitoring	Metamaterial Supported	NR, PPR, ZPR	Strain	Piezoresistive	Molding, Sputtering	$\nu = 0.07$	[15]
Monitoring light transmittance	Metamaterial Integrated	Rotating polygonal unit cells	Strain	Optical	Patterned cutting, thermal evaporation	Gauge factor of $GF \approx 10.5$	[60]
Health monitoring	Metamaterial Integrated	NPR	Pressure	Piezoresistive	Molding, freezing	$\nu = -4.2\%$, sensitivity of -5.4 kPa^{-1}	[16]
Wearable device	Metamaterial Integrated	NPR, Re-entrant unit cells	Pressure	Piezoresistive	Molding, assembling	$\nu = 0.18$, sensitivity of 7.08 kPa^{-1}	[12]
Monitoring force	Metamaterial Integrated	NPR	Pressure	Piezoresistive	Fused Deposition Modelling (FDM), Vacuum infiltration	Sensitivity of 2.68 Mpa^{-1}	[23]
Monitoring deformation	Metamaterial Integrated	Rotating polygonal unit cells	Strain	Electrical contact closing	Molding, Ink application	Logic gates (AND, NAND, OR, XOR, and XNOR)	[55]

deformation without failure, as demonstrated in figure 18(a). In another example, capacitive-based deformation sensors were developed using 3D printed functional materials integrated into a similarly 3D printed structure [294]. Here, a copper-based conductive filament was printed alongside a non-conductive TPU, both materials exhibiting comparable elasticity. This design approach minimized the likelihood of breakage at the intersection of these two materials after

repeated use. Figure 18(b) illustrates the developed structure featuring the two conductive materials.

The exploration of stiff island designs is attractive for providing localized areas of rigidity within the flexible matrix. Electronics, such as thin-film transistors or sensors, can be assembled on these islands, ensuring that the mechanical stress experienced by these devices is minimized during bending, stretching, or twisting [19, 58]. To exemplify it, mesa-shaped

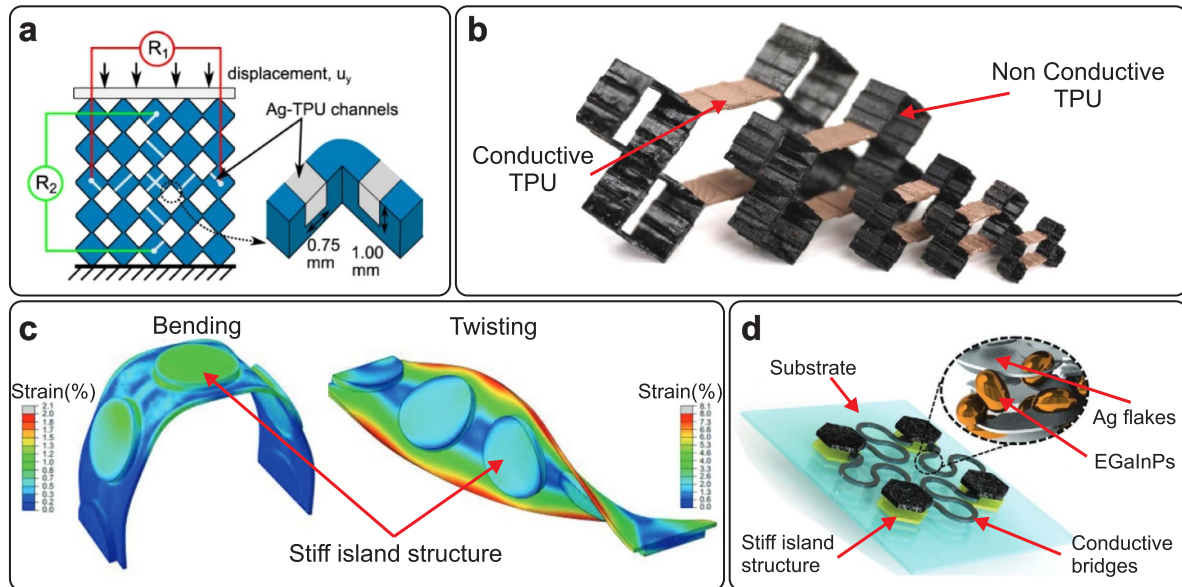


Figure 18. Solutions for mismatch of mechanical properties: (a) Use of composite ink with Ag microflakes mixed with TPU [55]. Reproduced from [55]. CC BY 4.0.; (b) Combination of conductive TPU with nonconductive TPU [294]. Reproduced with permission from [294]. [Copyright © 2021 ACM.]; (c) Stiff-island based PDMS substrate for TFT [58]. [58] John Wiley & Sons. [© 2018 WILEY-VCH Verlag GmbH & Co. KGaA, Weinheim]; (d) Stiff-island structure for electrochemical sensors [296]. [296] John Wiley & Sons. [© 2020 WILEY-VCH Verlag GmbH & Co. KGaA, Weinheim].

elastomeric substrates were developed using PDMS [58]. Amorphous indium-gallium-zinc-oxide InGaZnO thin-film transistors TFTs were directly fabricated on these stiff islands. The TFTs showed stable electrical performance even when subjected to bending to a radius of 6 mm, stretching up to 20%, and twisting to 180°, as demonstrated in figure 18(c). The stiff island design was also explored in the fabrication of a structure that could conform to the dynamic, non-flat surfaces of the human body without losing functionality [296]. The structure had electrochemical sensors fabricated on it and endured extreme mechanical deformations up to 250%, with a minimal influence on the performance of the sensors figure 18(d). Although not metamaterial-based, the design and application show good potential for metamaterial-supported applications.

When stiff island designs cannot be explored to protect the functional materials, the structure of the polymeric material can be engineered to ensure that its maximum strain does not exceed the maximum tolerable strain of the functional materials. For example, a metamaterial substrate exploring the rotation polygonal units was designed and analyzed through FEA to ensure that the areas experiencing maximum strain could withstand the deformation without causing breaks or delamination in the deposited gold Au layer [60]. Similarly, by employing an auxetic pattern and utilizing materials such as Dragon Skin silicone, the structure facilitated deformation up to 50%, effectively distributing strain and reducing the risk of mechanical failure in the gold layer. This approach was also explored in a ZPR structure [15], providing a distribution of the mechanical stress more evenly across the functional material—gold layers deposited to be stretched in two different orientations—allowing for a material strain up to of 20%.

This design minimized stress concentration, thereby reducing the risk of mechanical failure under strain.

5.1.2. Fabrication process compatibility. In the development of sensors involving 3D printed or even molded structures, compatibility issues between the fabrication steps and the employed materials often arise. This issue is more evident in functional materials being deposited through PVD techniques (section 4.6). For example, the sputter deposition on polymeric FDM 3D printed structures (section 4.2) resulted in the delamination of the object's printed layers [300]. This problem arised due to the low pressures—around 1.5×10^{-2} mbar—used during the PVD deposition process (section 4.6). It means that layer-by-layer printed structures tend to release air bubbles trapped within in fabrication processes that require low pressures, common in PVD processes, which not only degrades the mechanical properties of the structure but also leads to defects in the functional deposited material, resulting in non-uniform layer deposition. One alternative is to separate the fabrication of the sensors and later transfer them through, for example, transferring techniques (section 4.3).

5.1.3. Sensor positioning. Precision in the positioning of sensor components is essential for the successful incorporation of metamaterials into sensor design. The functionality of these sensors is dependent on how their components interact. For example, in thermistor sensors, performance is based on the precise patterning and connection of a semi-conductive functional material to conductive materials [283]. Any inaccuracies in the positioning of these materials can

significantly impair performance, leading to suboptimal outcomes or complete sensor failure. In incorporating metamaterials into sensor design, several strategies for positioning functional materials can be explored, including depositing [15, 17, 56, 60], patterning [201, 283, 301–303], and transferring [257, 261–268].

The importance of positioning sensor elements can be highlighted through split ring resonators (SRRs) carefully arranged on a kirigami substrate to maximize their effectiveness in sensing strain [18]. The SRRs were mounted on the hinges of the kirigami patterns. These hinges are the parts of the kirigami structure that undergo significant mechanical deformation (rotation and bending) when the material is strained. Positioning the resonators on these hinges allows the sensor to more effectively detect changes in strain, as these areas experience the most significant mechanical movement. Failing to position the SRRs accurately could result in a poor performance, as the resonators needed to be aligned such that the microwave fields interacted optimally with the resonators to detect the changes in the electromagnetic properties caused by the deformation. Bad positioning can also result in a premature mechanical failure of the sensor. For example, in a metamaterial-supported sensor fabricated exploring gold layers deposited on a ZPR-designed PDMS substrate [15], the inaccurate position in the deposition process may not align the functional layers with the strain concentration areas, leading to inefficient sensing and potential breakage under stress.

5.1.4. Electrical connections and wiring. The efficacy of metamaterial-based sensors depends on the quality of the contact interfaces between the electrical connections and the sensing elements. Dependable contacts ensure optimal signal transfer and enhance the sensitivity, ensuring minimal resistance at the junction and reliability of the sensor [15]. Poor contacts can result in signal attenuation, noise, and even electrical failure. Thus, maintaining robust and effective contacts is essential for the long-term stability and functionality of metamaterial-based sensors.

In metamaterial-supported sensors, the electrical contacts are only supported by the metamaterial structure and are directly connected to the sensors [15, 19, 54], while in metamaterial-integrated sensors, the electrical connections are directly in contact with the functional materials [12, 23, 55, 56, 198, 296]. The connection can be made through several materials, such as copper Cu wires [15, 17, 19, 54, 55, 195, 203], aluminum Al foil [14, 16], copper Cu tape [12, 59, 304], silver coated sheets [11, 56], conductive epoxy [296], silver Ag-based paste [19, 197], and conductive epoxy [115].

Moreover, the connection for sensor data acquisition can be performed wirelessly [18]. For example, the data acquisition from the kirigami-enabled microwave resonator arrays was carried out using a vector network analyzer (VNA), which measured the reflection coefficient S11 to gauge the sensor's response to strain. The VNA was configured with an IF bandwidth of 1 kHz, an output power of 0 dBm, and it scanned a frequency range from 2.2 GHz to 2.9 GHz. A standard horn antenna transmitted and received microwave signals,

enabling non-contact measurement of the sensor's electromagnetic response as the kirigami structure was mechanically strained.

5.1.5. Stability and lifetime. In sensor development, a fundamental aspect is ensuring that the device maintains its core functionality over its designed lifetime with no significant variation in behavior. This requires cycling tests and design optimization to ensure longevity and stability under operational stresses. Such performance parameters are particularly important in metamaterial-integrated or metamaterial-supported sensors, where the deformation of the unit-cell structure can significantly impact overall performance.

For metamaterial-supported sensors, the ability to endure repeated mechanical stress while keeping the embedded sensors protected from excessive loads and deformations is fundamental. The cycling tests are normally used to investigate how the signal coming from the sensor will be affected over long-term usage. For example, 10 000 cycles were applied to a piezoelectric origami-based sensor to monitor vehicle speed [54], revealing consistent electrical output over the testing period. Similarly, 1000 cycles were used to analyze a kirigami metamaterial structure used to protect flexible electronics [22], showing minimal performance degradation.

In the case of metamaterial-integrated sensors, the focus is on ensuring the durability of the metamaterial structure, since it is essential to the sensor's performance. The cycling tests can reveal the degradation of the metamaterial structure with repetitive deformations over time, which can influence the performance of the sensor. To illustrate it, a strain sensor exploring re-entrant structures endured 5000 cycles maintaining a consistent behavior, demonstrating durability along with sustained sensitivity [17]. A force sensor maintained approximately 90% of its initial response after 5000, illustrating minimal sensitivity degradation and excellent long-term applicability [23]. Additional examples highlight sensors that demonstrated minimal degradation in their sensing capabilities across numerous cycles, ensuring their functional integrity and mechanical properties are preserved for applications requiring high reliability [11, 14, 16, 18, 60].

5.1.6. Sensor calibration and drift of signals. Calibration and drift of signals can be critical issues in the performance of sensors, particularly those integrating mechanical metamaterials [12, 19, 56, 198, 203]. Calibration ensures accurate and reliable measurements from the outset. However, even well-calibrated sensors can experience signal drift [203], where the sensor's output gradually changes despite constant input conditions. This effect is especially common in sensors with functional materials embedded in a polymeric matrix. As the matrix deforms, such as in stretchable sensors, the conductive particles may shift from their original positions, resulting in altered conductive pathways and different outputs [203].

Carbon-based sensors, using materials like SWCNT [17, 198], MWCNTs [16], carbon black [19], and char [203] exemplify this issue. These sensors rely on the movement and

alignment of carbon particles within a matrix when subjected to mechanical deformation, such as bending, stretching, or compressing. The conductive properties of these particles facilitate their use in resistive or capacitive sensing mechanisms, where their relative positioning and contact networks change in response to external forces. However, these interactions are inherently unstable over extended periods or repeated cycles, leading to drift in the sensor's baseline signal. The GF, which quantifies the change in electrical resistance relative to mechanical strain, is a critical parameter in this context. A high GF indicates high sensitivity to strain but also underscores the susceptibility to signal drift due to the dynamic reconfiguration of conductive pathways.

6. Applications

The integration of metamaterials into sensor design has led to a variety of innovative sensing devices with enhanced capabilities by exploring the unique properties and attributes of metamaterials, such as negative Poisson's ratio, NTE, high strength-to-weight ratio, and programmability (sections 2 and 3). This section presents many examples of sensors, exploring how the materials, fabrication technologies, and design strategies presented in the previous sections were utilized to realize the sensors.

6.1. Pressure sensors

Metamaterial-supported and integrated pressure sensors can be fabricated by leveraging various aspects of mechanical metamaterials. Particularly, because pressure sensors are normally subjected to mechanical deformation, properties such as NPR, ZPR, and low relative density are highly beneficial. These properties can enhance the sensing components by inducing higher deformations and facilitating the formation of larger electrical pathways [11, 16, 23], or they can protect the sensors from localized excessive stress [19, 22].

To leverage the unconventional transversal expansion of NPR materials when they are subjected to longitudinal compression, anisotropic cellular foams with obliquely embedded hyperbolic microporous structures were explored to realize a metamaterial-integrated sensor [16], as shown in figure 19(a). The sensor was used for monitoring pressure distribution and athlete's gait. Here, the NPR structure explored an irregular structure instead of a well-defined pattern (section 3) through freeze casting a mixture of carbon nanotubes, polyvinylpyrrolidone, and TPUs with a controlled cooling rate of $-1\text{ }^{\circ}\text{C min}^{-1}$ from 0° to -80° . Figure 19(a) also shows the conceptual deformation of the structure, enabling more conductive pathways and decreasing the overall resistance of the foam. The configuration resulted in a Poisson's ratio of -4.2% at a longitudinal strain of 25% . The sensor showed a sensitivity of -5.4 kPa^{-1} under lower stresses and shifted to a sensitivity of -0.0054 kPa^{-1} when subjected to higher pressures.

A kirigami metamaterial-supported pressure sensor was developed, drawing inspiration from the rotating polygonal

units and snakeskin behavior [22]. This structure utilized a $100\text{ }\mu\text{m}$ -thick polyimide, which was enhanced in flexibility and bendability through cutting patterns, allowing it to conform to complex and curved surfaces as depicted in figures 19(b)–(c). The design incorporated rigid islands linked by silicone rubber hinges mixed with Ag microflakes, which helped to limit localized buckling, enhance conformability, and create electrical pathways. Flexible pressure sensors, based on a cavity structural design, were integrated into these hinges. These sensors were allocated along the longitudinal length of a tube-like structure, making it sensitive to both internal and external pressure variations, as illustrated in figure 19(d). The arrangement provided the structure with an out-of-plane loading sensitivity of 4.86 N^{-1} and an in-plane loading sensitivity of 0.1 N^{-1} . Additionally, the soft hinges facilitated the deployment of electrical interconnects which is advantageous for sensors and electronics mounted on the rigid islands, with the entire structure capable of stretching up to 25.9% without exceeding the critical yield strain.

To exemplify the use of relative density as a central parameter in the design of a metamaterial-integrated pressure sensor, a 3D-printed gyroid-structured pressure sensor was fabricated [23]. Figure 19(e) shows the conceptual image of the designed structure printed through FDM using a TPU filament and coated with carbon nanotubes. The sensor's mechanical and electrical properties, such as Young's modulus, sensing range, and sensitivity, can be tailored by varying the relative density of the gyroid structure. The sensor achieved a wide sensing range of up to 1.45 mPa and a sensitivity of 2.68 Mpa^{-1} . Regarding its lifetime span, it showed a stable and consistent response after 1000 cycles of loading with a relative density of 50% under a normal pressure of 200 kPa .

In another example, triboelectric materials were integrated with origami-enabled tubular metamaterials to realize a structure that senses the speed of vehicles when they pass over a bump [54]. This device utilizes an origami structure to facilitate multistable force-displacement behavior, serving as a stimulus for the triboelectric material. This arrangement allowed for the tuning of speed and weight-sensing capabilities. Optimal results were obtained with an octagonal-based origami configuration, where the open-circuit voltage, short-circuit current, and transferred charge reached 206.4 V , $4.66\text{ }\mu\text{A}$, and $0.38\text{ }\mu\text{C}$, respectively. Moreover, the maximum instantaneous power density obtained was $0.96\text{ }\mu\text{W cm}^{-2}$, achieved with a load resistance of $20\text{ M}\Omega$.

6.2. Biosensors

Biosensors for the precise measurement of human movements and physiological signals can greatly benefit from mechanical metamaterials [125]. By leveraging an auxetic configuration in the core sensing parts, a metamaterial-integrated approach can enhance the precision of sensors in measuring body movements and accurately monitoring pressure signals associated with various intra-body changes such as intra-ocular, intracranial, and internal jugular vein pressures [11–13]. Additionally, unit-cell configurations, such as chiral-based metamaterials, enable the development of nanoscale sensors [14]. Further

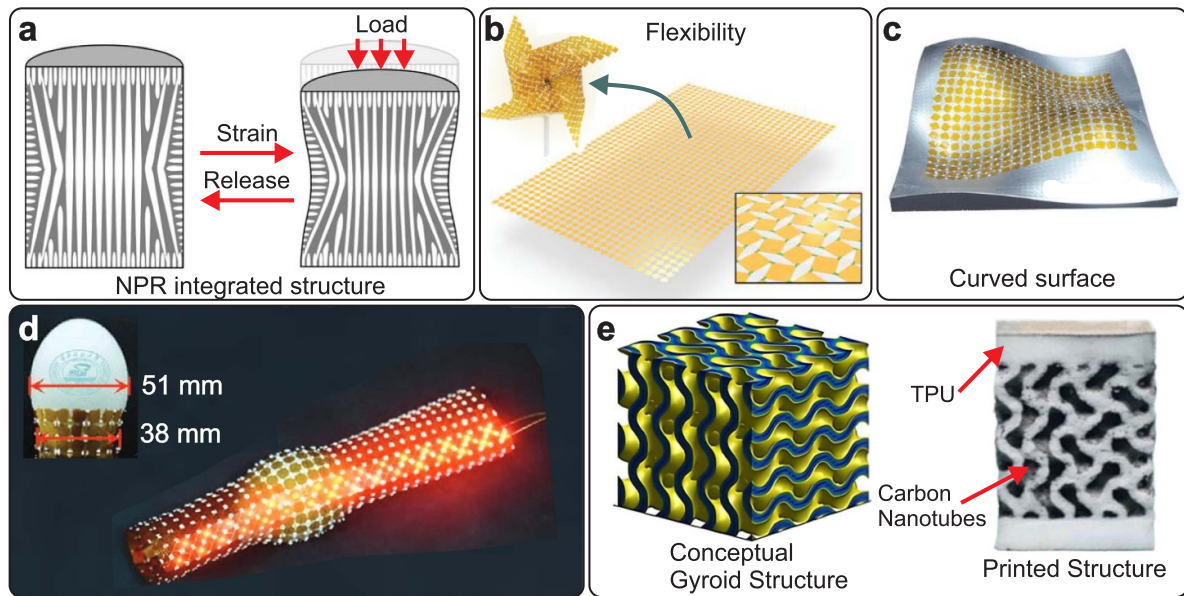


Figure 19. Metamaterial-based pressure sensors. (a) Anisotropic cellular foams with obliquely embedded hyperbolic microporous for pressure sensing [16]. Reprinted from [16], Copyright (2023), with permission from Elsevier.; (b) Flexibility of a kirigami metamaterial-supported pressure sensor [22]. [22] John Wiley & Sons. [© 2022 Wiley-VCH GmbH].; (c) Conformability of a kirigami metamaterial-supported pressure sensor [22]. [22] John Wiley & Sons. [© 2022 Wiley-VCH GmbH].; (d) Kirigami metamaterial-supported pressure sensors mimicking a snake behavior [22]. [22] John Wiley & Sons. [© 2022 Wiley-VCH GmbH].; (e) Gyroid-structured pressure sensor [23]. [23] John Wiley & Sons. [© 2023 Wiley-VCH GmbH].

details on these applications are discussed in the following paragraphs.

The negative Poisson's ratio can be explored with porous structures to realize sensors of human body movements. A re-entrant PDMS elastomer structure with a negative Poisson's ratio was embedded in a graphene-silicon rubber foam composite [12], as shown in figure 20(a). The NPR structure inside the foam helped in the formation of electrical pathways reducing the electrical resistance of the whole sensitive material. The Poisson's ratio of the whole sensitive structure reached 0.18 with a high linear sensitivity of 7.08 kPa^{-1} and 7.08 kPa^{-1} at the range of 0 kPa to 50 kPa and 50 kPa to 250 kPa, respectively.

Similarly, a conductive porous material based on re-entrant structures was investigated for the design of biosensors. A symmetric hyperbolic re-entrant pattern in the lateral parts combined with a rhombus pattern in the central part was developed to show NPR and high contraction in the transverse and longitudinal directions under compression [11], as shown in figure 20(b). The NPR varied with the compression experiments in the range of -0.48 to 0.175 with a maximum compressive strain of -80%. The NPR effect led to increased contact points allowing for the formation of conductive pathways and, consequently, a reduction in the electrical resistance with an improved sensitivity of 990.4 kPa^{-1} under a pressure of 30 Pa.

Chiral-based metamaterials can be explored even in the range of nanometers, as nanoscale molecular profiling structure was developed to leverage the deformation mechanism of chiral metamaterials [13] and profile biomolecules, as shown in figure 20(c). The chiral structure was fabricated using a

hydrogel responsive to temperature and redox activity functionalized with antibodies. When exposed to the antibodies, the metamaterial undergoes rapid re-organization upon the binding of antibodies within the hydrogel, amplifying changes in the mechanical deformation and diffraction patterns of the metamaterial, as verified in figures 20(c) and (d) illustrates the optical detection of the mechanical changes in the structures. The system reflects a significant enhancement in the limit of detection of approximately 1700 exosomes, which represents a 1000-fold over the conventional ELISA techniques [13, 305].

Exploring concepts of 4D printing, a Miura-ori-based origami structure was developed as a platform for triboelectric piezoelectric sensing function for tracking walking/running patterns [14], as verified in figure 20(e). The structure was embedded in a shoe sole showing a sensitivity of 4.68 V N^{-1} . Under various load tests, The maximum power density was 77 nW cm^{-2} under $100 \text{ M}\Omega$. The device was demonstrated to be reliable under 10 000 loading cycles.

6.3. Strain sensor

Most applications exploring mechanical metamaterials are related to strain measurement [15, 17, 18, 56, 59, 60]. Several combinations of properties to realize metamaterial-integrated and metamaterial-supported strain sensors have been developed. For example, combining PPR and NPR structures to protect sensing units [15], exploring re-entrant structures with functional materials to achieve higher sensitivity [60], and leveraging kirigami design with an array of microwave resonators to measure uniaxial deformation [18],

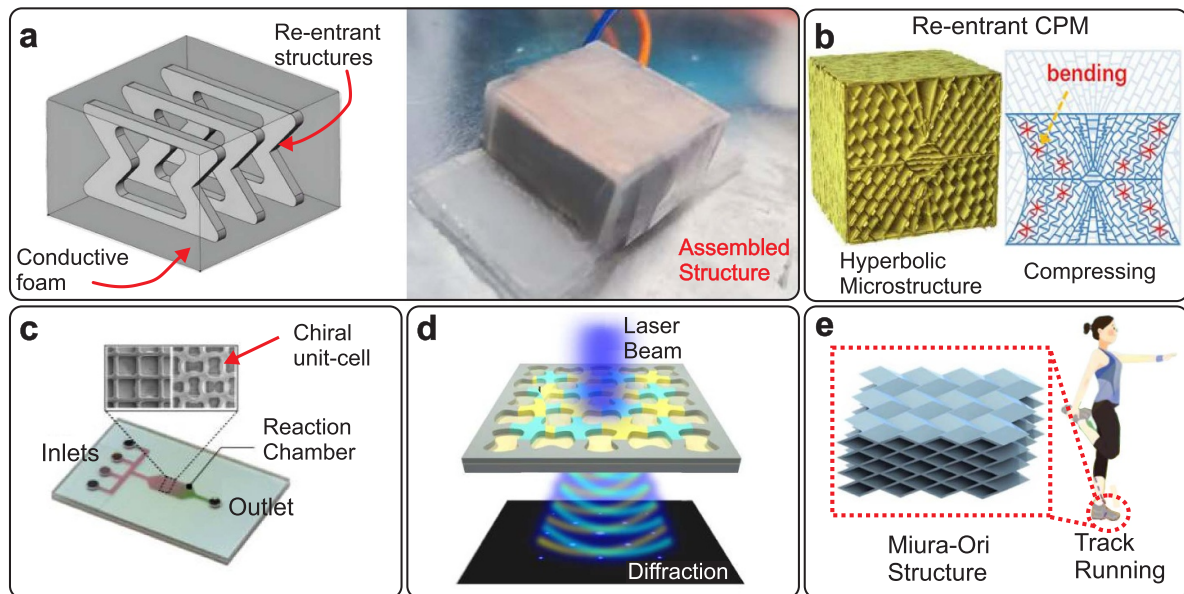


Figure 20. Biosensors. (a) Schematic and final assembly of a metamaterial-integrated human body movement sensor [12]. © [2023] IEEE. Reprinted, with permission, from [12].; (b) Conductive symmetric hyperbolic re-entrant pattern combined with rhombus structure to develop a biosensor [11]. Reprinted from [11], Copyright (2022), with permission from Elsevier.; (c) Chiral-based structure for profiling biomolecules [13]. Reproduced from [13], with permission from Springer Nature.; (d) Optical detection of mechanical change due to the presence of biomolecules [13]. Reproduced from [13], with permission from Springer Nature.; (e) Origami structure for walking/running patterns [14]. Reprinted from [14], Copyright (2023), with permission from Elsevier.

among others. More details on these combinations are discussed in the subsequent paragraphs.

By combining a PPR honeycomb hexagonal-based structure with a concave NPR structure, a hybrid ZPR structure was created exploring the superposition of the two Poisson's ratio [15], as verified schematically in figure 21(a). The structure achieved a Poisson's ratio of $\nu = 0.07$ for a uniaxial tensile strain of 10%. Because of its unique mechanical properties, the ZPR structure can protect the sensing units from deformation along a specific axis when subjected to stimuli from a perpendicular axis. Figure 21(a) also shows the sensors positioned in the x and y directions. This ensures the sensing units can independently detect uniaxial stimuli.

To explore the NPR property beyond application that enhances sensitivity, a self-powered piezo-transmittance-based strain sensor [60] was devised exploring bending-dominated rotation squared unit-cells, as shown in figure 21(b). These unit cells were mainly used because of the ultra-low stiffness they provide, which makes the target object experience a small influence when the metamaterial structure is used as a sensor. The structure could provide a gauge factor $GF \approx 10.5$, a hysteresis of $\sim 0.508\%$, a high linearity of $R^2 > 0.997$ and a long-term stability of more than 10 000 cycles without failure.

The high strength-to-weight ratio property was explored in the design of a multifunctional ceramic/graphene metamaterial [56], as demonstrated in figure 21(c). This structure was realized through a hierarchical honeycomb microstructure assembled with arch-arch-shell-shaped multi-nanolayer cellular walls working as basic unit cells. The structure exhibited a reversible compressibility of 80%, an electrical conductivity

of 1.02 S cm^{-3} , a high fatigue resistance, and a thermal insulation/flame-retardant around $0.05 \text{ W m}^{-1} \text{ K}^{-1}$ performance simultaneously. Although the metamaterial was not specifically designed to be used as a sensor, it demonstrates attractive properties for sensing strain/damage sensors, as it exhibits a synchronously sensitive response of electromechanical coupling performance by a positive piezo-resistance effect [56].

As an example of auxetic structures improving the performance of sensors, a re-entrant structure was employed in the design of a highly sensitive stretchable sensor [17] (figure 21(d)). This sensor comprises a one-unit auxetic metamaterial structure that is composed of SWCNT on top of a re-entrant structured PDMS. The stretching of the auxetic structure causes a specific deformation of the carbon nanotubes, which induces micro-cracks that are elongated by the auxetic meta-materials. The sensor was designed to work with a Poisson's ratio of range 0.41 to 0.19 with a GF around ≈ 835 for 15% of nominal strain.

Kirigami sheets-based mechanical metamaterial made up from a 0.127 mm-thick acetate sheets was combined with an array of wireless microwave resonator sensors to realize a highly sensitive, passive, wireless strain sensor [18]. The microwave sensing system was engineered to track changes in the S_{11} response of the resonators, correlating these alterations directly with the out-of-plane rotation of the Kirigami hinges, as shown in figure 21(e). The GF obtained was $GF = 15.51$ in the deformation range of 0.6%–21.3%.

The missing rib design approach was explored to develop expandable structural electronics through metamaterial structures [59]. Here, a conductive material was developed

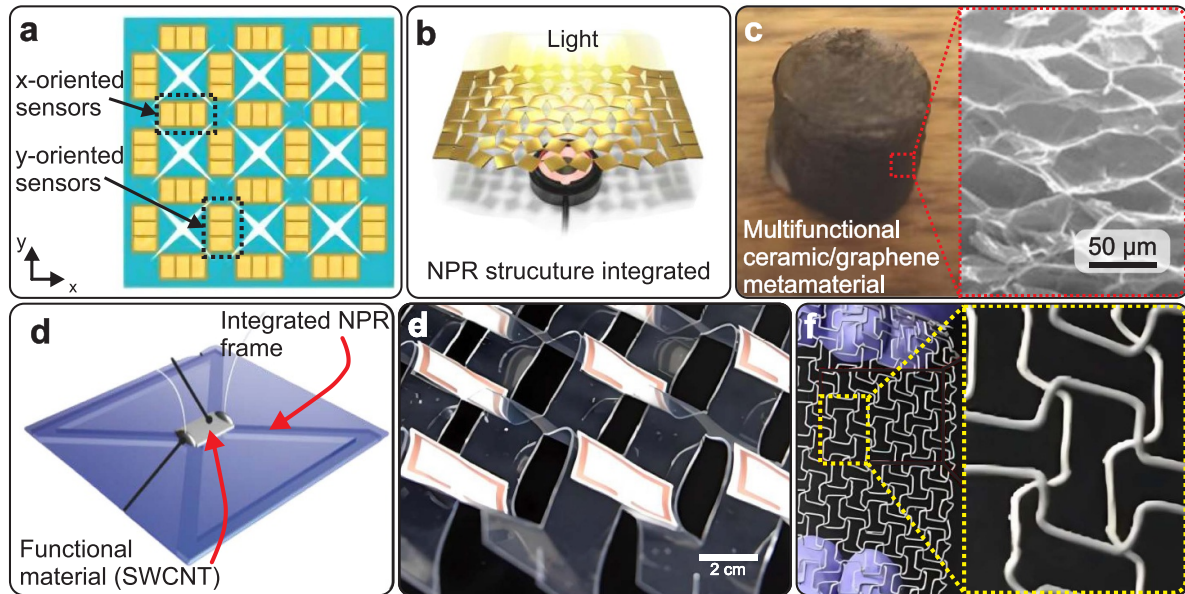


Figure 21. Strain sensors. (a) PPR and NPR structures to form a biaxial strain sensors [15]. Reproduced from [15]. CC BY 4.0.; (b) Sel-powered piezo-transmittance sensor [60]. Reprinted from [60], Copyright (2021), with permission from Elsevier.; (c) Multifunctional graphene-based sensor [56]. [56] John Wiley & Sons. [© 2017 WILEY-VCH Verlag GmbH & Co. KGaA, Weinheim].; (d) Re-entrant-based strain sensor [17]. [17] John Wiley & Sons. [© 2018 WILEY-VCH Verlag GmbH & Co. KGaA, Weinheim].; (e) Kirigami structured strain sensor based on microwave sensing [18]. Reprinted with permission from [18]. Copyright (2020) American Chemical Society.; (f) Expandable capacitive structure based on missing-rib design [59]. Reproduced from [59]. CC BY 4.0.

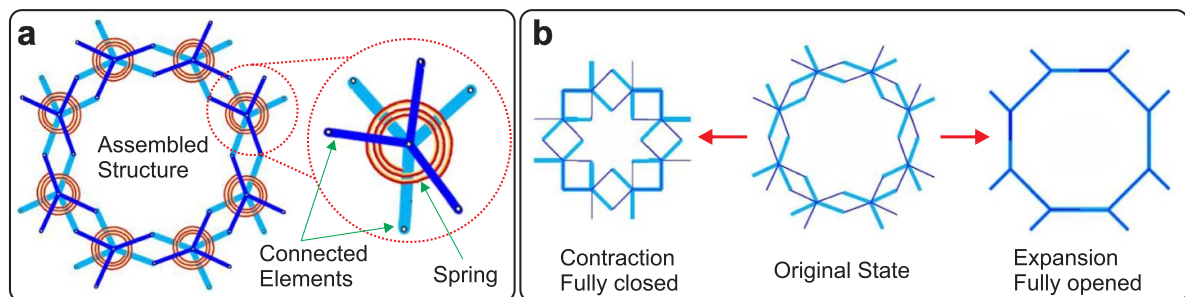


Figure 22. Temperature sensor. (a) Islamic geometric pattern for sensors design [20]. Reproduced from [20]. CC BY 4.0.; (b) Chiral structures to realize temperature sensors [20]. Reproduced from [20]. CC BY 4.0.

and optimized using room-temperature-vulcanizing silicone and RTV mixed with Ag (Ag-RTV). The material was 3D printed in an auxetic pattern to form a capacitive strain sensor (figure 21(f)), showing a variation of 66% decreasing from 6 pF to 2 pF under maximum pressure.

6.4. Temperature sensors

Temperature sensors demonstrate significant potential to benefit from NTE structures, as their behavior can be correlated with temperature changes to form metamaterial-integrated temperature sensors [20]. Additionally, the temperature can be precisely monitored by exploring mechanical metamaterial unit cells to detect changes in the resonance frequency of the sensor due to temperature shifts in the medium [21]. The following examples provide more details.

To investigate a metamaterial structure that can be leveraged as a sensor, a metamaterial inspired by an Islamic

geometrical pattern, capable of demonstrating adjustable positive and negative hygrothermal expansion was theoretically developed [20], as shown in figure 22(a). Here the analysis demonstrated that connecting rotating rods by a pin-joint with springs composed of two materials with different coefficients of thermal expansion can result in metamaterials that will deform with temperature differently when the temperature increases or decreases. Figure 22(b) shows the structure fully closed and fully opened because of temperature differences.

To take advantage of the chiral design for developing sensors and exploring chirality with activity, a chiral syndiotactic unit cell—which was composed of two chiral sub-cells and with inclined rods attached to octagonal plates—was employed as a temperature sensor for water, exploring the Fano resonance [21]. The structure is fabricated with acrylonitrile butadiene styrene (ABS) and can detect changes in the water's properties, such as density and viscosity, it works by measuring the shift in the resonance frequencies of the

material. The sensitivity is quantified by how much the resonance frequency shifts in response to changes in the liquid properties. For density variation of 1%, two resonance peaks were detected. The first peak took place at 1 kHz, with a correspondent sensitivity of 16 Hz m^{-3} , while the second peak was around 3 kHz, exhibiting a higher sensitivity of 100 Hz m^{-3} .

7. Summary and outlook

This review explores how mechanical metamaterials can enhance the performance of various types of sensors. Two main approaches to leveraging mechanical metamaterials in sensor design were identified: metamaterial-supported and metamaterial-integrated sensor designs. In metamaterial-supported, the metamaterial structure works primarily as support or framework for sensors that are otherwise capable of functioning independently [15, 18, 19, 22]. The metamaterial-integrated sensor embodies a design where the functional elements of the sensors are designed using metamaterial structures [11, 12, 14, 16, 17, 21, 23, 54, 55, 59, 60]. These sensors exploit the unique properties of metamaterials to enhance or enable their sensing capabilities. Several aspects of the design and fabrication, along with the materials necessary for the fabrication of the sensors, were discussed with examples.

Through unique properties such as negative and zero Poisson's ratios, negative and zero thermal expansions, and attributes like programmability, the metamaterial structures can deform in specific ways to protect the sensing parts of sensors or enhance their sensitivity [11, 12, 14–19, 21–23, 54, 55, 59, 60]. Additionally, the metamaterials enable increased energy dissipation and mechanical resilience, making them ideal for developing lightweight and robust sensors that can withstand physical deformations [56, 306]. Furthermore, their ability to be engineered at varying scales, from nano to macro [80, 81], allows for integration across a diverse array of applications, ensuring both versatility and functionality in sensor design.

The design of metamaterial-integrated or metamaterial-supported sensors benefits from traditional forward and inverse design methodologies, which encompass a range of concepts from the designer's know-how and knowledge to advanced optimization techniques and FEA simulations [66, 119, 170–174, 177–185, 187]. These approaches are especially utilized in the design of unit cells, such as re-entrant, semi re-entrant [17, 60, 124–126], chiral [31, 141, 143], and rotating polygonal units [135, 136], as well as origami and kirigami designs [14, 18, 22, 114, 148–152]. These techniques and methodologies enable the creation of complex structures that more efficiently utilize the unique properties of metamaterials.

The fabrication of mechanical metamaterials integrated with sensors encompasses various materials and techniques to enhance their functionality and durability. Additive manufacturing emerges as an important method, leveraging 3D

printing technologies such as FDM and SLA to create complex structures tailored to specific applications [23, 29, 34, 195, 196, 204]. Other fabrication technologies, including molding and patterned cutting techniques, enable rapid scaling of production, making it possible to produce many structures and samples [12, 15–17]. These techniques also allow for the creation of structures with fine details that are difficult to achieve manually.

Materials such as PDMS, PVDF, FEP, and various polymeric resins are often employed due to their mechanical properties and adaptability to different manufacturing processes [15, 19, 22, 60]. They provide the flexibility required for mechanical metamaterials and facilitate rapid prototyping and customization. These aspects are important for metamaterial-supported sensors, as they typically need to withstand deformation while protecting the embedded sensors from breakage [15, 19].

The selection of functional materials for fabricating metamaterial-integrated sensors is important for ensuring the performance and durability of these devices. Materials such as SWCNT, MWCNT, MXene, SNW, and conductive polymers like PEDOT:PSS are frequently used, as they provide superior electrical conductivity and mechanical flexibility [11, 16, 17, 23, 59]. These properties are essential for maintaining high sensitivity and stability under mechanical stress. Together, these material choices facilitate the development of sensors that are not only highly functional but also adaptable to various applications.

PVD and transfer techniques are essential fabrication in the fabrication of the sensor's sensitive part [13, 60], addressing specific challenges associated with material compatibility and structural design. PVD, which includes methods like sputtering and evaporation, allows for the precise deposition of thin films of metals and other conductive materials on a variety of substrates. Meanwhile, transfer techniques are employed to circumvent the limitations imposed by incompatible fabrication processes or substrates that cannot endure harsh conditions. These methods facilitate the integration of electronics fabricated on robust donor substrates onto more delicate or flexible metamaterial bases, thus expanding the functional scope and applicability of metamaterial-based sensors in fields requiring advanced mechanical and electronic integration.

The integration of metamaterials with sensors demands careful consideration of multiple factors, such as the compatibility of mechanical properties and fabrication processes [90], precision in sensor positioning [201, 283, 301–303], robustness of electrical connections [15, 17, 19, 54, 55, 195, 203], and stability over the sensor's operational life [11, 14, 16, 18, 60]. Material compatibility issues, particularly the mismatch in mechanical properties between polymers and functional materials, pose significant challenges in the realization of metamaterial-based sensors. Strategies such as the use of composite conductive materials [55], stiff island designs [58, 295–299], and engineering the polymeric structure [15, 19] to mitigate excessive deformation have been effective in addressing these challenges.

7.1. Prospects for design and fabrication

The design and fabrication of mechanical metamaterials are rapidly evolving due to advancements in artificial intelligence (AI) and 3D/4D printing technologies. AI, with its ability to analyze vast datasets and optimize complex systems, offers promising opportunities to design sensors with enhanced performance and adaptability. Simultaneously, 3D and 4D printing techniques enable the creation of complex and dynamic structures, enabling new possibilities for sensor development. This section will briefly cover the promising opportunities for utilizing metamaterials to make sensors even more precise, dependable, and robust through the integration of AI and 3D/4D printing technologies.

7.1.1. Artificial intelligence in the design of mechanical metamaterial sensors. AI refers to the capability of machines and software to perform tasks that typically require human intelligence, such as learning from data, recognizing patterns, making decisions, and adapting to new situations [10, 176, 182, 307, 308]. AI encompasses techniques like machine learning [309–311], and neural networks [216], enabling systems to analyze complex information and provide valuable insights.

AI models are trained on large datasets [10, 307, 311], allowing them to learn patterns and relationships within the data. During training, algorithms adjust their parameters to minimize prediction or classification errors [10, 307, 311]. In the context of designing mechanical metamaterial-based sensors, AI can leverage experimental and simulation data to understand the complex behavior and interactions of metamaterial structures and functional materials. By analyzing extensive datasets, AI can identify optimal design parameters and predict material properties under various conditions, facilitating the development of advanced sensors with enhanced performance and adaptability.

AI can potentially assist in developing mechanical metamaterial-based sensors by simultaneously considering various physical aspects, such as mechanical [311], electrical [312], thermal [313, 314], and electromagnetic properties. These models process complex, multidimensional data to optimize the interplay between these different physical phenomena [315], ensuring optimal sensor performance under diverse conditions. AI can determine the most effective material compositions and structural configurations by simulating interactions among these properties. This comprehensive approach enables the creation of highly sensitive, specific, robust, and adaptable sensors to varying environmental and operational demands.

Integrating AI into the design of metamaterial-supported and metamaterial-integrated sensors has the potential to demonstrate a significant advancement in sensor technology. AI's ability to analyze and optimize across multiple physical domains [315] can accelerate the development process and enhances the overall performance and reliability of the sensors.

7.1.2. 3D and 4D printing. A promising approach in the development of mechanical metamaterial-based sensors is the use of 4D printing [106, 230, 316–320]. This manufacturing technique builds on the capabilities of 3D printing by incorporating time-dependent changes [106, 319]. In 4D printing, objects are designed to change their shape, properties, or functionality in response to external stimuli such as heat, light, moisture, or magnetic fields [230, 316, 317]. This transformation is achieved through smart materials that react to these stimuli, allowing structures to evolve after fabrication.

In the context of mechanical metamaterial-based sensors, 4D printing can offer significant advantages. It enables the creation of dynamic structures that can adapt to environmental changes, enhancing sensor functionality and versatility [106]. For example, sensors can be designed to adjust their sensitivity or mechanical properties in real time, improving performance under varying conditions. Furthermore, 4D printing allows for the production of complex geometries and customized designs that are difficult or impossible to achieve with traditional manufacturing methods [106, 230, 316–318]. This flexibility might boost innovative sensor designs, leading to more efficient and responsive mechanical metamaterial-based sensors.

7.2. Perspectives on applications

The incorporation of metamaterials into sensor design enables numerous possibilities across a variety of fields, including soft robotics, textiles, biomedical applications, and environmental monitoring. This section highlights several potential applications that have been underexplored but hold considerable promise for development and further exploration. Figure 23 offers an overview of the recent advancements in metamaterial-supported and metamaterial-integrated sensors. Sections marked with a cross highlight areas needing further development to achieve maturity, while sections with examples demonstrate solid achievements.

7.2.1. Soft robots. There is great interest in integrating mechanical metamaterials with soft robotic systems [85] to augment the structural and actuation capabilities of soft robots [322, 323] and generate mechanically-preprogrammed (feed-forward) control schemes [97, 324]. However, little focus is directed toward the sensing capabilities, which are still underdeveloped in soft robotics and are paramount to enable feedback control. Similar to biological organisms, soft robots require a high density of sensing elements, potentially covering the entire body to allow proprioception of their deformable structures. In this context, the opportunities presented by metamaterial sensors are immense.

By embedding sensors within metamaterial structures that conform to the robot's flexible and compliant body, consistent sensor performance is maintained even under variable environmental interactions. These metamaterials also provide protective housing for sensors, safeguarding them from mechanical stresses and environmental conditions, which is crucial for

Type of sensor	Temperature	Strain	Pressure	Biosensor
Re-entrant		Exploring SWCNT	Exploring Graphene	Human body movement sensor
Rotating Polygonal Units		Self powered sensors		
Chiral	Exploring Fano frequencies			Profiling biomolecules
Origami			Self detectable speed bump	Walking pattern detection
Kirigami		Microwave sensing	Ultra Stretchable	Ultra Stretchable
Missing Rib		Sensor for soft actuator		

Figure 23. Outlook of the mechanical metamaterials unit-cells being used to realize diverse types of sensors: Auxetic structure with SWCNT integrated [17]; Pressure sensors with graphene oxide integrated [16]; Auxetic structure integrated with a foam-based material [12]; Self-powered strain sensor based on the piezo-transmittance of a mechanical metamaterial [60]; Exploring the low-frequency dual Fano resonances [21]; Profiling biomolecules using mechanical metamaterials [13]; Exploring origami with triboelectric materials to realize a self-detectable speed bump [54]; Leveraging Miura ori origami for detecting walking/running patterns [14]; Exploring out-of-plane rotating structures for strain sensing [18]; Exploring ultra-stretchable kirigami piezo-metamaterials to realize a pressure sensor [155]; Kirigami conductor of nanowire percolation Network for electronic skin applications [321]; Sensor for soft actuators [59]. [17] John Wiley & Sons. [© 2018 WILEY-VCH Verlag GmbH & Co. KGaA, Weinheim]. Reprinted from [16], Copyright (2023), with permission from Elsevier. © [2023] IEEE. Reprinted, with permission, from [12]. Reprinted from [60], Copyright (2021), with permission from Elsevier. Reprinted from [21], Copyright (2024), with permission from Elsevier. Reproduced from [13], with permission from Springer Nature. Reprinted with permission from [54]. Copyright (2023) American Chemical Society. Reprinted from [14], Copyright (2023), with permission from Elsevier. Reprinted with permission from [18]. Copyright (2020) American Chemical Society. Reproduced from [Hong *et al.*]. CC BY 4.0. Reproduced from [321]. CC BY 4.0. Reproduced from [59]. CC BY 4.0.

maintaining sensor integrity and reliability in dynamic robotic applications.

Metamaterial-integrated sensors offer a significant advantage by embodying sensor functionality directly into the programmable compliance of the metamaterials themselves. This approach allows for the precise measurement of mechanical changes within the robot’s structure, essential for real-time feedback control. These integrated sensors capitalize on the inherent properties of the metamaterials, such as multi-stability and variable stiffness, to enhance the robot’s sensory feedback system, thereby improving its interaction with the environment and overall performance in autonomous operations.

7.2.2. Textiles. Metamaterial-supported sensors can be integrated with various textile fabrication techniques—such as knitting [325], twisting [326], ring-spinning [327], wrap-spinning [328], and embroidering [329] — to embed sensors seamlessly within textiles. This integration allows the creation of textiles that are capable of enduring multiple types of

deformation while maintaining sensor functionality and integrity. By leveraging these traditional textile methods alongside advanced metamaterial designs, sensors can be effectively protected and incorporated into fabrics that are subjected to frequent and diverse mechanical stresses.

There is significant potential for incorporating functional materials, such as threads and yarns coated with conductive or semiconductive materials, into textiles. By leveraging specific unit cell designs, these enhanced materials can be integrated into the fabric to develop various types of sensors, including temperature and strain sensors. This approach not only allows for the creation of highly functional and adaptive textiles but also expands the capabilities of traditional fabrics to include sensing and interactive functionalities.

7.2.3. Biomedical devices. Metamaterial-supported sensors are particularly advantageous for applications requiring direct adherence to human body parts [296]. The unique structure of metamaterials facilitates enhanced conformability, allowing the sensor to maintain consistent contact and

functionality when adhered to the dynamic surface of the human body. Additionally, these structures can be designed to protect against deformations caused by bodily movements, ensuring reliable performance under various physiological conditions.

The sensing performance can be significantly enhanced through the metamaterial-integrated design approach. This is especially important for sensors that depend on the mechanical deformation of human body parts to detect biosignals, such as those used in measuring blood pressure. These materials enable the fabrication of sensors that are not only more responsive to subtle deformations but also more robust and reliable under the dynamic conditions of the human body

7.2.4. Environmental monitoring. Environmental sensors frequently operate under extreme conditions, including high humidity, varying temperatures, and corrosive environments. Metamaterials, with properties such as NTE (section 2), can be utilized in metamaterial-supported sensors to enhance their resilience. This adaptation provides crucial protection against excessive thermal expansion, which could otherwise lead to sensor breakage, thereby enhancing the longevity and reliability of sensors deployed in outdoor settings. Such enhancements are particularly beneficial for long-term environmental monitoring, reducing the need for frequent maintenance or replacement and ensuring consistent data collection.

Data availability statement

The data cannot be made publicly available upon publication because they are owned by a third party and the terms of use prevent public distribution. The data that support the findings of this study are available upon reasonable request from the authors.

Acknowledgments

This research was partially funded by the Autonomous Province of Bozen-Bolzano/South Tyrol through the International Joint-Project Cooperations South Tyrol-Switzerland (FLEXIBOTS, Grant N.: 2/34), South Tyrol-Luxembourg (V-SAFE, Grant N.: 7/34), the Autonomous Province of Bozen-Bolzano/South Tyrol's European Regional Development Fund Project: EFRE/FESR 1011-Smart Cover, and by the European Union—NextGenerationEU, in the framework of the iNEST—Interconnected Nord-Est Innovation Ecosystem (iNEST ECS0000043—CUP I43C22000250006). The views and opinions expressed are solely those of the authors and do not necessarily reflect those of the European Union, nor can the European Union be held responsible for them. EM and HSO acknowledge additional funding by the Deutsche Forschungsgemeinschaft (DFG, German Research Foundation) under Germany's Excellence Strategy-EXC-2193/1-390951807.

ORCID iDs

Hugo de Souza Oliveira  <https://orcid.org/0000-0003-1052-8127>
 Niloofar Saeedzadeh Khaanghah  <https://orcid.org/0000-0002-3343-6738>
 Giulia Elli  <https://orcid.org/0000-0003-3945-4440>
 Luisa Petti  <https://orcid.org/0000-0003-0264-7185>
 Giuseppe Cantarella  <https://orcid.org/0000-0002-6398-601X>
 Edoardo Milana  <https://orcid.org/0000-0003-3389-3039>
 Niko Münzenrieder  <https://orcid.org/0000-0003-4653-5927>

References

- [1] Zhu S and Zhang X 2018 Metamaterials: artificial materials beyond nature *Natl Sci. Rev.* **5** 131
- [2] Lees C, Vincent J F V and Hillerton J E 1991 Poisson's ratio in skin *Bio-Med. Mater. Eng.* **1** 19–23
- [3] Frolich L M, LaBarbera M and Stevens W P 1994 Poisson's ratio of a crossed fibre sheath: the skin of aquatic salamanders *J. Zool.* **232** 231–52
- [4] Iniguez-Rabago A, Li Y and Overvelde J T B 2019 Exploring multistability in prismatic metamaterials through local actuation *Nat. Commun.* **10** 1–10
- [5] Cui T J *et al* 2024 Roadmap on electromagnetic metamaterials and metasurfaces *J. Phys. Photonics* **6** 032502
- [6] Li L, Shi Y and Cui T J 2024 Introduction to electromagnetic metamaterials and metasurfaces *Electromagnetic Metamaterials and Metasurfaces: From Theory To Applications* (Springer) pp 1–20
- [7] Aydin G and San S E 2024 Breaking the limits of acoustic science: a review of acoustic metamaterials *Mater. Sci. Eng. B* **305** 117384
- [8] Nakayama M 2024 Acoustic metamaterials based on polymer sheets: from material design to applications as sound insulators and vibration dampers *Polym. J.* **56** 71–77
- [9] Jin H and Espinosa H D 2024 Mechanical metamaterials fabricated from self-assembly: a perspective *J. Appl. Mech.* **91** 144
- [10] Jiao P, Mueller J, Raney J R, Zheng X R and Alavi A H 2023 Mechanical metamaterials and beyond *Nat. Commun.* **14** 1–17
- [11] Shi X *et al* 2022 An auxetic cellular structure as a universal design for enhanced piezoresistive sensitivity *Matter* **5** 1547–62
- [12] Gao W, Yao J, Zhu K, Zhao P and Chen X 2023 Highly sensitive, wide-range pressure sensor based on negative Poisson's ratio for human motion detection *IEEE Sens. J.* **23** 12618–25
- [13] Zhao H *et al* 2023 A hydrogel-based mechanical metamaterial for the interferometric profiling of extracellular vesicles in patient samples *Nat. Biomed. Eng.* **7** 135–48
- [14] Zhao W *et al* 2023 4D printed shape memory metamaterials with sensing capability derived from the origami concept *Nano Energy* **115** 108697
- [15] Huang X *et al* 2024 Flexible sensors with zero Poisson's ratio *Natl. Sci. Rev.* **11** nwae027
- [16] Liu H, Li Y, Zhou M, Chen B, Chen Y and Zhai W 2023 Ambilateral convergent directional freeze casting meta-structured foams with a negative Poisson's ratio for high-performance piezoresistive sensors *Chem. Eng. J.* **454** 140436

- [17] Jiang Y *et al* 2018 Auxetic mechanical metamaterials to enhance sensitivity of stretchable strain sensors *Adv. Mater.* **30** 1706589
- [18] Dijvejin Z A, Kazemi K K, Alasvand Zarasvand K, Zarifi M H and Golovin K 2020 Kirigami-enabled microwave resonator arrays for wireless, flexible, passive strain sensing *ACS Appl. Mater. Interfaces* **12** 44256–64
- [19] de Souza Oliveira H *et al* 2022 Flexible auxetic structure as substrates for resistive pressure sensors 2022 *IEEE Sensors* (IEEE) pp 2022–02
- [20] Lim T-C 2023 Metamaterial with tunable positive and negative hygrothermal expansion inspired by a four-fold symmetrical islamic motif *Symmetry* **15** 462
- [21] Lemkalli B, Kadic M, El Badri Y, Guenneau S, Mir A and Achaoui Y 2024 The emergence of low-frequency dual Fano resonances in chiral twisting metamaterials *Wave Motion* **127** 103302
- [22] Jiang S, Liu J, Xiong W, Yang Z, Yin L, Li K and Huang Y 2022 A snakeskin-inspired, soft-hinge kirigami metamaterial for self-adaptive conformal electronic armor *Adv. Mater.* **34** 2204091
- [23] Kim H-G, Hajra S, Lee H, Kim N and Kim H J 2023 Additively manufactured mechanical metamaterial-based pressure sensor with tunable sensing properties for stance and motion analysis *Adv. Eng. Mater.* **25** 2201499
- [24] Chunder B J 1898 On the rotation of plane of polarisation of electric wave by a twisted structure *Proc. R. Soc.* **63** 146–52
- [25] Engheta N and Ziolkowski R W 2006 Introduction, history and selected topics in fundamental theories of metamaterials *Metamaterials: Physics and Engineering Explorations* (Wiley-IEEE Press) pp 1–41
- [26] Lindell I V, Sihvola A H and Kurkijarvi J 1992 Karl F. Lindman: the last Hertzian and a harbinger of electromagnetic chirality *IEEE Antennas Propag. Mag.* **34** 24–30
- [27] Kock W E 1948 Metallic delay lenses *Bell Syst. Tech. J.* **27** 58–82
- [28] Lakes R 1987 Foam structures with a negative Poisson's ratio *Science* **235** 1038–40
- [29] Choi Y K, Yoo Y J, Park S Y, Lim T, Jeong S-M and Ju S 2020 Metastructure-inspired ultraviolet and blue light filter *AIP Adv.* **10** 78
- [30] Bertoldi K, Vitelli V, Christensen J and van Hecke M 2017 Flexible mechanical metamaterials *Nat. Rev. Mater.* **10** 17066
- [31] Zhang Q and Sun Y 2024 A series of auxetic metamaterials with negative thermal expansion based on L-shaped microstructures *Thin-Walled Struct.* **197** 111596
- [32] Li Z, Gao W, Kessissoglou N, Oberst S, Wang M Y and Luo Z 2023 Multifunctional mechanical metamaterials with tunable double-negative isotropic properties *Mater. Des.* **232** 112146
- [33] Velu R, Vaheed N, Ramachandran M K and Raspall F 2020 Experimental investigation of robotic 3D printing of high-performance thermoplastics (PEEK): a critical perspective to support automated fibre placement process *Int. J. Adv. Manuf. Technol.* **108** 1007–25
- [34] Choi C, Bansal S, Münzenrieder N and Subramanian S 2021 Fabricating and assembling acoustic metamaterials and phononic crystals *Adv. Eng. Mater.* **23** 2000988
- [35] Ion A *et al* 2016 Metamaterial mechanisms *UIST'16: Proc. 29th Annual Symp. on User Interface Software and Technology* (Association for Computing Machinery) pp 529–39
- [36] Zhang Q, Lu W, Scarpa F, Barton D, Rankin K, Zhu Y, Lang Z-Q and Peng H-X 2021 Topological characteristics and mechanical properties of uniaxially thermoformed auxetic foam *Mater. Des.* **211** 110139
- [37] Zhang Q, Lu W, Scarpa F, Barton D, Lakes R S, Zhu Y, Lang Z and Peng H-X 2020 Large stiffness thermoformed open cell foams with auxeticity *Appl. Mater. Today* **20** 100775
- [38] Luo Y M, He C, Tao Z, Hao J, Xu H H, Zhang Y, Zhang F and Ren X 2024 A surface-wave seismic metamaterial filled with auxetic foam *Int. J. Mech. Sci.* **262** 108715
- [39] Kim J-S, Mahato M, Oh J-H and Oh I-K 2023 Multi-purpose auxetic foam with honeycomb concave micropattern for sound and shock energy absorbers *Adv. Mater. Interfaces* **10** 2202092
- [40] Meng H, Bailey Y, and Chen N, Wang L, Ciampa F, Fabro A, Chronopoulos D and Elmadih W 2020 3D rainbow phononic crystals for extended vibration attenuation bands *Sci. Rep.* **10** 1–9
- [41] Brandão A A T, de Paula A S and Fabro A T 2022 Rainbow gyroscopic disk metastructures for broadband vibration attenuation in rotors *J. Sound Vib.* **532** 116982
- [42] Sugino C, Leadenham S, Ruzzene M and Erturk A 2016 On the mechanism of bandgap formation in locally resonant finite elastic metamaterials *J. Appl. Phys.* **120** 48
- [43] Dalela S, Balaji P S and Jena D P 2022 A review on application of mechanical metamaterials for vibration control *Mech. Adv. Mater. Struct.* **29** 3237–62
- [44] Vellaparambil R, Han W-S, Di Giovanni P and Avril S 2023 Potential of auxetic designs in endovascular aortic repair: a computational study of their mechanical performance *J. Mech. Behav. Biomed. Mater.* **138** 105644
- [45] Zhou Y and Sun B 2023 A novel metamaterial-based stent with dual properties of auxetic and self-expanding *J. Phys.: Conf. Ser.* **2542** 012004
- [46] Jiang H, Ziegler H, Zhang Z, Zhang H, Le Barbenchon L, Atre S and Chen Y 2022 3D printed tubular lattice metamaterials for mechanically robust stents *Composites B* **236** 109809
- [47] Bhullar S K, Lekesiz H, Karaca A A, Cho Y, Willerth S M and Jun M B G 2022 Characterizing the mechanical performance of a bare-metal stent with an auxetic cell geometry *Appl. Sci.* **12** 910
- [48] Tomita S *et al* 2023 Transition of deformation modes from bending to auxetic compression in origami-based metamaterials for head protection from impact *Sci. Rep.* **13** 1–12
- [49] Pais V, Silva P, Bessa J, Dias H, Duarte M H, Cunha F and Figueiro R 2022 Low-velocity impact response of auxetic seamless knits combined with non-newtonian fluids *Polymers* **14** 2065
- [50] Zhang X G, Ren X, Jiang W, Zhang X Y, Luo C, Zhang Y and Xie Y M 2022 A novel auxetic chiral lattice composite: experimental and numerical study *Compos. Struct.* **282** 115043
- [51] Bronder S, Herter F, Röhrig A, Bähre D and Jung A 2022 Design Study for Multifunctional 3D Re-entrant Auxetics *Adv. Eng. Mater.* **24** 2100816
- [52] Wang Y 2022 Auxetic composite laminates with through-thickness negative Poisson's ratio for mitigating low velocity impact damage: a numerical study *Materials* **15** 6963
- [53] Duncan O *et al* 2018 Review of auxetic materials for sports applications: expanding options in comfort and protection *Appl. Sci.* **8** 941
- [54] Jiao P, Zhang H and Li W 2023 Origami tribo-metamaterials with mechano-electrical multistability *ACS Appl. Mater. Interfaces* **15** 2873–80
- [55] El Helou C, Buskohl P R, Tabor C E and Harne R L 2021 Digital logic gates in soft, conductive mechanical metamaterials *Nat. Commun.* **12** 1–8

- [56] Zhang Q *et al* 2017 Flyweight, superelastic, electrically conductive and flame-retardant 3D multi-nanolayer graphene/ceramic metamaterial *Adv. Mater.* **29** 1605506
- [57] Wang Z, Luan C, Liao G, Liu J, Yao X and Fu J 2021 High-performance auxetic bilayer conductive mesh-based multi-material integrated stretchable strain sensors *ACS Appl. Mater. Interfaces* **13** 23038–48
- [58] Cantarella G *et al* 2018 Design of engineered elastomeric substrate for stretchable active devices and sensors *Adv. Funct. Mater.* **28** 1705132
- [59] Lee J-Y, Oh M-H, Park J-H, Kang S-H and Kang S-K 2003 Three-dimensionally printed expandable structural electronics via multi-material printing room-temperature-vulcanizing (RTV) silicone/silver flake composite and RTV *Polymers* **15** 2023
- [60] Gu J *et al* 2021 Self-powered strain sensor based on the piezo-transmittance of a mechanical metamaterial *Nano Energy* **89** 106447
- [61] Wang H, Lyu Y, Bosiakov S, Zhu H and Ren Y 2023 A review on the mechanical metamaterials and their applications in the field of biomedical engineering *Front. Mater.* **10** 1273961
- [62] Pyo S and Park K 2024 Mechanical metamaterials for sensor and actuator applications *Int. J. Precis. Eng. Manuf.-Green. Tech.* **11** 291–320
- [63] Bertoldi K, Reis P M, Willshaw S and Mullin T 2010 Negative Poisson's ratio behavior induced by an elastic instability *Adv. Mater.* **22** 361–6
- [64] Lim T-C 2014 Introduction *Auxetic Materials and Structures* (Springer) pp 1–43
- [65] Reid D R, Pashine N, Wozniak J M, Jaeger H M, Liu A J, Nagel S R and de Pablo J J 2018 Auxetic metamaterials from disordered networks *Proc. Natl Acad. Sci. USA* **115** E1384–90
- [66] Zheng X, Chen T-T, Guo X, Samitsu S and Watanabe I 2021 Controllable inverse design of auxetic metamaterials using deep learning *Mater. Des.* **211** 110178
- [67] Rothenburg L, Berlin A I A I and Bathurst R J 1991 Microstructure of isotropic materials with negative Poisson's ratio *Nature* **354** 470–2
- [68] Ye M, Gao L, Wang F and Li H 2021 A novel design method for energy absorption property of chiral mechanical metamaterials *Materials* **14** 5386
- [69] Evans K E and Alderson A 2000 Auxetic materials: functional materials and structures from lateral thinking! *Adv. Mater.* **12** 617–28
- [70] Ramezani M J and Rahmani O 2024 Potential and applications of auxetic tubular: a review *Funct. Compos. Struct.* **6** 012001
- [71] Behravanrad A and Jafari M 2024 Thermo-mechanical behavior of 2D functionally graded porous-auxetic metamaterial rotating disk with an auxetic foundation *Aerosp. Sci. Technol.* **145** 108829
- [72] Lvov V A, Senatov F S, Veveris A A, Skrybykina V A and Diaz Lantada A 2022 Auxetic metamaterials for biomedical devices: current situation, main challenges and research trends *Materials* **15** 1439
- [73] Lipton J I, MacCurdy R, Manchester Z, Chin L, Cellucci D and Rus D 2018 Handedness in shearing auxetics creates rigid and compliant structures *Science* **360** 632–5
- [74] Evans K E, Nkansah M A, Hutchinson I J and Rogers S C 1991 Molecular network design *Nature* **353** 124
- [75] Jentzsch M, Badstöber M-C, Umlas F and Speck T 2022 Damage protection in fruits: Comparative analysis of the functional morphology of the fruit peels of five Citrus species via quasi-static compression tests *Front. Mater.* **9** 979151
- [76] Gorodtsov V A and Lisovenko D S 2020 Auxetics among materials with cubic anisotropy *Mech. Solids* **55** 461–74
- [77] Baughman R H, Shacklette J M, Zakhidov A A and Stafström S 1998 Negative Poisson's ratios as a common feature of cubic metals *Nature* **392** 362–5
- [78] Kolken H and Zadpoor A A 2017 Auxetic mechanical metamaterials *RSC Adv.* **7** 5111–29
- [79] Schwerdtfeger J, Wein F, Leugering G, Singer R F, Körner C, Stingl M and Schury F 2011 Design of auxetic structures via mathematical optimization *Adv. Mater.* **23** 2650–4
- [80] Zhang X and Yang D 2016 Mechanical properties of auxetic cellular material consisting of re-entrant hexagonal honeycombs *Materials* **9** 900
- [81] Grima J N, Gatt R, Alderson A and Evans K E 2005 On the potential of connected stars as auxetic systems *Mol. Simul.* **31** 925–35
- [82] He P, Du T, Zhao K, Dong J, Liang Y and Zhang Q 2023 Lightweight 3D graphene metamaterials with tunable negative thermal expansion *Adv. Mater.* **35** 2208562
- [83] Evtushok V Y, Ivanchikova I D, Zalomaeva O V, Gubanov A I, Kolesov B A, Glazneva T S and Kholdeeva O A 2024 Heterogeneous H₂O₂-based selective oxidations over zirconium tungstate α -ZrW₂O₈ *Dalton Trans.* **53** 1528–40
- [84] Zhang Q and Sun Y 2024 Novel metamaterial structures with negative thermal expansion and tunable mechanical properties *Int. J. Mech. Sci.* **261** 108692
- [85] Rafsanjani A, Bertoldi K and Studart A R 2019 Programming soft robots with flexible mechanical metamaterials *Sci. Robot.* **4** eaav7874
- [86] Zhang J, Lu G, Wang Z, Ruan D, Alomarah A and Durandet Y 2018 Large deformation of an auxetic structure in tension: experiments and finite element analysis *Compos. Struct.* **184** 92–101
- [87] Wu Y and Yang L 2020 The effect of unit cell size and topology on tensile failure behavior of 2D lattice structures *Int. J. Mech. Sci.* **170** 105342
- [88] Veloso F, Gomes-Fonseca J, Morais P, Correia-Pinto J, Pinho A C M and Vilaça J L 2022 Overview of methods and software for the design of functionally graded lattice structures *Adv. Eng. Mater.* **24** 2200483
- [89] Zhang W, Zhao S, Sun R, Scarpa F and Wang J 2021 Mechanical properties of a hybrid auxetic metamaterial and metastructure system *J. Reinf. Plast. Compos.* **40** 785–99
- [90] Surjadi J U, Gao L, Du H, Li X, Xiong X, Fang N X and Lu Y 2019 Mechanical metamaterials and their engineering applications *Adv. Eng. Mater.* **21** 1800864
- [91] Hartmann A, Murer K, de Bie R A and de Bruin E D 2009 Reproducibility of spatio-temporal gait parameters under different conditions in older adults using a trunk tri-axial accelerometer system *Gait Posture* **30** 351–5
- [92] Khan S, Ali S and Bermak A 2019 Recent developments in printing flexible and wearable sensing electronics for healthcare applications *Sensors* **19** 1230
- [93] Yi J and Xianyu Y 2022 Gold nanomaterials-implemented wearable sensors for healthcare applications *Adv. Funct. Mater.* **32** 2113012
- [94] Sun Y, Song K, Ju J and Zhou X 2024 Curved-creased origami mechanical metamaterials with programmable stabilities and stiffnesses *Int. J. Mech. Sci.* **262** 108729
- [95] Xiao B, Liu Y, Xu W, Wei R, Chen M and Jiang H 2024 A bistable honeycomb mechanical metamaterial with transformable Poisson's ratio and tunable vibration isolation properties *Thin-Walled Struct.* **198** 111718
- [96] Choe J K, Yi J, Jang H, Won H, Lee S, Lee H, Jang Y, Song H and Kim J 2024 Digital mechanical metamaterial: encoding mechanical information with graphical

- stiffness pattern for adaptive soft machines *Adv. Mater.* **36** 2304302
- [97] Van Raemdonck B, Milana E, De Volder M, Reynaerts D and Gorissen B 2023 Nonlinear inflatable actuators for distributed control in soft robots *Adv. Mater.* **35** 2301487
- [98] Zhou W, Wu B, Muhammad M, Du Q, Huang G, Lü C and Chen W 2018 Actively tunable transverse waves in soft membrane-type acoustic metamaterials *J. Appl. Phys.* **123** 79
- [99] Montgomery S M *et al* 2021 Magneto-mechanical metamaterials with widely tunable mechanical properties and acoustic bandgaps *Adv. Funct. Mater.* **31** 2005319
- [100] Galea R, Dudek K K, Farrugia P-S, Zammit Mangion L, Grima J N and Gatt R 2022 Reconfigurable magneto-mechanical metamaterials guided by magnetic fields *Compos. Struct.* **280** 114921
- [101] Slesarenko V 2020 Planar mechanical metamaterials with embedded permanent magnets *Materials* **13** 1313
- [102] Ma C, Chang Y, Wu S and Zhao R R 2022 Deep learning-accelerated designs of tunable magneto-mechanical metamaterials *ACS Appl. Mater. Interfaces* **14** 33892–902
- [103] Zhu R, Chen Y Y, Barnhart M V, Hu G K, Sun C T and Huang G L 2016 Experimental study of an adaptive elastic metamaterial controlled by electric circuits *Appl. Phys. Lett.* **108** 46
- [104] Elefante G, De Bellis M L and Bacigalupo A 2023 Electrically-tunable active metamaterials for damped elastic wave propagation control *Int. J. Solids Struct.* **276** 112306
- [105] Zhao Z, Yuan C, Lei M, Yang L, Zhang Q, Chen H, Qi H J and Fang D 2019 Three-dimensionally printed mechanical metamaterials with thermally tunable auxetic behavior *Phys. Rev. Appl.* **11** 044074
- [106] Bodaghi M and Liao W H 2019 4D printed tunable mechanical metamaterials with shape memory operations *Smart Mater. Struct.* **28** 045019
- [107] Grima-Cornish J N, Cauchi R, Attard D, Gatt R and Grima J N 2020 Smart Honeycomb “Mechanical Metamaterials” with Tunable Poisson’s Ratios *Phys. Status Solidi b* **257** 1900707
- [108] Ni X, Guo X, Li J, Huang Y, Zhang Y and Rogers J A 2019 2D mechanical metamaterials with widely tunable unusual modes of thermal expansion *Adv. Mater.* **31** 1905405
- [109] Barri K, Zhang Q, Jiao P, Wang Z L and Alavi A H 2021 Multifunctional metamaterial sensor and nanogenerator *Proc. Volume 11589, Behavior and Mechanics of Multifunctional Materials XV* vol 11589 (SPIE) pp 43–48
- [110] Babaee S, Overvelde J T B, Chen E R, Tournat V and Bertoldi K 2016 Reconfigurable origami-inspired acoustic waveguides *Sci. Adv.* **2** 19
- [111] Florijn B, Coulais C and van Hecke M 2014 Programmable mechanical metamaterials *Phys. Rev. Lett.* **113** 175503
- [112] Felton S M, Tolley M T and Wood R J 2014 Mechanically programmed self-folding at the millimeter scale *2014 IEEE Int. Conf. on Automation Science and Engineering (CASE)* (IEEE) pp 18–22
- [113] Gregg C E *et al* 2024 Ultralight, strong and self-reprogrammable mechanical metamaterials *Sci. Rob.* **9** eadi2746
- [114] Hu X, Tan T, Wang B and Yan Z 2023 A reprogrammable mechanical metamaterial with origami functional-group transformation and ring reconfiguration *Nat. Commun.* **14** 1–13
- [115] Tolley M T, Felton S M, Miyashita S, Aukes D, Rus D and Wood R J 2014 Self-folding origami: shape memory composites activated by uniform heating *Smart Mater. Struct.* **23** 094006
- [116] Kolken H M A, Janbaz S, Leeflang S M A, Lietaert K, Weinans H H and Zadpoor A A 2018 Rationally designed meta-implants: a combination of auxetic and conventional meta-biomaterials *Mater. Horiz.* **5** 28–35
- [117] Farhangdoust S, Georgeson G and Ihn J-B 2022 MetaMembranes for the sensitivity enhancement of wearable piezoelectric metasensors *Sensors* **22** 1909
- [118] Lee Y-J *et al* 2019 Auxetic elastomers: Mechanically programmable meta-elastomers with an unusual Poisson’s ratio overcome the gauge limit of a capacitive type strain sensor *Extreme Mech. Lett.* **31** 100516
- [119] Li D, Bu X, Xu Z, Luo Y and Bai H 2020 Bioinspired multifunctional cellular plastics with a negative Poisson’s ratio for high energy dissipation *Adv. Mater.* **32** 2001222
- [120] Zheng X, Guo X and Watanabe I 2021 A mathematically defined 3D auxetic metamaterial with tunable mechanical and conduction properties *Mater. Des.* **198** 109313
- [121] Soyarslan C, Blümer V and Bargmann S 2019 Tunable auxeticity and elastomechanical symmetry in a class of very low density core-shell cubic crystals *Acta Mater.* **177** 280–92
- [122] Zhou L, Zheng X, Du K, Guo X, Yin Q, Lu A and Yi Y 2021 Parametric and experiment studies of 3D auxetic lattices based on hollow shell cuboctahedron *Smart Mater. Struct.* **30** 025042
- [123] Li T, Chen Y, Hu X, Li Y and Wang L 2018 Exploiting negative Poisson’s ratio to design 3D-printed composites with enhanced mechanical properties *Mater. Des.* **142** 247–58
- [124] Bao S, Ren X, Qi Y J, Li H R, Han D, Li W, Luo C and Song Z Z 2022 Quasi-static mechanical properties of a modified auxetic re-entrant honeycomb metamaterial *Phys. Status Solidi b* **259** 2200270
- [125] Wong J *et al* 2019 3D printing ionogel auxetic frameworks for stretchable sensors *Adv. Mater. Technol.* **4** 1900452
- [126] Wu C *et al* 2022 Tailoring auxetic mechanical metamaterials to achieve patterned wire strain sensors with controllable high sensitivity *Chem. Eng. J.* **442** 136317
- [127] Masters I G and Evans K E 1996 Models for the elastic deformation of honeycombs *Compos. Struct.* **35** 403–22
- [128] Wan H, Ohtaki H, Kotosaka S and Hu G 2004 A study of negative Poisson’s ratios in auxetic honeycombs based on a large deflection model *Eur. J. Mech. A Solids* **23** 95–106
- [129] Liu W, Wang N, Huang J and Zhong H 2014 The effect of irregularity, residual convex units and stresses on the effective mechanical properties of 2D auxetic cellular structure *Mater. Sci. Eng. A* **609** 26–33
- [130] Shen J, Zeng Q, Wang J, Ge J, Gao F and Liang J 2023 Study of mechanical properties of a new 3D re-entrant lattice auxetic structure under bending *Adv. Eng. Mater.* **25** 2201509
- [131] Yang H, Wang B and Ma L 2019 Mechanical properties of 3D double-U auxetic structures *Int. J. Solids Struct.* **180-181** 13–29
- [132] Zhang C, Xiao S-H, Qin Q-H and Wang H 2021 Tunable compressive properties of a novel auxetic tubular material with low stress level *Thin-Walled Struct.* **164** 107882
- [133] Zhao X, Wei L, Wen D, Zhu G, Yu Q and Ma Z D 2021 Bending response and energy absorption of sandwich beams with novel auxetic honeycomb core *Eng. Struct.* **247** 113204
- [134] Dudek K K, Gatt R, Mizzi L, Dudek M R, Attard D and Grima J N 2017 Global rotation of mechanical metamaterials induced by their internal deformation *AIP Adv.* **7** 98
- [135] Grima-Cornish J N, Attard D, Grima J N and Evans K E 2022 Auxetic behavior and other negative thermomechanical properties from rotating rigid units *Phys. Status Solidi RRL* **16** 2100322

- [136] Lim T-C 2023 A metamaterial with sign-programmable thermal expansivity and Poisson's ratio constructed from a hybrid of rotating and non-rotating rigid units *Int. J. Solids Struct.* **284** 112510
- [137] Grima J N and Evans K E 2000 Auxetic behavior from rotating squares *J. Mater. Sci. Lett.* **19** 1563–5
- [138] Hur J M and Kim D-N 2023 Auxetic meta-disk for independent control of flexural and torsional waves *Int. J. Mech. Sci.* **243** 108050
- [139] Lim T-C 2023 A metamaterial with negative thermal expansivity and programmable Poisson's ratio based on rotating triangles and quivering rhombi *Eur. J. Mech. A Solids* **100** 104986
- [140] Wallbanks M, Khan M F, Bodaghi M, Triantaphyllou A and Serjouei A 2021 On the design workflow of auxetic metamaterials for structural applications *Smart Mater. Struct.* **31** 023002
- [141] Wu W, Hu W, Qian G, Liao H, Xu X and Berto F 2019 Mechanical design and multifunctional applications of chiral mechanical metamaterials: a review *Mater. Des.* **180** 107950
- [142] Xu W, Liu Z, Wang L and Zhu P 2022 3D chiral metamaterial modular design with highly-tunable tension-twisting properties *Mater. Today Commun.* **30** 103006
- [143] Fernandez-Corbaton I *et al* 2019 New twists of 3D chiral metamaterials *Adv. Mater.* **31** 1807742
- [144] Srivatsa S, Kumar R S, Selva D and Silberstein M N 2022 Examining the impact of asymmetry in lattice-based mechanical metamaterials *Mech. Mater.* **172** 104386
- [145] Fei X, Jin L, Zhang X, Li X and Lu M 2020 Three-dimensional anti-chiral auxetic metamaterial with tunable phononic bandgap *Appl. Phys. Lett.* **116** 89
- [146] Lu F, Lin B, Ling X, Zhang C and Zhu Y 2023 Controllable design of bi-material metamaterials with programmable thermal expansion and Poisson's ratio *Compos. Struct.* **322** 117417
- [147] Bai L, Wang W, Xu W, Cheng S and Yu X 2023 Dual-constituent anti-tetra-chiral lattice metamaterial with tailorable coefficient of thermal expansion and excellent bandgap *Mater. Today Commun.* **34** 105047
- [148] Silverberg J L, Evans A A, McLeod L, Hayward R C, Hull T, Santangelo C D and Cohen I 2014 Using origami design principles to fold reprogrammable mechanical metamaterials *Science* **345** 647–50
- [149] Meng Z, Liu M, Yan H, Genin G M and Chen C Q 2022 Deployable mechanical metamaterials with multistep programmable transformation *Sci. Adv.* **8** 60
- [150] Jamalimehr A, Mirzajanzadeh M, Akbarzadeh A and Pasini D 2022 Rigidly flat-foldable class of lockable origami-inspired metamaterials with topological stiff states *Nat. Commun.* **13** 1–14
- [151] Ye H, Liu Q, Cheng J, Li H, Jian B, Wang R, Sun Z, Lu Y and Ge Q 2023 Multimaterial 3D printed self-locking thick-panel origami metamaterials *Nat. Commun.* **14** 1–12
- [152] Wickeler A L and Naguib H E 2020 Novel origami-inspired metamaterials: Design, mechanical testing and finite element modelling *Mater. Des.* **186** 108242
- [153] Overvelde J T B *et al* 2016 A three-dimensional actuated origami-inspired transformable metamaterial with multiple degrees of freedom *Nat. Commun.* **7** 1–8
- [154] McClintock H D *et al* 2021 A fabrication strategy for reconfigurable millimeter-scale metamaterials *Adv. Funct. Mater.* **31** 2103428
- [155] Hong L, Zhang H, Kraus T and Jiao P 2024 Ultra-stretchable kirigami piezo-metamaterials for sensing coupled large deformations *Adv. Sci.* **11** 2303674
- [156] Liu X, Zhang K, Shi H, Hong F, Liu H and Deng Z 2024 Origami-inspired metamaterial with compression–twist coupling effect for low-frequency vibration isolation *Mech. Syst. Sig. Process.* **208** 111076
- [157] Wen G, Zhang S, Wang H, Wang Z-P, He J, Chen Z, Liu J and Xie Y M 2023 Origami-based acoustic metamaterial for tunable and broadband sound attenuation *Int. J. Mech. Sci.* **239** 107872
- [158] Han H, Sorokin V, Tang L and Cao D 2023 Origami-based tunable mechanical memory metamaterial for vibration attenuation *Mech. Syst. Sig. Process.* **188** 110033
- [159] Sadegh Ebrahimi M, Noruzi M, Hamzehei R, Etemadi E and Hashemi R 2023 Revolutionary auxetic intravascular medical stents for angioplasty applications *Mater. Des.* **235** 112393
- [160] Zhang H and Paik J 2022 Kirigami design and modeling for strong, lightweight metamaterials *Adv. Funct. Mater.* **32** 2107401
- [161] Lee G, Lee S-J, Rho J and Kim M 2023 Acoustic and mechanical metamaterials for energy harvesting and self-powered sensing applications *Mater. Today Energy* **37** 101387
- [162] Ning C, Xiang S, Sun X, Zhao X, Wei C, Li L, Zheng G and Dong K 2024 Highly stretchable kirigami-patterned nanofiber-based nanogenerators for harvesting human motion energy to power wearable electronics *Mater. Futures* **3** 025101
- [163] Qi Y, Kuang Y, Liu Y, Liu G, Zeng J, Zhao J, Wang L, Zhu M and Zhang C 2022 Kirigami-inspired triboelectric nanogenerator as ultra-wide-band vibrational energy harvester and self-powered acceleration sensor *Appl. Energy* **327** 120092
- [164] Brooks A K, Chakravarty S, Ali M and Yadavalli V K 2022 Kirigami-inspired biodesign for applications in healthcare *Adv. Mater.* **34** 2109550
- [165] Meng K *et al* 2022 Kirigami-inspired pressure sensors for wearable dynamic cardiovascular monitoring *Adv. Mater.* **34** 2202478
- [166] Xu Z *et al* 2021 Implantable cardiac kirigami-inspired lead-based energy harvester fabricated by enhanced piezoelectric composite film *Adv. Healthcare Mater.* **10** 2002100
- [167] Farrugia P-S, Gatt R, Lonardelli E Z, Grima J N and Evans K E 2019 Different deformation mechanisms leading to auxetic behavior exhibited by missing rib square grid structures *Phys. Status Solidi b* **256** 1800186
- [168] Zhang W, Zhao S, Scarpa F, Wang J and Sun R 2021 In-plane mechanical behavior of novel auxetic hybrid metamaterials *Thin-Walled Struct.* **159** 107191
- [169] Das R, Khan F and Kumar G S 2023 Design of novel auxetic hybrid metamaterials: experimental and numerical study *2023 14th Int. Conf. on Mechanical and Aerospace Engineering (ICMAE)* (IEEE) pp 18–21
- [170] Ha C S *et al* 2023 Rapid inverse design of metamaterials based on prescribed mechanical behavior through machine learning *Nat. Commun.* **14** 1–11
- [171] Garland A P, White B C, Jensen S C and Boyce B L 2021 Pragmatic generative optimization of novel structural lattice metamaterials with machine learning *Mater. Des.* **203** 109632
- [172] Loonen R C G M, de Vries S and Goia F 2022 Inverse design for advanced building envelope materials, systems and operation *Rethinking Building Skins* (Woodhead Publishing) pp 377–402
- [173] Deng B, Zareei A, Ding X, Weaver J C, Rycroft C H and Bertoldi K 2022 Inverse design of mechanical metamaterials with target nonlinear response via a neural accelerated evolution strategy *Adv. Mater.* **34** 2206238

- [174] Zheng X, Zhang X, Chen T-T and Watanabe I 2023 Deep learning in mechanical metamaterials: from prediction and generation to inverse design *Adv. Mater.* **35** 2302530
- [175] Ronellenfitch H, Stoop N, Yu J, Forrow A and Dunkel J 2019 Inverse design of discrete mechanical metamaterials *Phys. Rev. Mater.* **3** 095201
- [176] Bastek J-H and Kochmann D M 2023 Inverse design of nonlinear mechanical metamaterials via video denoising diffusion models *Nat. Mach. Intell.* **5** 1466–75
- [177] Rahman O, Uddin K Z, Muthulingam J, Youssef G, Shen C and Koohbor B 2022 Density-graded cellular solids: mechanics, fabrication and applications *Adv. Eng. Mater.* **24** 2100646
- [178] Dong L and Wang D 2022 Optimal design of three-dimensional voxel printed multimaterial lattice metamaterials via machine learning and evolutionary algorithm *Phys. Rev. Appl.* **18** 054050
- [179] Wang Y, Zeng Q, Wang J, Li Y and Fang D 2022 Inverse design of shell-based mechanical metamaterial with customized loading curves based on machine learning and genetic algorithm *Comput. Methods Appl. Mech. Eng.* **401** 115571
- [180] Zeng Q, Duan S, Zhao Z, Wang P and Lei H 2023 Inverse design of energy-absorbing metamaterials by topology optimization *Adv. Sci.* **10** 2204977
- [181] Liang K, Wang Y, Luo Y, Takezawa A, Zhang X and Kang Z 2023 Programmable and multistable metamaterials made of precisely tailored bistable cells *Mater. Des.* **227** 111810
- [182] Zheng L, Karapiperis K, Kumar S and Kochmann D M 2023 Unifying the design space and optimizing linear and nonlinear truss metamaterials by generative modeling *Nat. Commun.* **14** 1–14
- [183] Cerniauskas G, Sadia H and Alam P 2024 Machine intelligence in metamaterials design: a review *Oxf. Open Mater. Sci.* **4** itae001
- [184] Ahmadpour A, Yetisen A K and Tasoglu S 2023 Piezoelectric metamaterial blood pressure sensor *ACS Appl. Electron. Mater.* **5** 3280–90
- [185] Mohammadi A, Tan Y, Choong P and Oetomo D 2021 Flexible mechanical metamaterials enabling soft tactile sensors with multiple sensitivities at multiple force sensing ranges *Sci. Rep.* **11** 1–9
- [186] Oliveri G and Overvelde J T B 2020 Inverse design of mechanical metamaterials that undergo buckling *Adv. Funct. Mater.* **30** 1909033
- [187] Bacigalupo A, Gnecco G, Lepidi M and Gambarotta L 2021 Computational design of innovative mechanical metafilters via adaptive surrogate-based optimization *Comput. Methods Appl. Mech. Eng.* **375** 113623
- [188] Zhang G and Khandelwal K 2019 Computational design of finite strain auxetic metamaterials via topology optimization and nonlinear homogenization *Comput. Methods Appl. Mech. Eng.* **356** 490–527
- [189] Ma K and Zhao Q 2024 Multi-objective topology optimization for thermo-elastic systems based on periodic constraints *J. Therm. Stresses* **47** 695–725
- [190] Baishya M J, Muthu N and Khanikar P 2024 In pursuit of a high-performance mechanical metamaterial: simple-cubic-octahedral plate lattice *Int. J. Mech. Sci.* **272** 109189
- [191] Meier T, Li R, Mavrikos S, Blankenship B, Vangelatos Z, Yildizdag M E and Grigoropoulos C P 2024 Obtaining auxetic and isotropic metamaterials in counterintuitive design spaces: an automated optimization approach and experimental characterization *npj Comput. Mater.* **10** 1–12
- [192] Montazeri A, Bahmanpour E and Safarabadi M 2023 A Poisson's ratio sign-switching mechanical metamaterial with tunable stiffness *Int. J. Mech. Sci.* **260** 108670
- [193] Kim H W *et al* 2018 Hygroscopic auxetic on-skin sensors for easy-to-handle repeated daily use *ACS Appl. Mater. Interfaces* **10** 40141–8
- [194] Stavric M and Wiltche A 2019 Geometrical elaboration of auxetic structures *Nexus Netw. J.* **21** 79–90
- [195] Gao Z, Ren P, Wang H, Tang Z, Wu Y and Wang H 2024 Additive manufacture of ultrasoft bioinspired metamaterials *Int. J. Mach. Tools Manuf.* **195** 104101
- [196] Zhang K P *et al* 2021 3D printed embedded metamaterials *Small* **17** 2103262
- [197] Tiller B, Reid A, Zhu B, Guerreiro J, Domingo-Roca R, Curt Jackson J and Windmill J F C 2019 Piezoelectric microphone via a digital light processing 3D printing process *Mater. Des.* **165** 107593
- [198] Shi L, Xiao X, Liu T, Liao W and Kong L 2022 Design and performance of a flexible broadband metamaterial absorbing structure fabricated based on the direct ink writing 3D printing *J. Appl. Phys.* **55** 455001
- [199] Gao H-Z, Xu W-R, Li M-C, Ilyas N, Wang J-M, Li W and Jiang X-D 2022 Hyperbolic metamaterials based on multilayer ag/tin alloy structure for spr refractive index sensors *Opt. Laser Technol.* **151** 108034
- [200] Valerini D, Cretì A, Caricato A P, Lomascolo M, Rella R and Martino M 2010 Optical gas sensing through nanostructured ZnO films with different morphologies *Sens. Actuators B* **145** 167–73
- [201] Catania F, de Souza Oliveira H, Lugoda P, Cantarella G and Münzenrieder N 2022 Thin-film electronics on active substrates: review of materials, technologies and applications *J. Appl. Phys.* **55** 323002
- [202] Catania F, Oliveira H D S, Costa Angeli M A, Ciocca M, Pané S, Münzenrieder N and Cantarella G 2022 The influence of climate conditions and on-skin positioning on InGaZnO thin-film transistor performance *Front. Electron.* **2** 786601
- [203] de Souza Oliveira H, Catania F, Cantarella G, Benedetti V, Baratieri M and Münzenrieder N 2021 Recycled carbon-based strain sensors: an ecofriendly approach using char and coconut oil *2021 IEEE Int. Flexible Electronics Technology Conf. (IFETC)* (IEEE) pp 08–11
- [204] Kaffe A, Luis E, Silwal R, Pan H M, Shrestha P L and Bastola A K 2021 3D/4D printing of polymers: fused deposition modelling (FDM), selective laser sintering (SLS) and stereolithography (SLA) *Polymers* **13** 3101
- [205] Ngo T D, Kashani A, Imbalzano G, Nguyen K T Q and Hui D 2018 Additive manufacturing (3D printing): a review of materials, methods, applications and challenges *Composites B* **143** 172–96
- [206] Choudhry N K, Panda B and Dixit U S 2023 Energy absorption characteristics of fused deposition modeling 3D printed auxetic re-entrant structures: a review *J. Mater. Eng. Perform.* **32** 8981–99
- [207] Tunay M and Cetin E 2023 Energy absorption of 2D auxetic structures fabricated by fused deposition modeling *J. Braz. Soc. Mech. Sci. Eng.* **45** 1–16
- [208] Vyavahare S and Kumar S 2020 Re-entrant auxetic structures fabricated by fused deposition modeling: an experimental study of influence of process parameters under compressive loading *Polym. Eng. Sci.* **60** 3183–96
- [209] Mocerino D, Ricciardi M R, Antonucci V and Papa I 2023 Fused deposition modelling of polymeric auxetic structures: a review *Polymers* **15** 1008
- [210] Soman P, Fozdar D Y, Lee J W, Phadke A, Varghese S and Chen S 2012 A three-dimensional polymer scaffolding material exhibiting a zero Poisson's ratio *Soft Matter* **8** 4946–51
- [211] Attar M, Aydin S S, Arabaci A and Mutlu I 2020 Mechanical meta-material-based polymer skin graft production by

- rapid prototyping and replica method *Rapid Protot. J.* **27** 278–87
- [212] Warner J J, Gillies A R, Hwang H H, Zhang H, Lieber R L and Chen S 2017 3D-printed biomaterials with regional auxetic properties *J. Mech. Behav. Biomed. Mater.* **76** 145–52
- [213] Joseph A, Mahesh V and Harursampath D 2021 On the application of additive manufacturing methods for auxetic structures: a review *Adv. Manuf.* **9** 342–68
- [214] Varas D, Pernas-Sánchez J, Fjeldberg N and Martin-Montal J 2023 Experimental analysis at different loading rates of 3D printed polymeric auxetic structure based on cylindrical elements *Polym. Test.* **119** 107930
- [215] Zhang Q, Weng S, Zhao Z, Qi H J and Fang D 2021 Soft pneumatic actuators by digital light processing combined with injection-assisted post-curing *Appl. Math. Mech.* **42** 159–72
- [216] Patel D K, Sakhaei A H, Layani M, Zhang B, Ge Q and Magdassi S 2017 Highly stretchable and UV curable elastomers for digital light processing based 3D printing *Adv. Mater.* **29** 1606000
- [217] Wan J, Sun L and Du T 2023 Design and applications of soft actuators based on digital light processing (DLP) 3D printing *IEEE Access* **11** 86227–42
- [218] Zhou X, Parida K, Chen J, Xiong J, Zhou Z, Jiang F, Xin Y, Magdassi S and Lee P S 2023 3D printed auxetic structure-assisted piezoelectric energy harvesting and sensing *Adv. Energy Mater.* **13** 2301159
- [219] Saadi O W, Uddin M A, Schiffer A and Kumar S 2023 Digital light processing of 2D lattice composites for tunable self-sensing and mechanical performance *Adv. Eng. Mater.* **n/a** 2300473
- [220] Ahmed I, Sullivan K and Priye A 2022 Multi-resin masked stereolithography (MSLA) 3D printing for rapid and inexpensive prototyping of microfluidic chips with integrated functional components *Biosensors* **12** 652
- [221] Junk S and Bär F 2023 Design guidelines for Additive Manufacturing using Masked Stereolithography mSLA *Procedia CIRP* **119** 1122–7
- [222] Valizadeh I, Al Aboud A, Dörsam E and Weeger O 2021 Tailoring of functionally graded hyperelastic materials via grayscale mask stereolithography 3D printing *Addit. Manuf.* **47** 102108
- [223] Keneth E S, Kamyshny A, Totaro M, Beccai L and Magdassi S 2021 3D printing materials for soft robotics *Adv. Mater.* **33** 2003387
- [224] Biasetto L, Gleadall A and Gastaldi V 2023 Ink tuning for direct ink writing of planar metallic lattices *Adv. Eng. Mater.* **25** 2201858
- [225] Yan W, Tian X, Zhang D, Zhou Y and Wang Q 2023 3D printing of stretchable strain sensor based on continuous fiber reinforced auxetic structure *Chin. J. Mech. Eng.* **2** 100073
- [226] Vo T H, Lam P K, Sheng Y-J and Tsao H-K 2023 Jammed microgels in deep eutectic solvents as a green and low-cost ink for 3D printing of reliable auxetic strain sensors *ACS Appl. Mater. Interfaces* **15** 33109–18
- [227] Carrillo C S and Sanchez M 2021 Design and 3D printing of four multimaterial mechanical metamaterial using polyjet technology and digital materials for impact injury prevention 2021 43rd Annual Int. Conf. of the IEEE Engineering in Medicine & Biology Society (EMBC) (IEEE) pp 01–05
- [228] Patpatiya P, Chaudhary K, Shastri A and Sharma S 2022 A review on polyjet 3D printing of polymers and multi-material structures *Proc. Inst. Mech. Eng. C* **236** 7899–926
- [229] Wang K, Chang Y-H, Chen Y, Zhang C and Wang B 2015 Designable dual-material auxetic metamaterials using three-dimensional printing *Mater. Des.* **67** 159–64
- [230] Zhou X, Ren L, Song Z, Li G, Zhang J, Li B, Wu Q, Li W, Ren L and Liu Q 2023 Advances in 3D/4D printing of mechanical metamaterials: from manufacturing to applications *Composites B* **254** 110585
- [231] Wu L, Xue J, Tian X, Liu T and Li D 2023 3D-printed metamaterials with versatile functionalities *Chin. J. Mech. Eng.* **2** 100091
- [232] Yuan S, Chua C K and Zhou K 2019 3D-printed mechanical metamaterials with high energy absorption *Adv. Mater. Technol.* **4** 1800419
- [233] Li N, Xue C, Chen S, Aiyiti W, Khan S B, Liang J, Zhou J and Lu B 2023 3D printing of flexible mechanical metamaterials: synergistic design of process and geometric parameters *Polymers* **15** 4523
- [234] Falco A, Petrelli M, Bezzeccheri E, Abdelhalim A and Lugli P 2016 Towards 3D-printed organic electronics: planarization and spray-deposition of functional layers onto 3D-printed objects *Org. Electron.* **39** 340–7
- [235] Chen L, Zhang X and Gan S 2020 Effects of laser polishing on surface quality and mechanical properties of PLA parts built by fused deposition modeling *J. Appl. Polym. Sci.* **137** 48288
- [236] Gordeev E G, Galushko A S and Ananikov V P 2018 Improvement of quality of 3D printed objects by elimination of microscopic structural defects in fused deposition modeling *PLoS One* **13** e0198370
- [237] Cano-Vicent A *et al* 2021 Fused deposition modelling: current status, methodology, applications and future prospects *Addit. Manuf.* **47** 102378
- [238] Srivastava K and Kumar Y 2023 A review on fused deposition modeling of thermoplastics *Advances in Additive Manufacturing and Metal Joining* (Springer) pp 3–16
- [239] Penumakala P K, Santo J and Thomas A 2020 A critical review on the fused deposition modeling of thermoplastic polymer composites *Composites B* **201** 108336
- [240] Medellín-Castillo H I and Zaragoza-Siqueiros J 2019 Design and manufacturing strategies for fused deposition modelling in additive manufacturing: a review *Chin. J. Mech. Eng.* **32** 1–16
- [241] Rajan K *et al* 2022 Fused deposition modeling: process, materials, parameters, properties and applications *Int. J. Adv. Manuf. Technol.* **120** 1531–70
- [242] Mwema F M and Akinlabi E T 2020 Basics of fused deposition modelling (FDM) *Fused Deposition Modeling: Strategies for Quality Enhancement* (Springer) pp 1–15
- [243] Arretche I and Matlack K H 2019 Experimental testing of vibration mitigation in 3D-printed architected metastructures *J. Appl. Mech.* **86** 35
- [244] Al Rifaie M, Abdulhadi H and Mian A 2022 Advances in mechanical metamaterials for vibration isolation: a review *Adv. Mech. Eng.* **14** 16878132221082872
- [245] Monkova K, Vasina M, Zaludek M, Monka P P and Tkac J 2021 Mechanical vibration damping and compression properties of a lattice structure *Materials* **14** 1502
- [246] Matlack K H, Bauhofer A, Krödel S, Palermo A and Daraio C 2016 Composite 3D-printed metastructures for low-frequency and broadband vibration absorption *Proc. Natl Acad. Sci. USA* **113** 8386–90
- [247] Vyavahare S, Teraiya S and Kumar S 2023 FDM manufactured auxetic structures: an investigation of mechanical properties using machine learning techniques *Int. J. Solids Struct.* **265–266** 112126
- [248] Mohan A, Mondal P and Rengaswamy J 2023 Impact behavior of auxetic structures: experimental and numerical analysis *Mater. Today: Proc.* **87** 292–8

- [249] Baila D I and Tonoiu S 2022 Properties of photo-curable polyurethane resins used in SLA manufacturing *IOP Conf. Ser.: Mater. Sci. Eng.* **1268** 012006
- [250] Ren L, Wu W, Ren L, Song Z, Liu Q, Li B, Wu Q and Zhou X 2022 3D printing of auxetic metamaterials with high-temperature and programmable mechanical properties *Adv. Mater. Technol.* **7** 2101546
- [251] Manapat J Z, Chen Q, Ye P and Advincula R C 2017 3D printing of polymer nanocomposites via stereolithography *Macromol. Mater. Eng.* **302** 1600553
- [252] Sultan M T, Lee O J, Lee J S and Park C H 2022 Three-dimensional digital light-processing bioprinting using silk fibroin-based bio-ink: recent advancements in biomedical applications *Biomedicine* **10** 3224
- [253] Kim S-Y, Shin Y-S, Jung H-D, Hwang C-J, Baik H-S and Cha J-Y 2018 Precision and trueness of dental models manufactured with different 3-dimensional printing techniques *Am. J. Orthod. Dentofacial Orthop.* **153** 144–53
- [254] Knowlton S, Yu C H, Ersoy F, Emadi S, Khademhosseini A and Tasoglu S 2016 3D-printed microfluidic chips with patterned, cell-laden hydrogel constructs *Biofabrication* **8** 025019
- [255] Slesarenko V and Rudykh S 2018 Towards mechanical characterization of soft digital materials for multimaterial 3D-printing *Int. J. Eng. Sci.* **123** 62–72
- [256] Linghu C, Zhang S, Wang C and Song J 2018 Transfer printing techniques for flexible and stretchable inorganic electronics *npj Flexible Electr.* **2** 26
- [257] De Souza Oliveira H, Catania F, Lanthaler A H, Carrasco-Pena A, Cantarella G and Mützenrieder N 2023 Substrate-free transfer of large-area ultra-thin electronics *Adv. Electron. Mater.* **9** 2201281
- [258] Giannakou P, Tas M O, Le Borgne B and Shkunov M 2020 Water-transferred, inkjet-printed supercapacitors toward conformal and epidermal energy storage *ACS Appl. Mater. Interfaces* **12** 8456–65
- [259] Kim M-G, Kanatzidis M G, Facchetti A and Marks T J 2011 Low-temperature fabrication of high-performance metal oxide thin-film electronics via combustion processing *Nat. Mater.* **10** 382–8
- [260] Park J, Lee Y, Lee H and Ko H 2020 Transfer printing of electronic functions on arbitrary complex surfaces *ACS Nano* **14** 12–20
- [261] Lee C H, Kim D R and Zheng X 2011 Fabrication of nanowire electronics on nonconventional substrates by water-assisted transfer printing method *Nano Lett.* **11** 3435–9
- [262] Ko H *et al* 2010 Ultrathin compound semiconductor on insulator layers for high-performance nanoscale transistors *Nature* **468** 286–9
- [263] Jin S H *et al* 2015 Water-soluble thin film transistors and circuits based on amorphous indium–gallium–zinc oxide *ACS Appl. Mater. Interfaces* **7** 8268–74
- [264] Zhang J *et al* 2019 High-performance acetone soluble tape transfer printing method for heterogeneous integration *Sci. Rep.* **9** 15769
- [265] Lee C H *et al* 2013 Peel-and-stick: mechanism study for efficient fabrication of flexible/transparent thin-film electronics *Sci. Rep.* **3** 2917
- [266] Le Borgne B, Liu S, Morvan X, Crand S, Sporea R A, Lu N and Harnois M 2019 Water transfer printing enhanced by water-induced pattern expansion: toward large-area 3D electronics *Adv. Mater. Technol.* **4** 1800600
- [267] Le Borgne B, Jacques E and Harnois M 2018 The use of a water soluble flexible substrate to embed electronics in additively manufactured objects: from tattoo to water transfer printed electronics *Micromachines* **9** 474
- [268] Chen Y, Liu X, Ma Y, Chen Y, Lu B and Feng X 2021 Interfacial liquid film transfer printing of versatile flexible electronic devices with high yield ratio *Adv. Mater. Interfaces* **8** 2100287
- [269] Xu R, Chen C, Sun J, He Y, Li X, Lu M-H and Chen Y 2023 The design, manufacture and application of multistable mechanical metamaterials—a state-of-the-art review *Int. J. Extreme Manuf.* **5** 042013
- [270] Shan S *et al* 2015 Multistable architected materials for trapping elastic strain energy *Adv. Mater.* **27** 4296–301
- [271] Li W, Wang F, Sigmund O and Zhang X S 2022 Digital synthesis of free-form multimaterial structures for realization of arbitrary programmed mechanical responses *Proc. Natl Acad. Sci. USA* **119** e2120563119
- [272] Bell M A, Becker K P and Wood R J 2022 Injection molding of soft robots *Adv. Mater. Technol.* **7** 2100605
- [273] Schmitt F, Piccin O, Barbé L and Bayle B 2018 Soft robots manufacturing: a review *Front. Rob. AI* **5** 344386
- [274] Laschi C, Mazzolai B and Cianchetti M 2016 Soft robotics: technologies and systems pushing the boundaries of robot abilities *Sci. Rob.* **1** eaah3690
- [275] Xue Y, Wang X, Wang W, Zhong X and Han F 2018 Compressive property of Al-based auxetic lattice structures fabricated by 3-D printing combined with investment casting *Mater. Sci. Eng., A* **722** 255–62
- [276] Yao D 2009 Micromolding of polymers *Advances in Polymer Processing* (Woodhead Publishing) pp 552–78
- [277] Rossnagel S 2003 Thin film deposition with physical vapor deposition and related technologies *J. Vac. Sci. Technol. A* **21** S74–S87
- [278] Weimer P K 1962 The tft a new thin-film transistor *Proc. IRE* **50** 1462–9
- [279] Yao B, Chan Y and Wang N 2002 Formation of zno nanostructures by a simple way of thermal evaporation *Appl. Phys. Lett.* **81** 757–9
- [280] Awan T I, Bashir A and Tehseen A 2020 *Chemistry of Nanomaterials: Fundamentals and Applications* (Elsevier)
- [281] Baptista A *et al* 2018 On the physical vapour deposition (PVD): evolution of magnetron sputtering processes for industrial applications *Proc. Manuf.* **17** 746–57
- [282] Dai Z R, Pan Z W and Wang Z L 2003 Novel nanostructures of functional oxides synthesized by thermal evaporation *Adv. Funct. Mater.* **13** 9–24
- [283] de Souza Oliveira H *et al* 2023 Permeable thermistor temperature sensors based on porous melamine foam *IEEE Sens. Lett.* **7** 2500904
- [284] Berg S and Nyberg T 2005 Fundamental understanding and modeling of reactive sputtering processes *Thin Solid Films* **476** 215–30
- [285] Kelly P J and Arnell R D 2000 Magnetron sputtering: a review of recent developments and applications *Vacuum* **56** 159–72
- [286] Williams P 1979 The sputtering process and sputtered ion emission *Surf. Sci.* **90** 588–634
- [287] Posadowski W, Wiatrowski A, Dora J and Radzinski Z 2008 Magnetron sputtering process control by medium-frequency power supply parameter *Thin Solid Films* **516** 4478–82
- [288] Pethe S A, Takahashi E, Kaul A and Dhere N G 2012 Effect of sputtering process parameters on film properties of molybdenum back contact *Sol. Energy Mater. Sol. Cells* **100** 1–5
- [289] OjedaGP A, Döbeli M and Lippert T 2018 Influence of plume properties on thin film composition in pulsed laser deposition *Adv. Mater. Interfaces* **5** 1701062
- [290] Chrisey D B *et al* 1994 *Pulsed Laser Deposition of Thin Films* ed G K Hubler (Wiley)
- [291] Masood K B, Kumar P, Malik M A and Singh J 2021 A comprehensive tutorial on the pulsed laser deposition

- technique and developments in the fabrication of low dimensional systems and nanostructures *Emer. Mater.* **4** 737–54
- [292] Sunu S, Prabhu E, Jayaraman V, Gnanasekar K and Gnanasekaran T 2003 Gas sensing properties of pld made moo3 films *Sensors Actuators B* **94** 189–96
- [293] Xu L, Shyu T C and Kotov N A 2017 Origami and kirigami nanocomposites *ACS Nano* **11** 7587–99
- [294] Gong J, Seow O, Honnet C, Forman J and Mueller S 2021 MetaSense: integrating sensing capabilities into mechanical metamaterial *UIST'21: The 34th Annual ACM Symp. on User Interface Software and Technology* (Association for Computing Machinery) pp 1063–73
- [295] Gao H, Li J, Wang Z, Xue Z and Meng X 2024 Design of porous partition elastomer substrates for the island–bridge structures in stretchable inorganic electronics *J. Appl. Mech.* **91** 67
- [296] Silva C A *et al* 2020 Liquid metal based island-bridge architectures for all printed stretchable electrochemical devices *Adv. Funct. Mater.* **30** 2002041
- [297] Li K, Shuai Y, Cheng X, Luan H, Liu S, Yang C, Xue Z, Huang Y and Zhang Y 2022 Island effect in stretchable inorganic electronics *Small* **18** 2107879
- [298] Song X, Bian Z, Zhou X and Huang Z 2022 Vibration characteristics of island-bridge structure on porous PDMS substrates for stretchable electronics *J. Appl. Mech.* **89** 90
- [299] Tang R and Fu H 2020 Mechanics of buckled kirigami membranes for stretchable interconnects in island-bridge structures *J. Appl. Mech.* **87** 3
- [300] Romani A, Mantelli A, Tralli P, Turri S, Levi M and Suriano R 2021 Metallization of thermoplastic polymers and composites 3D printed by fused filament fabrication *Technologies* **9** 49
- [301] Khaanghah N S *et al* 2023 Stone-based substrates for thin-film thermistor temperature sensors *2023 IEEE SENSORS* (IEEE) pp 2023–01
- [302] Khaanghah N S *et al* 2024 Application of stone-derived substrates in thin-film temperature sensing *IEEE Sens. J.* **24** 40179–87
- [303] Khaanghah N S *et al* 2023 Silicone/carbon black-filled elastomer-based self-healing strain sensor *IEEE Sens. Lett.* **7** 2501204
- [304] Lanthaler A H *et al* 2023 Thin-film temperature sensor on flexible PEEK fabric *2023 IEEE Int. Flexible Electronics Technology Conf. (IFETC)* (IEEE) pp 13–16
- [305] Hayrapetyan H, Tran T, Tellez-Corrales E and Madiraju C 2023 Enzyme-linked immunosorbent assay: types and applications *ELISA* (Springer) pp 1–17
- [306] Chen X Y and Rodrigue D 2023 Conversion of polystyrene foams into auxetic metamaterials *Polym. Eng. Sci.* **63** 2193–203
- [307] Jiao P and Alavi A H 2021 Artificial intelligence-enabled smart mechanical metamaterials: advent and future trends *Int. Mater. Rev.* **66** 365–93
- [308] Song J, Lee J, Kim N and Min K 2024 Artificial intelligence in the design of innovative metamaterials: a comprehensive review *Int. J. Precis. Eng. Manuf.* **25** 225–44
- [309] Jenis J, Ondriga J, Hrcek S, Brumerick F, Cuchor M and Sadovsky E 2023 Engineering applications of artificial intelligence in mechanical design and optimization *Machines* **11** 577
- [310] Patel A R, Ramaiya K K, Bhatia C V, Shah H N and Bhavsar S N 2020 artificial intelligence: prospect in mechanical engineering field—a review *Data Science and Intelligent Applications* (Springer) pp 267–82
- [311] Guo K, Yang Z, Yu C-H and Buehler M J 2021 Artificial intelligence and machine learning in design of mechanical materials *Mater. Horiz.* **8** 1153–72
- [312] Zhao S, Blaabjerg F and Wang H 2020 An overview of artificial intelligence applications for power electronics *IEEE Trans. Power Electron.* **36** 4633–58
- [313] Sridharan M 2020 Applications of artificial intelligence techniques in heat exchanger systems *Advanced Analytic and Control Techniques for Thermal Systems With Heat Exchangers* (Academic) pp 325–34
- [314] Guillen D P, Abboud A W and Bennink J 2022 Topology optimization of an airfoil fin microchannel heat exchanger using artificial intelligence *Nucl. Eng. Des.* **391** 111737
- [315] Ye Z, Shao W, Ding X, Wang B-Z and Sun S 2022 Knowledge-based neural network for multiphysical field modeling *IEEE Trans. Microwave Theory Tech.* **71** 1967–76
- [316] van Manen T, Janbaz S, Jansen K M B and Zadpoor A A 2021 4D printing of reconfigurable metamaterials and devices *Commun. Mater.* **2** 1–8
- [317] Bodaghi M, Damanpack A R and Liao W H 2017 Adaptive metamaterials by functionally graded 4D printing *Mater. Des.* **135** 26–36
- [318] Xin X, Liu L, Liu Y and Leng J 2020 4D printing auxetic metamaterials with tunable, programmable and reconfigurable mechanical properties *Adv. Funct. Mater.* **30** 2004226
- [319] Tao R, Xi L, Wu W, Li Y, Liao B, Liu L, Leng J and Fang D 2020 4D printed multi-stable metamaterials with mechanically tunable performance *Compos. Struct.* **252** 112663
- [320] Chen J, Virrueta C, Zhang S, Mao C and Wang J 2024 4D printing: the spotlight for 3D printed smart materials *Mater. Today* **77** 66–91
- [321] Won P *et al* 2019 Stretchable and transparent kirigami conductor of nanowire percolation network for electronic skin applications *Nano Lett.* **19** 6087–96
- [322] Mark A G, Palagi S, Qiu T and Fischer P 2016 Auxetic metamaterial simplifies soft robot design *2016 IEEE Int. Conf. on Robotics and Automation (ICRA)* (IEEE) pp 4951–6
- [323] Pan Q, Chen S, Chen F and Zhu X 2020 Programmable soft bending actuators with auxetic metamaterials *Sci. China Technol. Sci.* **63** 2518–26
- [324] Rafsanjani A, Zhang Y, Liu B, Rubinstein S M and Bertoldi K 2018 Kirigami skins make a simple soft actuator crawl *Sci. Robot.* **3** eaar7555
- [325] Aigner R, Haberfellner M A and Haller M 2022 spaceR: knitting ready-made, tactile and highly responsive spacer-fabric force sensors for continuous input *UIST'22: Proc. 35th Annual ACM Symp. on User Interface Software and Technology* (Association for Computing Machinery) pp 1–15
- [326] Jang Y, Kim S M, Spinks G M and Kim S J 2020 Carbon nanotube yarn for fiber-shaped electrical sensors, actuators and energy storage for smart systems *Adv. Mater.* **32** 1902670
- [327] Özen O, Yilmaz D and Yapici K 2022 A novel method for the production of conductive ring spun yarn *Cellulose* **29** 4767–85
- [328] Bar M, Alagirusamy R and Das A 2018 Properties of flax-polypropylene composites made through hybrid yarn and film stacking methods *Compos. Struct.* **197** 63–71
- [329] Preindl T, Honnet C, Pointner A, Aigner R, Paradiso J A and Haller M 2020 Sonoflex: embroidered speakers without permanent magnets *UIST'20: Proc. 33rd Annual ACM Symp. on User Interface Software and Technology* (Association for Computing Machinery) pp 675–85